COUPLING OF AN ELECTROLYZER WITH RANKINE CYCLE FOR SUSTAINABLE HYDROGEN PRODUCTION VIA THERMAL SOLAR ENERGY

by

Mohamed Shahin Shahin

A Thesis Presented to the Faculty of the
American University of Sharjah
College of Engineering
in Partial Fulfillment
of the Requirements
for the Degree of

Masters of Science in
Mechanical Engineering

Sharjah, United Arab Emirates

May 2015

Approval Signatures

We, the undersigned, approve the Master's Thesis of Mohamed Shahin Shahin.

Thesis Title: Coupling of an Electrolyzer with Rankine Cycle for Sustainable Hydrogen Production via Thermal Solar Energy.

Signature	**Date of Signature** (dd/mm/yyyy)
_____	_____
Dr. Mehmet Fatih Orhan Assistant Professor, Department of Mechanical Engineering Thesis Advisor	
_____	_____
Dr. Mamoun Abdel-Hafez Associate Professor, Department of Mechanical Engineering Thesis Committee Member	
_____	_____
Dr. Mehmet Egilmez Assistant Professor, Department of Physics College of Arts and Science Thesis Committee Member	
_____	_____
Dr. Essam Wahba Interim Head, Department of Mechanical Engineering	
_____	_____
Dr. Mohamed El-Tarhuni Associate Dean, College of Engineering	
_____	_____
Dr. Leland Blank Dean, College of Engineering	
_____	_____
Dr. Khaled Assaleh Director of Graduate Studies	

Acknowledgements

I would like to express my extreme gratitude to my thesis advisor, Dr. Mehmet Fatih Orhan for his continuous support and guidance in my thesis and for his patience, expertise, and kindness. I am very thankful to him for supporting and encouraging me during my hardest times and over the course of my study here at AUS.

My thanks and appreciation goes to my thesis committee members Dr. Mehmet Egilmez and Dr. Mamoun Abdel-Hafez for reviewing my thesis report and allocating the time to read it.

Also, many thanks to my parents, brother, and sister for their continuous support over the course of 7 years I spent at AUS. Without their encouragement and sacrifices, I would have not been able to carry out my work.

Finally, I would like to greet and thank the American University of Sharjah (AUS) for providing me with the Master's scholarship and opportunity to further increase my knowledge in Mechanical Engineering through my degree.

Abstract

Due to the global challenges faced everyday by our planet earth, several groundbreaking energy solutions are needed to reduce the environmental pollution caused by fossil fuels and improve energy sustainability for the future generations. The increase in fossil fuel prices, environmental pollution, and limitations in fossil fuel reserves, stresses the need of an alternative energy source that is clean, not hazardous, and dependable. Hydrogen is believed to be the future energy carrier that will reduce environmental pollution and solve the current energy crises especially when produced from a renewable energy source. Solar energy is a renewable source that has been used in the production of hydrogen for years because it is inexhaustible, clean, and a free energy source. Hydrogen is produced by a means of a water splitting process, mainly electrolysis, which requires energy input provided by harvesting solar energy. The proposed model integrates the solar harvesting system to a conventional Rankine cycle, producing electric and thermal power, used in domestic applications, and production of hydrogen by high temperature electrolysis (HTE) using a solid oxide steam electrolyzer (SOSE). The objective of this research is to carry out thermodynamic energy analysis on the proposed system to study the performance and efficiency of the system. The system is divided into three subsystems; solar collector(s), steam cycle, and electrolysis subsystem, where thermodynamic analysis is done using equations from the literature and Engineering Equations Solver (EES). Moreover, parametric analysis will be carried out with the results obtained from EES to study the performance of the system under different conditions. The analysis that will be carried out is to study the effect of varying the solar flux and varying the area of the solar collector on the rate of hydrogen produced. Finally, a comparative analysis will be done with a parabolic trough and heliostat field to investigate which works most effectively with the plant and has the highest rate of hydrogen produced.

Search Terms: Hydrogen production; solar; Rankine cycle; thermodynamic analysis; electrolyzer; parabolic trough; heliostat field

Table of Contents

List of Figures

List of Tables

List of Abbreviations

$\dot{m}$	Mass flow rate
Cp	Specific heat
T	Temperature
A	Area
F_R	Heat removal factor
S	Heat absorbed by receiver
U	Collector heat loss coefficient
D	Diameter
L	Length
G_b	Solar irradiation
K_r	Incident angle modifier
w	Width
F_1	Efficiency factor
Nus	Nusselt number
Pr	Prandtl number
h	Heat transfer coefficient
Re	Reynolds number
V	Velocity
K	Thermal conductivity
Col	Number of solar collectors
$\dot{Q}$	Heat rate
s	Entropy
h	Enthalpy

Ex	Exergy
g	Acceleration due to gravity
z	Elevation
F_r	View factor
C	Concentration ratio
d	Diameter
$\dot{W}$	Power output

Subscripts

ri	Receiver's inlet
ro	Receiver's outlet
i	Inner
o	Outer
r	Receiver
ap	Aperture
c	Cover
a	Ambient
c,o	Cover outlet
c,i	Cover inlet
r,int	Internal receiver
0	Ambient
r,ca	Between ambient and receiver cover
c,ca	Between cover and ambient
r,cr	Between receiver and cover
r,avg	Average, receiver

c,r,in	Between cover and receiver, input
r,cross	Cross sectional, receiver
th	Thermal
u	Useful
rec	Receiver
s	Solar
rec,surf	Surface of receiver
insi	Inside
H	Heliostat field
em	Emissive heat
ref	Reflective heat
conv	Convective heat
cond	Conductive heat
fc	Forced convection
nc	Natural convection
H2	Hydrogen
insu	Insulation
ms	Molten salt
turb	Turbine
st	Steam
p	Pump
cond	Condenser
ex	Exergy
en	Energy

abs	Absorbed
isen	Isentropic
elect	Electrolyzer

Greek Letters

η	Efficiency
ρ_c	Reflectance
γ	Intercept factor
τ	Transmittance
α	Absorbance
σ	Stefan Boltzmann constant
ε_r	Emittance of the cover
υ	Kinematic viscosity
ρ	Density
ε_w	Wall's emissivity
δ	Thickness
λ	Thermal conductivity

Acronyms

LHV	Low heating value
HTF	Heat transfer fluid
UAE	United Arab Emirates
SOEC	Solid oxide electrolyzer cell
CO2	Carbon dioxide
H2	Hydrogen

NaOH	Sodium hydroxide
KOH	Potassium hydroxide
HTSE	High temperature steam electrolysis
VHTR	Very high temperature reactor
ORC	Organic Rankine cycle
PEM	Particle exchange membrane
OTEC	Ocean thermal energy conversion
HRHG	Heat recovery heat generator
HRSG	Heat recovery steam generator
EES	Engineering Equations Solver
THE	High temperature electrolysis
S-I	Sulfur iodine
Cu-Cl	Copper chlorine
SI	System of innovation
LCOE	Localized cost of electricity

Chapter 1: Introduction

Energy plays a crucial role in the human life nowadays. The increase in technological equipment and appliances require energy now more than ever. Not only is it dependent on what people use at home, but also on other activities such as agriculture, construction, manufacturing, and health. With the technological increase over the past century, solutions are required to accelerate the production of energy. The growth in population and human desire to increase life standards is what drives energy demand. Clean energy sources are now needed to protect the environment and make our lives more productive, safer, and healthier. Renewable energy sources are now attractive to many countries for meeting the energy demands without relying on fossil fuels. The burning of fossil fuels increased environmental pollution and changes in climate. The endless dependency on fossil fuels to be the future energy carrier raises doubts. The depletion of those fuels over time and the hikes in prices of oil and gas require an alternative energy carrier. Hydrogen is promised to be the future energy carrier because it is the most abundant chemical source. In the Gulf region, and especially the United Arab Emirates (UAE), the demand for energy is increasing and the best renewable energy source available is solar energy. In the future, fossil fuels will no longer be the main energy source, with hydrogen to be the energy carrier, making it appealing to utilize the solar energy available. The use of solar energy in the UAE is slowly increasing due to the promising performance of the systems and the increase in research topics of systems utilizing solar energy. Recent researches has been done on harvesting solar energy with existing systems such as the Rankine cycle with hydrogen production using water electrolysis.

1.1 Background and Motivation

Renewable energies are emerging day after day in every-day applications to save the planet earth from environmental pollution, ozone depletion, and global warming. Solar energy coming from the sun is used as a means of energy in agriculture, transport, thermal heating, and electricity production.

The UAE is in rapid development since the past decade, which in turn increases the energy demand to maintain the high living standards. The population growth in the UAE is very rapid which is leading to increased energy demand.

Currently, the UAE is heavily dependent on hydrocarbons such as oil and gas for the production of electricity, holding the world's seventh largest reserves of oil (97.8 billion barrels), according to the Oil and Gas Journal of the year 2012. This continuous use of fossil fuels and natural gas has had a dramatic effect on climate change and the increase in greenhouse gas emissions according to the U.S Energy Information Administration as shown in Figure 1.

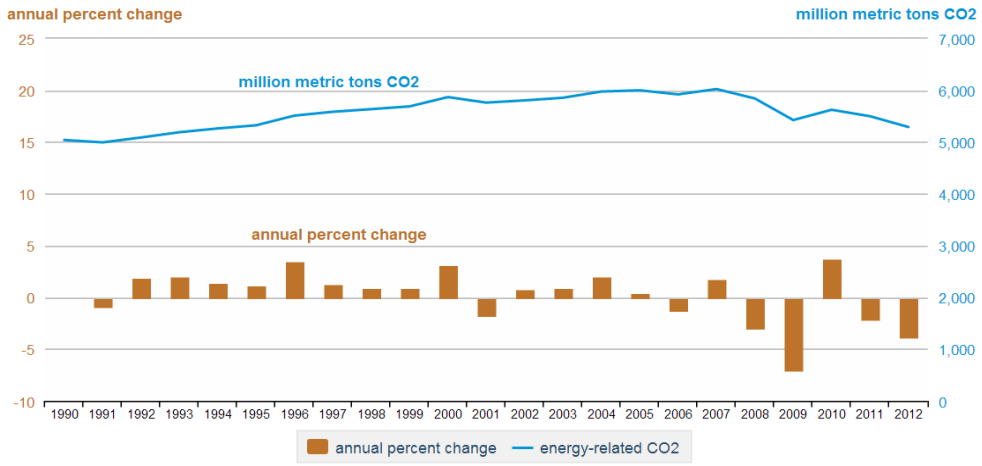

Figure 1: Annual greenhouse gas emissions (CO2) in 2013 [1]

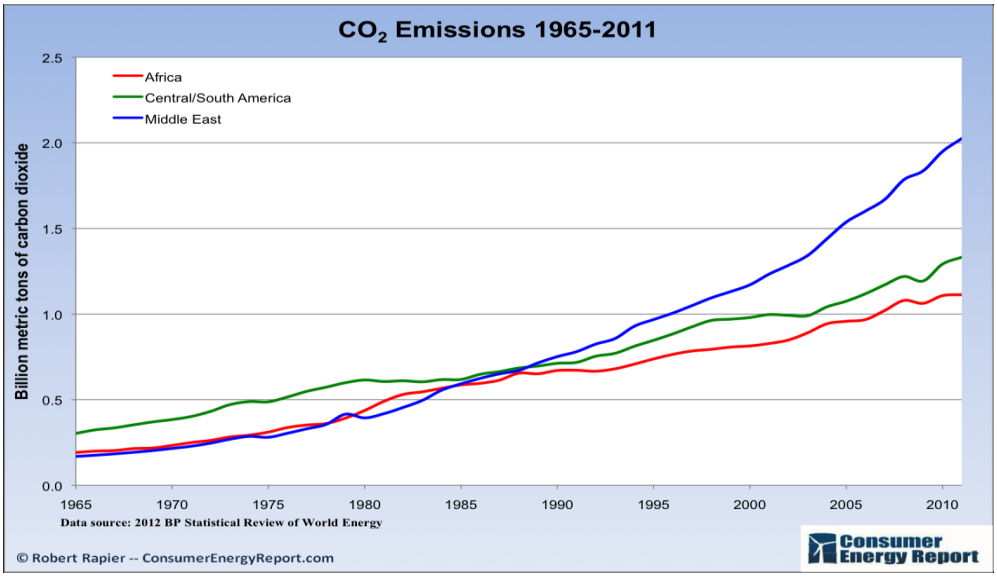

Figure 2: Greenhouse gas emissions (CO2) in Africa, Central/South America, and Middle East (1965-2011) [2]

The increased greenhouse gas emissions led countries like the UAE to hunt for better energy sources and carriers. As seen from Figure 2, the increase in CO_2 emissions in the Middle East is the highest compared to Africa and Central/South America, which is not surprising as the use of fossil fuels in the Middle East is rapidly

increasing due to the development and high living standards. The emission from the UAE alone is 40.1 tons of CO_2 per person in the year 2010 compared to the year 1992 where the emission was only 4 tons of CO_2 per person, a 90% increase.

1.1.1 Solar energy sources.

Planet earth receives 174 PW (petawatts) of solar radiation, 30% of which is reflected back to space leaving the other percentage to be absorbed by clouds, surfaces, and oceans [3]. The solar energy absorbed by the atmosphere is approximately 3,850,000 EJ (exajoules) per year. This huge amount of solar energy reaching the sun is so massive that it is twice that obtained from non-renewable sources in one year [4]. Therefore, this free energy can be harnessed using two methods. These methods are passive or active. In passive solar, thermal energy is used directly for heating purposes like greenhouses, sunrooms, and solariums. The sun's rays pass through glass windows and the interior retain the heat. In active solar, solar collectors are available for harnessing thermal energy, and they vary from flat plate collectors, parabolic troughs, heliostat fields, to parabolic dish technologies. These technologies are all concentrated collectors to focus the sun's energy on one point raising the temperature of a fluid flowing in an absorber tube. The types of concentrated solar collectors used in this thesis are as follows:

1.1.1.1 Parabolic trough solar collectors.

Parabolic trough solar collectors are a type of concentrating collectors used in thermal power plants. They consist of a reflective mirror in the shape of a parabola, a tubular receiver, and support structures. The collector uses the solar incident rays from the sun, reflecting them onto a tubular receiver containing a heat transfer fluid (HTF) to produce heat. This heat is then used to convert water to superheated steam in a Rankine cycle to produce electricity. The tubular receiver sits at the focal point of the parabola for effective reflection of the sun's rays onto the fluid inside the receiver. The tube is covered by a sealed glass containing a vacuum to avoid heat loss to the surroundings. Moreover, the HTF must have good thermal properties to achieve high temperature, and also avoid cavitation and corrosion inside the pipe where the fluid flows. The support structures are designed in a way to track the incident rays over the day for the highest possible efficiency. This type of solar collector is very effective in areas with high incident solar flux such as Abu Dhabi and also the quality of heat

depends on the availability and level of solar irradiation. New technologies use a different type of reflecting mirror material which is lighter and more efficient than conventional mirrors, therefore reducing capital and running costs. Figure 3 shows the schematic of a conventional parabolic trough collector.

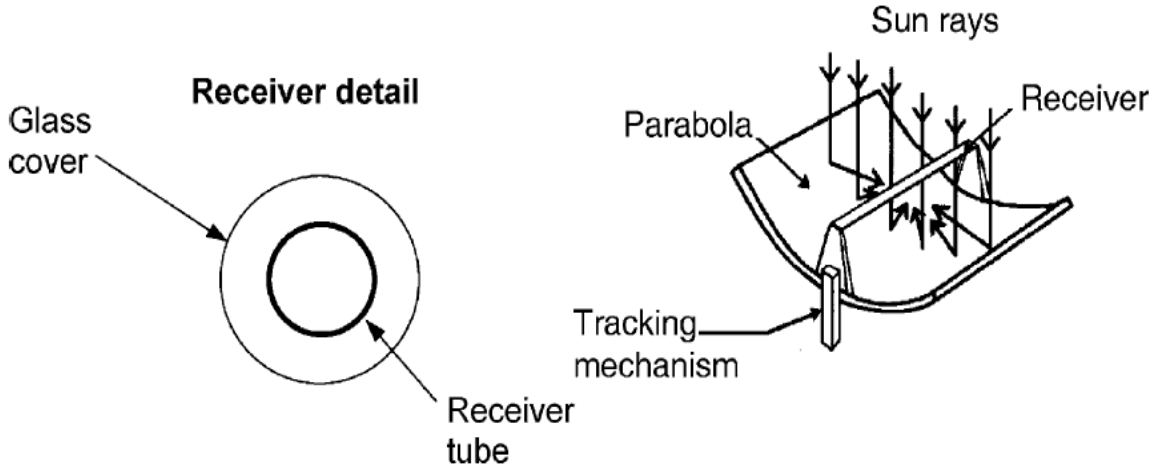

Figure 3: Schematic of a parabolic trough collector [5]

1.1.1.2 Heliostat field solar collectors.

For centralized heat production high temperature solar technologies, heliostat fields have an operating temperature range of 150-2000℃ [5]. High temperature solar collectors are important in larger power production and efficiency. The flexibility of the operating temperatures in a heliostat field is what makes it the best choice for the application at hand. A heliostat field collector consists of several reflecting mirrors and a tower with a central receiver where molten salt flows and absorbs the heat reflected. The wide field of mirrors focuses the sun's incident rays onto a single receiver to heat up the molten salt. The molten salt then travels through a heat exchanger where heat is lost to the water and high temperature superheated steam is produced. This high temperature steam is then expanded in a steam turbine and electricity is generated. The cost of a heliostat field represents 30-50% of the initial capital investment for solar thermal power plants depending on the location of the country, energy policy, and the economic framework. New technologies incorporate a secondary sandwich-type mirror on top of the conventional mirror referred to as a glass/metal heliostat. This type of new heliostat field is an attempt to lower the cost of the heliostat field by replacing the conventional heliostat field with one that uses

fewer and lighter materials [6]. Figure 4 shows the schematic diagram of a conventional heliostat field in a solar thermal power plant.

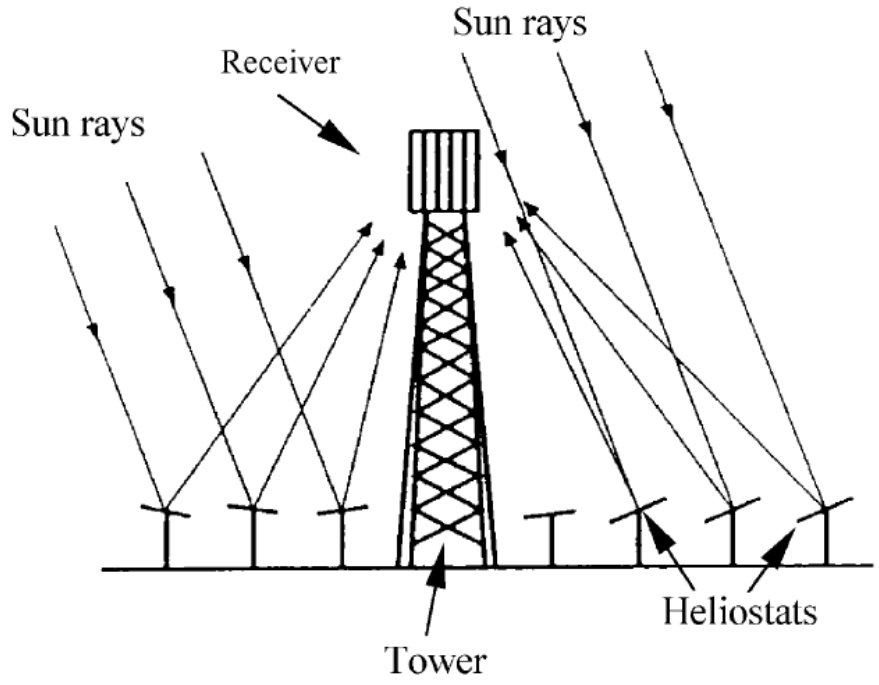

Figure 4: Schematic of a heliostat field collector [5]

1.1.2 Rankine cycle.

The cycle responsible for generating electrical power to the electrolyzer is the famous Rankine cycle as shown in Figure 5. The cycle below consists of a heat exchanger, two steam turbines, a condenser, and a water pump. The efficiency of the Rankine cycle is mainly dependent on the high heat vaporization of the fluid; therefore, for high efficiency of a Rankine cycle, the temperature and pressure of water needs to reach a critical level. The typical entering temperature value at the steam turbine is around 550°C which gives a theoretical maximum Carnot efficiency of around 63% [7]. The molten salt inside the heat exchanger receives the heat in the receiver of the solar collector and gets heated up to a high temperature. This high temperature molten salt transfers the heat to the subcooled water entering the heat exchanger where high temperature steam is generated. The high temperature steam enters the two stage steam turbines where steam loses energy to produce power. Heat is lost in the condenser cooled by the cooling tower and the cycle is repeated. The power produced by the cycle is used to power the pumps and the electrolyzer.

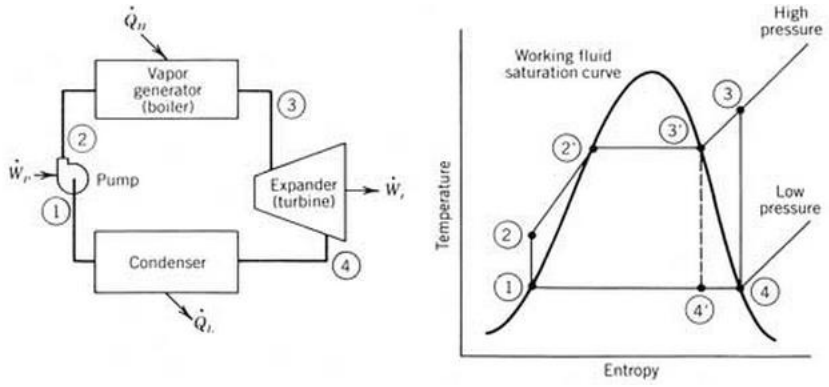

Figure 5: Rankine cycle schematic with the T-s diagram [7]

1.1.3 Water electrolysis.

As discussed earlier, hydrogen is believed to be the energy carrier of the future. However, hydrogen is not freely available and needs to be produced using existing and renewable sources. Hydrogen serves the same purpose as a battery, since it is an energy carrier, unlike coal which is a primary energy source [8]. The production of hydrogen includes vast methods such as steam reformation of hydrocarbons, water electrolysis, and thermochemical splitting of water. 96% of the hydrogen produced nowadays is by conventional methods using fossil fuels, whereas the other 4% is produced by water electrolysis.

Thermochemical splitting of water is the most covered area in recent research. It uses heat to split water into hydrogen and oxygen molecules, thus producing hydrogen [9]. The heat used in this method can be produced from renewable energy sources, such as wind, solar, and geothermal power. It is the most favorable method in the future since renewable sources will most likely contribute to the energy demand in the future.

Steam reformation of hydrocarbons is the production of hydrogen using fuels such as natural gas. This process is carried out in a reformer where fossil fuels react with steam at very high temperatures, where hydrogen is produced and provided to fuel cells [10]. The issue with this method is that it utilizes hydrocarbons which produce CO_2 emissions upon reaction in the reformer-fuel-cell system. Considering this emission, global warming issues will arise and the idea of using renewable sources is overlooked.

The most favorable method of hydrogen production, especially considering both renewable energy sources and the Rankine cycle, is the water electrolysis

method. Water electrolysis uses electricity generated from a steam turbine, where electric current is passed through water and water is decomposed into hydrogen and oxygen. Hydrogen is produced in an electrolyzer cell at the cathode, and oxygen at the anode, with a power source in between. A huge amount of energy is required to break the strong bond between hydrogen and oxygen inside the water molecule; therefore, catalysts are used to loosen the bond such as sodium hydroxide (NaOH) or potassium hydroxide (KOH). The most common electrolyzer used in thermal power plants with high temperatures is the solid oxide electrolyzer cell (SOEC).

1.1.3.1 Solid oxide electrolyzer cell.

In water electrolysis, the electricity used to produce hydrogen is from renewable sources making it more convenient than other production methods [11]. As mentioned before, the electrolyzer used in the system is a solid oxide electrolyzer cell (SOEC) which utilizes high temperature electrolysis (THE). SOEC single cell consists of three main layers as shown in Figure 6. The upper layer is the negative fuel electrode made of Ni having good oxide and electron conductivity and a porous structure where the gases can meet and react. The middle layer is oxide ion-conducting electrolyte that insulates the gas entrapped [12]. The operation temperature of the SOEC is over 1023 K [13]. The modeling of the process phenomena inside the cell is done using planar rectangular SOECs in order to estimate the electric potential and the energy needs of the cell. This type of modeling is used because of the flexibility, easy-production, and compactness characteristics describing the performance. A single unitary celled SOEC is shown in Figure 7.

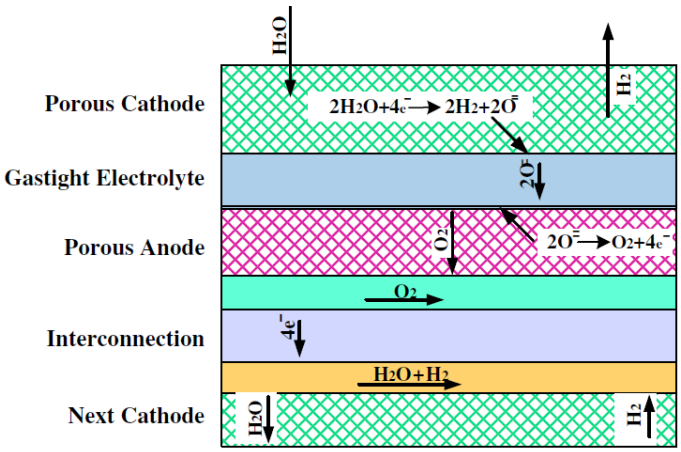

Figure 6: Structure of a SOEC single cell [12]

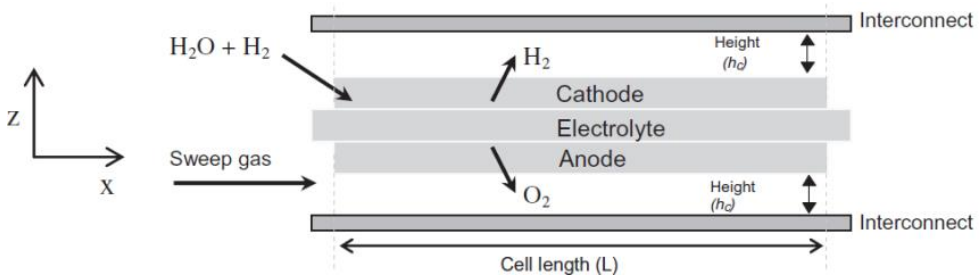

Figure 7: SOEC unitary cell [14]

The selection of the appropriate electrolyzer cell for hydrogen production is based on several criteria as shown below:

I. Process Temperature

Water electrolysis requires high temperatures ranging from 400 to 3000°C, which is difficult to achieve in commercial applications. The usage of concentrated solar collectors achieves these high temperatures but the constraint on materials used is a challenge.

II. Process Safety and Environmental Factors

Some cycles which use high amounts of cadmium, mercury, and even bromine can achieve the suitable temperature limit, but they are hazardous to the environment. On the other hand, some cells use non-hazardous materials and are very environmentally-friendly.

III. Process Complexity

Several thermodynamic cycles involve many complex and difficult gas separation steps. However, some electrolyzers split water molecules in simple steps with the provision of a water supply and electrical power.

The selection of the electrolyzer was based on the criteria above, and the SOEC is chosen. The SOEC has an operating temperature which can be reached using the parabolic and heliostat collectors, and uses simple materials which are environmentally friendly and non-hazardous. The most famous high temperature electrolysis is the Solid Oxide Electrolyzer Cell (SOEC) designed by Donitz and Erdle in the 1980s [15]. In a SOEC, water acts as a reactant and is supplied to the cathode part of the electrolyzer, where oxygen ions are transported to the anode part through the electrolyte, leaving hydrogen produced at the cathode side as shown in Figure 8 below [16]. The thermodynamic reaction of electrolysis is shown in the following equations:

$$H_2O \rightarrow H_2 + \frac{1}{2}O_2 \quad (1)$$

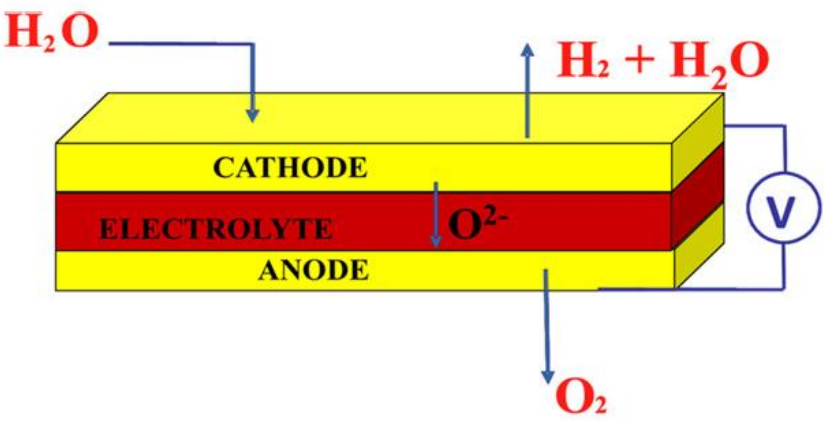

Figure 8: SOEC operating under electrolysis mode [16]

The reactions at the anode and cathode sides are:

$$H_2O + 2e^- \rightarrow H_2(g) + O^{2-}(\text{Cathode})$$

$$O^{2-} \rightarrow \frac{1}{2}O_2(g) + 2e^-(\text{Anode})$$

High temperature electrolysis is favored because it requires low electrical energy at high temperatures and because the electrolysis of water is highly endothermic with increasing temperatures [16]. For this purpose, hydrogen production through renewable sources is a great motivation to utilize these existing technologies and reduce environmental pollution on planet earth.

1.2 Problem Statement

The problem faced in most countries for the past several years has been the future replacement of fossil fuels that will grant sustainable development. Hydrogen is believed to be the future energy carrier since it is the most abundant chemical substance in the world [17]. It is an energy carrier, not an energy source, and therefore has to be produced. The proposed system utilizes solar collection technologies, existing power production cycles, and a hydrogen production unit. The proposed system consists of three parts: solar collectors, Rankine cycle, and the electrolyzer. The solar collector sub-system reflects the sun's rays to an absorber tube containing a heat transfer fluid and the temperature is raised. The primary advantage of molten salts as the heat transfer fluid is their capability to reach very high temperatures

(~560℃). This in turn allows high temperature steam to be generated at utility temperatures, achieving higher efficiencies in modern Rankine cycles. The heat from the molten salt is transferred to the water in the steam cycle through a heat exchanger where water is converted to steam at high pressure and temperature. The second sub-system is the Rankine cycle where the thermal energy (steam) is converted to electrical energy with the aid of the steam turbine. Water is then condensed using cold water from the cooling tower and is re-circulated to be heated again. The third sub-system is the hydrogen production part where water electrolysis takes place. High temperature electrolysis using the Solid Oxide Electrolyzer Cell (SOEC) is used where both electrical and thermal heat inputs are required for the production of gaseous hydrogen and oxygen. Solar radiation values for Abu Dhabi will be used since the global radiations in Abu Dhabi are very high.

This thesis is very important in the energy field and will provide a solution to the increasing energy demands in the UAE. With the solar incident availability and intensity and existing power production cycles, this proposed method could provide the UAE with a clean, sustainable, and long term solution to its energy needs and an answer for the future energy carrier question.

1.3 Objectives

The objective of this research is to carry out intensive thermodynamic analysis on the proposed system. These objectives can be specified as:

a. Examine and investigate the operating conditions and principles of the solar energy sources, Rankine cycle, hydrogen production through HTSE, and hydrogen storage.
b. Carry out energy and exergy analysis on the overall hydrogen production system and evaluate the performance. The evaluation will be in terms of the net-work output, rate of hydrogen produced, and energy and exergy efficiency of the sub-systems and overall system.
c. Parametric analysis will be carried out to investigate the effect of solar radiation and electrolyzer temperature on the power output and rate of hydrogen produced.

Finally, a comparative analysis will be done to see the difference in performance using a parabolic trough and heliostat field separately.

1.4 Significance of this Research

The increase in energy demands in recent years has led countries to invest in renewable energies for sustainable development. This research is of crucial importance since it could give long lasting answers and solutions to the problems faced in developing countries. Such systems where hydrogen is produced from a free and clean source of energy (solar) can utilize the hydrogen for power output using fuel cells. Moreover, automotive industries are moving in the direction of finding a replacement for diesel and petrol as a fuel, and hydrogen can be used as a fuel when it is compressed into liquid form. We can also make use of such fuel cells to run future automobiles.

1.5 Literature Review

Many challenges exist around the globe to find energy solutions that are capable of reducing environmental pollution that is caused by fossil fuels to produce electricity and energy output. These challenges are mainly focused on renewable energies as a means to produce electricity and improve sustainability for the upcoming generation. Hydrogen energy is under heavy research since it is believed to be the future energy carrier and will play important roles in reducing environmental emissions when it is produced from renewable energies [18]. However, the cost of implementing these new technologies is very high and they lack quality, density, and durability. Therefore, new research is being conducted to combine several renewable sources which could provide a promising energy supply to meet the future demands. Hydrogen can be produced from fossil fuels such as coal (carbon sequestration), natural gas, and renewable energy sources such as wind, solar, geothermal wells, and hydroelectric power [19].

Solar thermal energy is one of the renewable sources that can be used in the production of hydrogen. The solar flux from the sun reaching the earth's surface contains a tremendous amount of energy that can be utilized in power production. For centralized power, high temperature solar thermal technology is used since it has high power production and higher efficiencies compared to PV or PV/T systems [20]. The Rankine cycle is the most competitive approach to utilize the sun's energy and produce power. Organic substances and carbon dioxide are used instead of water to make better use of the thermal energy and hence are called the organic Rankine cycle

(ORC). Carbon dioxide is the most researched substance to be used in the Rankine cycle since it is non-explosive, non-flammable, and naturally abundant [21]. Moreover, carbon dioxide reaches its supercritical state (7.38 MPa and 31.1℃) easily and has a better temperature profile to match the heat source temperature because there is no isothermal evaporation of these supercritical fluids [22]. Yang et al. proposed a solar-powered-Rankine-based hybrid power generation system consisting of a solar collector-Rankine cycle and a hydrogen producing and storage system. Incident solar radiation is collected by means of parabolic trough solar collectors and concentrated on the absorber tubes. The working fluid is evaporated in the absorber tubes which are then passed through steam turbines for power production. Excess power is then used in the electrolyzer to produce hydrogen and during off-peak conditions the hydrogen stored is used for auxiliary heating. Using meteorological data taken in 1984 by the Space Research Laboratory, the hybrid cycle produced a net power of 7.886 kWh for the 15^{th} of January and 15.41 kWh for the 16^{th} of July. The 15^{th} of January was a sunny and cold winter day, while the 16^{th} of July was a hot summer day with partial clouds in the late morning hours. The proposed system had a cycle efficiency of 14.47% for 1/15 and 15.08% for 7/16. It is concluded also that, ideally, 39.3 kWh of energy input is needed per kilogram of hydrogen produced, and that it is sufficient that the hydrogen is stored as compressed gas since it loses energy in liquid form due to the liquefaction process [23].

Hydrogen can be produced using water electrolysis (splitting of water into hydrogen and oxygen) with the aid of electrical energy. Water electrolysis is of three types: solid oxide, alkaline, and particle exchange membrane (PEM) electrolysis [24]. PEM electrolysis is the favorite type of water splitting process because it uses a solid electrolyte membrane that is expected to increase the lifetime of the electrolyzer. The advantages of PEM electrolysis over conventional alkaline electrolysis are that it is simple, cost effective, and sustainable technology for producing and storing hydrogen [25]. Tinoco et al. investigated high temperature electrolysis which is the most efficient and sustainable process for the production of hydrogen. Since it operates in the auto-thermal mode, it does not require a high temperature source for the electrolysis but rather an energy source to supply enough heat to vaporize water. The electrolyzer used in the study is Solid Oxide Electrolysis Cells (SOECs) operating at a temperature over 1023 K. A simplified economic model was used in order to assess

the impact of temperature, pressure, and thermal energy cost of the heat source on the process competitiveness. The results showed that the exothermal mode in the electrolyzer cells (high current density) seemed efficient towards low production cost but in return diminishes the lifespan of the cells leading to high costs for hydrogen production. The study established a hydrogen production cost of $170 per kW electricity produced which certainly shows low production cost but the lifespan of the electrolyzer cells is shortened [14].

With reference to high temperature electrolysis, Shin et al. [26] proposed a study where a very high temperature gas-cooled reactor (VHTR) is coupled with a power cycle and a high temperature steam electrolyzer (HTSE) in a cycle to produce pure hydrogen. The electrochemical thermodynamic properties and overall efficiency of the cycle was calculated in the range of 600-1000 ℃ operating temperature. The overall thermal efficiency of the system was calculated to be around 48% at 1000℃ operating temperature [26]. This thermal efficiency is energy saving compared to the efficiencies of conventional electrolysis (alkaline solution) which is about 27%, showing that HTSE can be two times as energy saving.

Mingyi et al. [27] also performed thermodynamic analysis on the efficiency of high temperature steam electrolysis (HTSE) with a Solid Oxide Fuel Cell (SOFC). HTSE is the primary energy source as well as providing thermal energy to the SOFC, where electrolysis of the high temperature steam takes place producing hydrogen. Electrical efficiency, electrolysis efficiency, thermal efficiency, and overall efficiency of the system were investigated. The temperature increase from 500-1000℃ decreased the overall and electrical efficiencies, while increasing the thermal efficiency. The overall efficiency of the system (HTSE) coupled with a solar reactor was calculated to be 59% more than the conventional alkaline electrolysis systems having 33% [27].

Research all over the world shows several configurations of the system being described to ensure sustainable hydrogen production and higher efficiencies. High temperature solar thermal technologies are available such as parabolic troughs, heliostat fields, and solar dishes. The operating temperature of these technologies is different and depending on the system required, each can be used for the production of hydrogen through thermodynamic systems. Parabolic troughs have an operation temperature range of 60-300℃, solar dishes have a range of 100-500℃, and heliostat fields have a range of 150-2000℃ [5]. Zhang et al. [28] presented a new solar-driven

high temperature steam electrolysis for which energy consumption was studied. The system is composed of a solar concentrating beam splitting system, a Solid Oxide Steam Electrolyzer (SOSE), two heat exchangers, a separator, and storage tanks. Parametric studies were run to investigate the effect of current density with the efficiency of the SOSE, showing that the anode-supported SOSE had the best performance as it has the least electrical energy requirement. Further parametric analysis was done on the effect of operating temperature on the efficiency of the SOSE, resulting in a maximum efficiency at a certain operating temperature. The thermal energy and electrical energy distribution from the solar concentrated beam splitting system was further investigated which is very important in the optimal design of high temperature electrolysis. The balance parameter which is the ratio of the thermal to the electrical energy from the solar collector and the current density, were studied for different operating temperatures. The results showed an increase in the balance parameter with decreasing operating temperature, but the effects are comparatively small at lower and higher current density. It is concluded in this study that the thermal and electrical energy should be distributed reasonably for the optimum operation of the SOSE with the solar concentrated beam splitting system [28].

Several renewable energy sources can be implemented in the design of a hydrogen production system. Dincer and Ratlamwala [29] discussed five renewable energy systems based on hydrogen production systems and published a comparative study showing the advantages and disadvantages in terms of energy efficiency. The first system was the integrated Cu-Cl system with hydrolysis, oxygen production, hydrogen production, and drying. High temperature steam is mixed with $CuCl_2$ to bring out aqueous HCl and solid Cu_2OCl_2 where it is passed through a heat exchanger and then separated into CuCl and oxygen. The CuCl and HCl mixture is then passed to the electrolyzer where the electrical energy converts the mixture into aqueous $CuCl_2$ and H_2. The second system is the integrated HyS system where the temperature of water and sulfuric acid leaving the electrolyzer are increased in the concentrator (heating). The pressure is then brought down in the concentrator (flashing) in order to produce vapor. At the end, sulfur dioxide enters the anode side of the electrolyzer and aqueous sulphuric acid enters the cathode side producing hydrogen, and with the help of the isobutene cycle, further hydrogen is produced. The third system is the

integrated quintuple flash system which utilizes the geothermal steam passing through an expansion valve lowering its pressure and has a saturated mixture state. The mixture is then flashed, separating the steam from water at different states and then the high pressure vapor is expanded in steam turbines producing power that drives the electrolyzer in which water is disassociated into oxygen and hydrogen. The fourth and fifth systems are the same, utilizing solar power such as heliostat fields and photovoltaic collectors to heat up molten salt which exchanges heat to the water in the heat exchanger where steam is produced. The steam is expanded in the two-stage steam turbines before entering the condenser where heat is released to the isobutene cycle. The power produced by the two cycles is then used to drive the pumps and the electrolyzer where hydrogen is produced. The authors carried out energy and exergy analysis on the five systems on the basis of hydrogen production, energy efficiency, sustainability index, and energy required producing L/s of hydrogen. The results showed that ambient conditions do not affect the energy efficiencies for the five systems. The energy efficiency, sustainability index, and energy required to produce L/s hydrogen produced are 59%, 83%, 5.9%, and 16.58 kW, respectively concluding that the first system (Kalina Cu-Cl) cycle is the best [20]. The results are carried out for the heliostat field system with the organic Rankine cycle (ORC) showing an optimized energy and exergy efficiency of 18.74% and 39.55%, and a rate of hydrogen produced of 1571 L/s. In the study, parametric analysis was done to investigate the effect of heliostat fields and solar flux on the energy efficiency, net power, and rate of hydrogen produced. The results were an increase of hydrogen production rate from 0.006 kg/s to 0.063 kg/s when the heliostat field area was increased from 8000 m^2 to 50,000 m^2, and an increase from 0.005 kg/s to 0.018 kg/s when the solar flux was increased from 400 W/m^2 to 1200 W/m^2 [29].

Another study by Ahmadi et al. [30] displays the energy and exergy analysis for hydrogen production by ocean thermal energy conversion (OTEC) coupled with a proton exchange membrane electrolyzer (PEM). The system in this study consists of a flat solar collector, turbine, evaporator, and a PEM electrolyzer. The warm surface seawater is used to evaporate a working fluid (ammonia or freon) driving a turbine to produce electrical power, then to drive the PEM electrolyzer to produce hydrogen. The cycle for power production is an organic Rankine cycle and was used in the energy and exergy analysis. The results of the system's analysis showed an exergy

efficiency of 22.7%. This efficiency and the results show that any increase in solar radiation intensity increases the exergy efficiency and hydrogen production rate. The ambient temperature, on the other hand, decreased the exergy efficiency and sustainability index decreased when below 298 K, but increased the exergy efficiency and sustainability index when above 298 K [30].

Geothermal energy is another renewable source that is implemented in hydrogen production power plants to achieve sustainable development. Yilmaz and Kanoglu proposed a binary geothermal power plant where water is used as the heat source coupled with an organic Rankine cycle with a low boiling temperature working fluid such as isobutane, pentane, and isopentane. The work output from the ORC is used as a means of driving the particle exchange membrane (PEM) electrolyzer and the electrolysis water is preheated using the waste geothermal water. Thermodynamic and parametric analysis was carried out on the binary system to evaluate the performance. The geothermal source considered in the system is at 160 ℃ at a rate of 100 kg/s, and the effect of geothermal water and electrolysis temperatures on the amount of hydrogen produced is studied. The results show 3810 kW power produced at the turbine of the ORC which is all used for the electrolysis process. Electrolysis water is preheated to 80℃ using the waste geothermal water and the hydrogen production rate from the PEM electrolysis is at 0.0340 kg/s with a thermal energy efficiency of the geothermal plant of 11.4% and 45.1% exergy efficiency. Electrolysis process efficiencies are 64% and 61.6%, respectively, accounting for overall system efficiencies of 6.7% energy efficiency and 23.8% exergy efficiency. The parametric analysis results showed the geothermal water and electrolysis temperatures are directly proportional to the amount of hydrogen produced [31].

Moreover, AlZaharani et al. [11] proposed an integrated system for power, hydrogen, and heat production utilizing geothermal energy. The proposed system consisted of a supercritical carbon dioxide Rankine cycle cascaded by an organic Rankine cycle (ORC) coupled with an electrolyzer and heat recovery system. The power output from the Rankine cycle is used to drive the electrolyzer, and the thermal energy output is utilized for space heating. The results of the thermodynamic analysis (energy and exergy analysis) showed the capability of the proposed system to produce 245 kg/h of hydrogen for a net power output of 18.59 MW used in the electrolyzer. The overall energy and exergy efficiencies are 13.37% and 32.27%, respectively with

a total exergetic effectiveness of 43.22%. Also, the results showed that increasing the temperature of the geothermal source led to an increase in the overall exergetic efficiency of the system [11].

Another way of utilizing free solar power is co-generation, where a simple process produces two commodities, electricity and heat, including the use of waste heat from electricity to produce heating. Co-generation systems typically have energy efficiencies in the range of 40-50% [32]. Ahmadi et al. [33] proposed a multigeneration system plant based on an ejector refrigeration cycle and PEM electrolysis including a heat recovery heat generator (HRSG) driven by power from solar energy. The refrigeration cycle in the plant is the organic Rankine cycle (ORC) since solar energy is a low-grade source. The vapor generated in the HRSG is expanded in a turbine to produce power, with a low pressure extraction point driven to a supersonic nozzle and mixed with the exhaust from the turbine to be pre-heated before entering the HRSG. The low pressure and temperature vapor after preheating enters an evaporator providing a cooling effect that is utilized domestically. Some of the power produced is used for domestic use and the rest is used to drive the electrolyzer producing hydrogen. Exergy analysis confirmed that the energy efficiency was increased by about 60% compared to a single generation system, claiming that the system can provide the energy requirements for 1897 houses (214 m^2 living area) and hot water production for 16,928 houses [33].

Ozturk and Dincer [34] similarly performed thermodynamic analysis on a multigeneration plant producing power, heating, cooling, hot water, and hydrogen. The system consisted of four parts namely a Rankine cycle sub-system, organic Rankine cycle sub-system, hydrogen production sub-system, absorption and cooling sub-system, and hydrogen utilization sub-system. The hydrogen production sub-system utilizes high temperature steam electrolysis (HTSE) where power is needed in terms of electricity and thermal heat. The absorption sub-system is used instead of a conventional refrigeration system to utilize surplus heat in the system. The overall thermal energy and exergy efficiency of the system was found to be 52.71% and 57.35%, respectively, having a large amount of heat recovery within the system since the sub-systems efficiencies were lower. The results also showed the largest exergy destructed was in the parabolic trough solar collector of around 17% on average mainly due to the high temperature difference between the working fluid going into

the collector and the surface temperature of the receiver tubes. Finally, parametric analysis showed that the increase in solar flux and collector receiver temperature increased the exergy efficiency [34].

1.6 Methodology

The objective behind this research is to calculate the overall energy and exergy efficiency of the proposed system, net power output from the Rankine cycle, and hydrogen production rate, and carry out parametric analysis to investigate the effect of controlled and uncontrolled variables on the performance of the system. The outline of the research is shown in Figure 9. To carry out the thermodynamic analysis, engineering software will be used making it easier for future adjustments and parametric analysis. The program that will be used is Engineering Equations Solver (EES). EES will be used to utilize the energy and exergy equations of each subsystem, calculating the efficiency, temperatures at each state, power output, and hydrogen production rate. Also, parametric analysis on the system is done to investigate the behavior of each subsystem and the overall system by varying different parameters. The program uses the energy equation listed in the mathematical modeling and then uses the optimization toolbox imbedded to study the effect of varying one parameter on the other. Bar charts and graphs are generated to simulate the results visually.

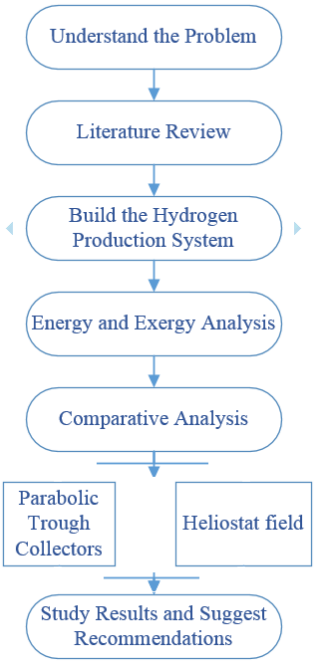

Figure 9: Methodology chart

1.6.1 Phase I: Literature survey.

A literature survey was carried out on the existing hydrogen production systems and the renewable sources used in producing the power required for the production of hydrogen. Also, research was done on the various types of electrolysis processes used in the production of hydrogen to select the most effective method. Finally, more literature reviews were carried out to access the thermodynamic equations that will be used in the energy and exergy analysis.

1.6.2 Phase II: Thermodynamics energy analysis.

Energy analysis will be carried out on the hydrogen production system proposed earlier using the thermodynamic equations listed in the literature. The proposed system can be divided into three main parts to carry out the analysis:

1. Solar Collector(s): For the proposed system, a particular location is needed in order to extract the global solar radiations to be used as an initial assumption for solar energy. The location that will be used is Abu Dhabi (24.43°N, 54.45°E), since the solar radiation in the UAE is very high. The solar radiation for Abu Dhabi is shown in Table 1 below:

Table 1: Global solar radiation in Abu Dhabi [35]

	Global solar radiation (W/m^2)
Highest daily solar radiation	369
Monthly mean solar radiation	290
Highest average one-minute average daily	1041

2. Rankine Cycle: The equations for the Rankine cycle found in thermodynamic books will be used to calculate the power output from the steam turbine, thermal energy and exergetic efficiencies, and the mass flow rate of steam in the cycle.
3. Water Electrolysis: The water splitting technology that will be used is high temperature electrolysis (HTE) since it operates at very high temperatures and takes in thermal input which is cheaper than electrical input. Solid oxide

electrolyzer cells (SOECs) are used because they allow high temperature electrolysis to happen.

1.6.3 Phase III: Comparative analysis.

Energy and exergy analyses will be carried out for three different configurations in the solar collector. The parabolic solar trough and heliostat field will be analyzed differently with the proposed system stating the advantages and disadvantages for using the three collectors. The two different solar collectors which will be compared in terms of performance are shown in Figure 10. This comparative analysis will be a beneficial way to know which collector will be best used for the proposed system.

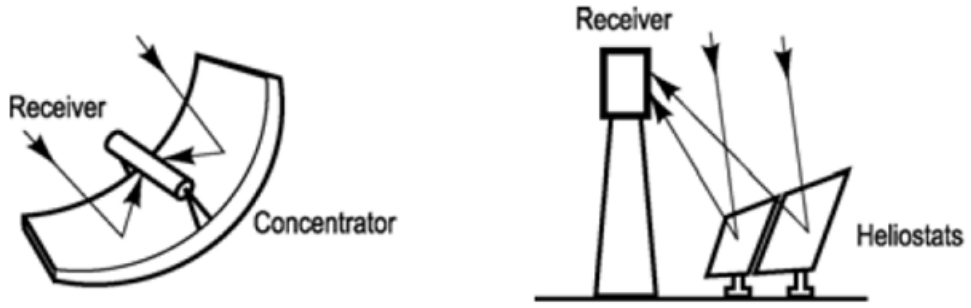

Figure 10: Parabolic trough and heliostat field solar collectors

1.7 Thesis Organization

In this chapter, the effects of increased energy demand, high living standards, and environmental pollution were explained in detail. Moreover, the existing solar collector technologies, Rankine cycle, and hydrogen production systems were discussed and how they can be incorporated together. The expected outcome of this thesis was also discussed. The literature review of existing research papers was also shown, along with a clear objective of the thesis and its significance.

In Chapter 2, the proposed system's schematic and description is shown and discussed with the two solar collectors used. The use of solar collectors with existing steam cycles for the production of hydrogen is also shown. A detailed description of each subsystem is shown as well as the capability of the system to meet the demand as required.

Chapter 3 shows the thermodynamic analysis in terms of energy and exergy equations of each subsystem with its components. Mathematical modeling is done on two different solar collectors (parabolic and heliostat), the steam cycle (Rankine cycle), and the electrolyzer. An overall analysis is performed on the whole system coupled together to determine the efficiencies and hydrogen production rate.

Chapter 4 shows the results of the analysis on each subsystem and the overall system with the parametric analysis done by varying the independent variables to investigate the effects on the performance. The analysis results are shown in terms of simulated graphs and results for a base case scenario. Discussions on the output graphs are shown and optimized results for both overall systems are shown.

Chapter 5 shows a validation on the models being studied with existing cycles in literature. The validation is based on both proposed systems.

Finally, chapter 6 provides a conclusion of the analysis on both systems and recommendations on future analysis of both systems to increase their output and thermal efficiencies. Suggestions for future work on the system are also listed. . There is also a discussion of the research findings.

Chapter 2: System Description

2.1 System Description

Figures 10 and 11 show the schematic diagram of the solar collectors (parabolic trough and heliostat field) integrated with a Rankine cycle. Both of the proposed systems utilize concentrated solar collectors with receivers carrying a heat transfer fluid (HTF), molten salt in the heliostat central receiver, and Therminol VP-1 in the parabolic trough receiver. The molten salt contains 60% $NaNO_3$ and 40% KNO_3 [36]. The first schematic shows the parabolic solar trough coupled with a Rankine cycle with a heat exchanger producing a net power output at the turbine shaft which runs the electrolyzer for hydrogen production. The second schematic differs in the solar collector part where a heliostat field is used to collect the heat from the sun and heat the water in the steam cycle.

The analysis is only based on the energy analysis of the system, and hence the thermal storage subsystem will not be included in the analysis. The overall system can be studied as four subsystems: the solar collector subsystem, thermal heat exchanger, Rankine cycle, and the electrolyzer. The first subsystem will be analyzed using two different solar collectors: the parabolic trough and the heliostat field solar collector. The parabolic trough solar collector reflects the heat coming from the sun (solar flux) using a parabolic-shaped mirror onto a vacuum-sealed pipe where the HTF (Therminol VP-1) is heated up to high temperatures. Similarly, the heliostat field uses several numbers of projected mirrors to reflect the sun's rays onto a central receiver achieving higher temperatures of molten salt. The high temperature heat transfer fluid then passes through the heat exchanger, typically in a counter flow mode, and the heat is transferred to the water in the Rankine cycle where superheated steam is generated. The superheated steam is then expanded in the two-stage steam turbine generating shaft work, which is then converted to electrical power using the electrical generator.

Mathematical modeling for each subsystem is done using equations from the literature. Firstly, thermodynamic analysis is conducted on the solar energy sources. Thermal efficiencies are carried out on the parabolic and heliostat solar collectors using a base case scenario for the variables. Secondly, the Rankine cycle performance is done with the aid of heat absorbed by the heat transfer fluid inside the collector receivers. Thirdly, the analysis on the hydrogen production unit at the electrolyzer is

carried out to determine the rate of hydrogen produced. Lastly, the overall system analysis is carried out using the output from each subsystem to calculate the efficiencies and overall performance. The complete schematic diagrams for both proposed models are shown in Figures 11 and 12.

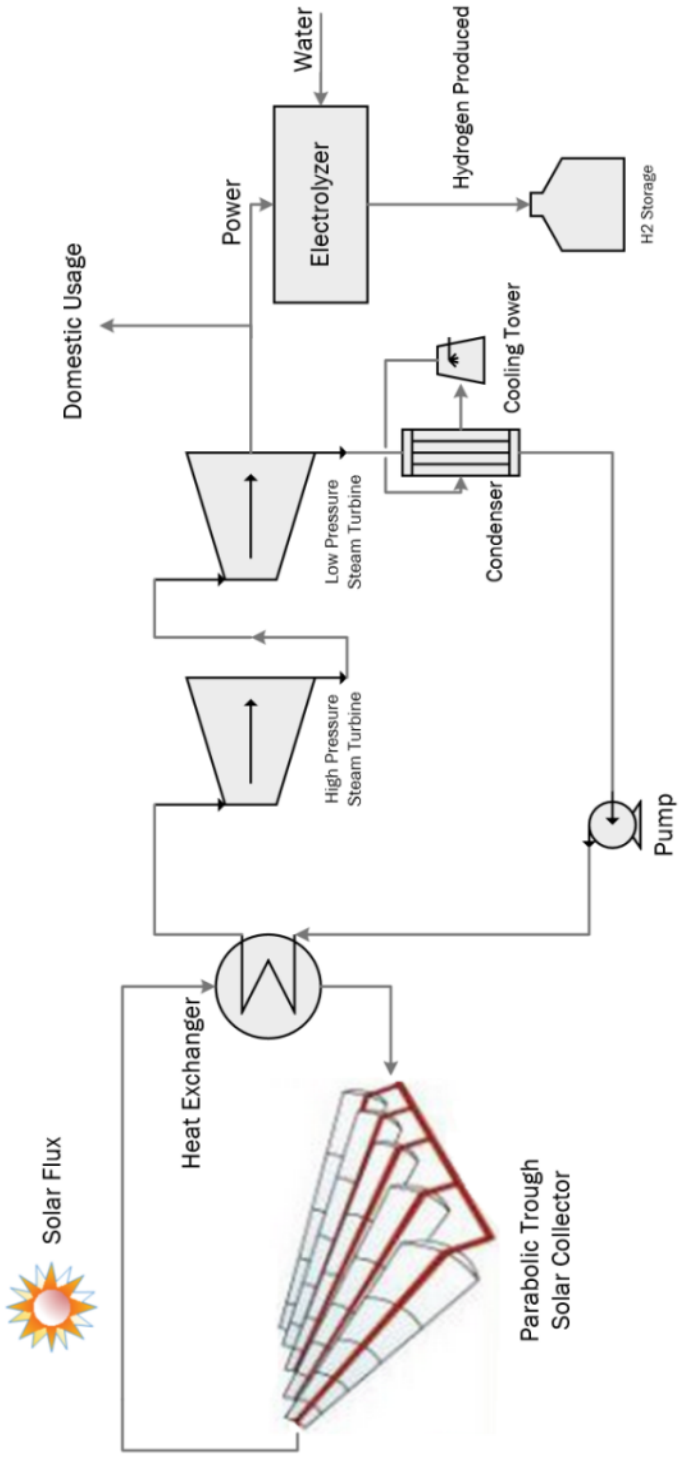

Figure 11: Overall proposed system with parabolic trough solar collector

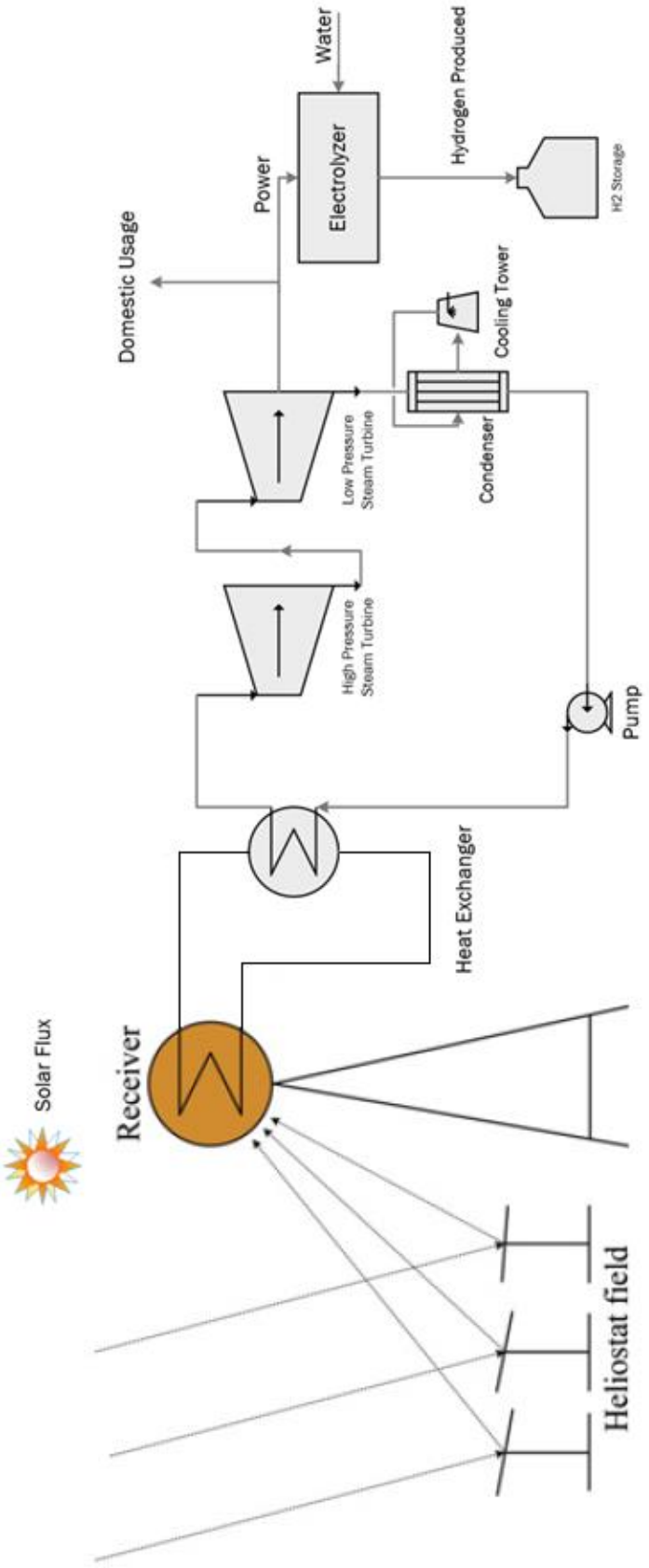

Figure 12: Proposed overall system with heliostat field solar collector

Chapter 3: Thermodynamic Analysis

In this chapter, a thermodynamic analysis in terms of energy and exergy equations is presented for each component in each subsystem. The thermodynamic analysis is shown first for the solar collectors, then for the steam cycle (Rankine cycle) for power production, and then for the SOEC electrolyzer for hydrogen production.

3.1 Solar Energy Sources

Below, the thermodynamic analysis of heat transfer is shown for both parabolic trough and heliostat field collectors as energy analysis of the heat losses and heat absorbed inside each of the receivers. Temperatures of the receiver cover, heat transfer fluid temperature, thermal efficiency, and useful energy in the receiver are shown below. The analysis is carried out in order to have a better understanding of the best collector to use. The efficiency of a solar collector depends mainly on the inlet temperature, outlet temperature, ambient temperature, and wind speeds. The input values for the variables used in the analysis are shown for each solar collector in their respective tables. Other variables like the solar irradiation in the UAE are taken from Table 1.

3.1.1 Energy analysis.

3.1.1.1 Parabolic trough solar collector.

3.1.1.1.1 Energy analysis.

The solar field with the parabolic trough collector type consists of hundreds of solar collector rows, with 10 modules of collectors in each row. Each module has a length of 12.27m and a width of 5.76m [37, 38]. The data for the LS-3 solar collector is found in Table 2. The LS-3 is the most used solar collector in the design of SEGS plants with proven performance. The maximum practical operating temperature of the oil flowing in the receiver has an exit temperature of 663K (39 ℃) [39]. The selected oil is Thermonil-VP1 since it has good heat transfer properties and good temperature control [40]. The mass flow rate of the heat transfer fluid per row is 0.35-0.8 kg/s [41].

Table 2: LS-3 solar collector geometric values [42]

Parameter	**Symbol**	**Values**
Single collector width	w	5.76 m
Single collector length	L	12.27 m
Receiver inner diameter	$D_{r,i}$	0.066 m
Receiver outer diameter	$D_{r,o}$	0.07 m
Cover inner diameter	$D_{c,i}$	0.115 m
Cover outer diameter	$D_{c,o}$	0.121 m
Emittance of the cover	ε_{cv}	0.86
Emittance of the receiver	ε_r	0.15
Reflectance of the mirror	ρ_c	0.94
Intercept factor	γ	0.93
Transmittance of the glass cover	τ	0.96
Absorbance of the receiver	α	0.96
Incidence angle modifier	K_r	1
Number of collector in series	Col_s	10

The mathematical representation of the parabolic collector is shown in this section. The energy analysis is based on the equations presented in [43]. It is assumed that the systems are in steady state with no pressure change.

The collector's useful energy output is defined as:

$$\dot{Q}_u = \dot{m}_r(Cp_{ro}T_{r0} - Cp_{ri}T_{ri}) \tag{2}$$

where $\dot{m}_r$ the mass flow rate in the receiver is, Cp is the specific heat, and T is the temperature. The subscripts ro and ri refer to the receiver's inlet and outlet.

The specific heat of Therminol-VP1 is calculated using equation 2 derived from the experimental measurements in the study [44].

$$Cp = 0.0025T + 1.5497 \tag{3}$$

Also, the useful energy is calculated as shown:

$$\dot{Q}_u = A_{ap}F_R\left(S - \frac{A_r}{A_{ap}}U_L(T_{ri} - T_o)\right) \tag{4}$$

where A_{ap} is the receiver area, F_R is the heat removal factor, S is the heat absorbed by the receiver, and U_L is the solar collector overall heat loss coefficient.

The area of the receiver and cover is the surface area calculated as shown:

$$A_r = \pi D_{r,o}L \tag{5}$$

$$A_c = \pi D_{c,o} L \tag{6}$$

The heat absorbed by the receiver is given below as:

$$S = G_b \eta_r \tag{7}$$

where G_b the direct radiation is heat and η_r is the efficiency of the receiver given by [43].

$$\eta_r = \rho_c \gamma \tau \alpha K_\gamma \tag{8}$$

where ρ_c the reflectance of the mirror is, γ is the intercept factor, τ is the transmittance of the glass cover, α is the absorbance of the receiver, and K_r is the incidence angle modifier.

The aperture area is defined as:

$$A_{ap} = (w - D_{ro})L \tag{9}$$

where L is the collector length, w is the collector width, and D_{co} is the receiver cover outer diameter.

The heat removal factor is defined as:

$$F_R = \frac{\dot{m}_r Cp_r}{A_{r,int} U_L}\left[1 - exp\left(-\frac{A_{r,int} U_L F_1}{\dot{m}_r Cp_r}\right)\right] \tag{10}$$

where $\dot{m}_r$ the mass flow rate in the receiver, Cp_r is the specific heat of the HTF in the receiver calculated at the average temperature between the inlet and outlet, and F_1 is the efficiency factor of the collector defined as:

$$F_1 = \frac{U_o}{U_L} \tag{11}$$

The solar collector heat loss coefficient is given as:

$$U_L = \left[\frac{A_r}{(h_{c,ca} + h_{r,ca})A_c} + \frac{1}{h_{r,cr}}\right]^{-1} \tag{12}$$

where the radiation heat coefficient between ambient conditions and the receiver cover is defined as:

$$h_{r,ca} = \varepsilon_{cv} \sigma (T_c + T_a)(T_c^2 + T_a^2) \tag{13}$$

where ε_{cv} represents the emittance of the cover and σ represents the Stefan-Boltzmann constant equal to ($\sigma = 5.67 \times 10^{-8}\ W/m^2K^4$). The radiation heat coefficient between the receiver and the cover is given as:

$$h_{r,cr} = \frac{\sigma\left(T_c + T_{r,av}\right)\left(T_c^2 + T_{r,av}^2\right)}{\frac{1}{\varepsilon_r} + \frac{A_r}{A_c}\left(\frac{1}{\varepsilon_{cv}} - 1\right)} \tag{14}$$

where ε_r represents the emittance of the receiver and $T_{r,av}$ represents the average temperature between the receiver inlet and outlet. The convection heat loss coefficient between the cover and the ambient conditions is defined as:

$$h_{c,ca} = \left(\frac{Nusk_{air}}{D_{c,o}}\right) \tag{15}$$

where Nus the Nusselt is number and k_{air} is the thermal conductivity of the air.

$$Nus = 0.3Re_a^{0.6} \tag{16}$$

$$Re_a = \frac{V_{air}D_{r,o}}{\upsilon_{air}} \tag{17}$$

The average wind speed in the UAE is estimated at $V_{air} = 4\ m/s$.

The kinematic viscosity of air is given as $\upsilon_{air} = 1.56 \times 10^{-5}\ m^2/s$.

The overall heat coefficient U_o from the surroundings to the fluid is calculated as:

$$U_o = \left[\frac{1}{U_L} + \frac{D_{r,o}}{h_{c,r,in}D_{r,i}} + \left(\frac{D_{r,o}}{2k_r} ln\left(\frac{D_{r,o}}{D_{r,i}}\right)\right)\right]^{-1} \tag{18}$$

The thermal conductivity of the HTF in the receiver (k_r), which is the Therminol-VP1 is given in [40] as $k_r = 0.096\ W/m.K$.

Where $h_{c,r,in}$ the heat loss coefficient between the cover and the receiver is calculated as:

$$h_{c,r,in} = \frac{Nus_r k_r}{D_{r,i}} \tag{19}$$

where Nus_r the Nusselt is number of the HTF in the receiver and k_r is the thermal conductivity of the Therminol-VP1.

$$Nus = 0.3Re_{HTF}^{0.6} \tag{20}$$

$$Re_{HTF} = \frac{V_{HTF} D_{r,i}}{\upsilon_{HTF}} \tag{21}$$

$$V_{HTF} = \frac{\dot{m}_r}{\rho_{HTF} A_{r,cross}} \tag{22}$$

The kinematic viscosity of Therminol at 400 ℃ is given as $\upsilon_{HTF} = 9.9 \times 10^{-7}\ m^2/s$.
The mass flow rate of Therminol-VP1 per row of modules is taken as 0.8 kg/s.
The cross sectional area of the receiver pipe is:

$$A_{r,cross} = \frac{\pi D_{r,i}^2}{4} \tag{23}$$

The temperature of the receiver cover is calculated as:

$$T_c = \frac{h_{r,cr} T_{r,a} + \frac{A_c}{A_r}\left(h_{c,ca} + h_{r,ca}\right) T_0}{h_{r,cr} + \frac{A_c}{A_r}\left(h_{c,ca} + h_{r,ca}\right)} \tag{24}$$

Therefore, the amount of solar radiation that is reflected on the collector and is a heat input into the system is defined by:

$$\dot{Q}_{solar} = A_{ap} F_R SCol_r Col_s \tag{25}$$

where Col_r and Col_s are the total number of solar collector modules in rows and in series, respectively.
The thermal efficiency of the solar collector is therefore written as:

$$\eta_{c,th} = \frac{\dot{Q}_u}{G_b A_{ap}} \tag{26}$$

3.1.1.1.2 Exergy analysis.

Exergy is the measure of the departure of the system's state from the surrounding state, which is the maximum output that the system can produce when interacting with the equilibrium (surrounding) state [45]. The balance of exergy on a control volume is shown as:

$$0 = \sum_j \left(1 - \frac{T_0}{T_j}\right) \dot{Q}_j - \dot{W}_{cv} + \sum_i \dot{m}_i ex_i - \sum_e \dot{m}_e ex_e - \dot{E}x_d \tag{27}$$

where $\dot{E}x_d$, ex, and T are the rate of exergy destructed, exergy per mass flow rate and temperature, respectively. The subscripts i and e refer to the state at the inlet and exit, whereas the subscript 0 refers to the surrounding state.

The exergy per mass flow rate (ex) is given as [45]:

$$ex = (h - h_0) - T_0(s - s_0) + \left(\frac{V^2 - V_0^2}{2}\right) + g(z - z_0) \tag{28}$$

The velocity and elevation components are neglected because their values are very small when compared to the other components. The exergy efficiency is defined as the actual theoretical efficiency divided by the maximum reversible thermal efficiency under the same conditions. The electrical exergy efficiency is calculated as:

$$\eta_{ex,el} = \frac{\dot{W}_{net}}{Ex_{in}} \tag{29}$$

where Ex_{in} is the inlet exergy to the system dependent on the sun's surface temperature (5800 K), which is defined in [46] as:

$$\dot{E}x_{in} = A_{ap,t}G_b\left(1 + \frac{1}{3}\left(\frac{T_o}{T_s}\right)^4 - \frac{4}{3}\left(\frac{T_o}{T_s}\right)\right) \tag{30}$$

The exergetic fuel depletion ratio (Y_d) and irreversibility ration (Y_d^*) are defined in [47]. Also, the improvement potential (IP) of component j in the proposed system is defined as:

$$Y_{d,j} = \frac{Ex_{d,j}}{Ex_{total,in}} \tag{31}$$

$$Y_{d,j}^* = \frac{Ex_{d,j}}{Ex_{D,total}} \tag{32}$$

$$IP = \left(1 - \frac{\eta_{ex,el}}{100}\right) Ex_{d,j} \tag{33}$$

3.1.1.2 Heliostat field solar collector.

For centralized heat production high temperature solar technologies, heliostat fields have an operating temperature range of 150-2000℃ [5]. High temperature solar collectors are important in larger power production and efficiency. The flexibility of

the operating temperatures in a heliostat field is what makes it the best choice for the application at hand. The receiver of the heliostat field is coupled with a heat exchanger with molten salt to transfer the heat to the working fluid of the Rankine cycle (i.e. water). The molten salt is a mixture of 60 wt% $NaNO_3$ and 40 wt% KNO_3 [36].

Density [36]: $\rho = 2090 - 0.636 \times T(℃)$

Specific Heat [36]: $c_p = 1443 + 0.172 \times T(℃)$

Thermal Conductivity [36]: $\lambda = 0.443 + 1.9 \times 10^{-4} \times T(℃)$

Table 3: Properties of the Heliostat Field (adopted from [45])

Parameter	**Symbol**	**Values**
Total heliostat aperture area	A_{field}	10,000 m^2
Central receiver aperture area	$A_{rec,surf}$	12.5 m^2
Heliostat efficiency	η_H	75% [48]
Inlet temperature of molten salt	$T_{ms,in}$	290°C
Outlet temperature of molten salt	$T_{ms,o}$	565°C
View Factor	F_r	0.8
Tube diameter	d	0.019 m
Tube Thickness	-	0.00165 m
Emissivity	ε_w	0.8
Reflectivity	ρ	0.04
Wind Velocity	-	5 m/s
Passes	-	20
Insulation Thickness	δ_{insu}	0.07 m
Concentration Ratio	C	1000

3.1.1.2.1 Energy analysis.

The energy analysis is based on the equations provided in [29] and the heliostat model is based on the model provided in [48].

The rate of heat received by the solar irradiation is calculated as:

$$\dot{Q}_s = I \times A_{field} \tag{34}$$

where I represents the region's solar light intensity and A_{field} represents the area of the heliostat field.

The rate of heat received by the central receiver is:

$$\eta_H = \frac{\dot{Q}_{rec}}{\dot{Q}_s} \tag{35}$$

where η_H the efficiency of the heliostat field is, $\dot{Q}_{rec}$ is the rate of heat received by the central receiver, and $\dot{Q}_s$ is the rate of heat received by solar irradiation.

The central receiver emissivity is defined as:

$$\varepsilon_{avg} = \frac{\varepsilon_w}{\varepsilon_w + (1 - \varepsilon_w)F_r} \tag{36}$$

where ε_w represents the wall's emissivity of the central receiver and F_r represents the view factor.

The temperature of the inner side of the central receiver is:

$$T_{insi} = \frac{T_{rec,surf} + T_0}{2} \tag{37}$$

where $T_{rec,surf}$ represents the temperature of the receiver's surface and T_0 represents the ambient temperature of the surroundings.

The surface area and the aperture area of the central receiver are calculated as:

$$A_{rec,surf} = \frac{A_{field}}{C \times F_r} \tag{38}$$

$$A_{ap} = \frac{A_{field}}{C} \tag{39}$$

where A_{field} represents the area of the collector field, C represents the concentration ratio, and F_r represents the view factor.

The rate of heat loss in the central receiver due to emissivity is defined by:

$$\dot{Q}_{rec,em} = \frac{\varepsilon_{avg} \times \sigma\left(T_{rec,surf}^4 - T_0^4\right)A_{field}}{C} \tag{40}$$

where ε_{avg} represents the central receiver emissivity and σ represents the Stefan-Boltzmann constant.

The rate of heat loss in the central receiver due to reflection is defined by:

$$Q_{rec,ref} = \dot{Q}_{rec} \times \rho \times F_r \tag{41}$$

The rate of heat loss in the central receiver due to convection is defined by:

$$\dot{Q}_{rec,conv} = \frac{\frac{\left(h_{air,fc,insi}\left(T_{rec,surf} - T_0\right) + h_{air,nc,insi}\left(T_{rec,surf} - T_0\right)\right)}{F_r}A_{field}}{C} \tag{42}$$

where $h_{air,fc,insi}$ and $h_{air,nc,insi}$ are the force and natural convective heat transfer coefficients of the inside side of the receiver, respectively.

The convective heat transfer coefficients for natural and forced convection can be determined from the Nusselt number. The natural convection heat coefficient is obtained by the following relation by Siebers and Kraabel [49]:

$$h_{air,nc,insi} = 0.81\left(T_{rec,surf} - T_0\right)^{0.426} \tag{43}$$

The forced convective heat transfer coefficient is calculated from the Nusselt number given below [49]:

$$Nu_{air,fc,insi} = 0.0287 \cdot Re_{air,insi}^{0.8} \cdot Pr_{air,insi}^{\frac{1}{3}} \tag{44}$$

where Re represents the Reynolds number of the air inside the receiver tube and Pr is the Prandtl number. The reference temperature for the air properties calculations is $T_{air,insi} = \frac{T_{rec,surf}+T_0}{2}$, and the characteristic length for the Reynolds number is the height of the receiver. Therefore, the forced convective heat transfer coefficient is calculated from:

$$Nu = \frac{h_{air,fc,insi}L}{k} \tag{45}$$

where L represents the characteristic length and k represents the thermal conductivity of air.

The rate of heat loss in the central receiver due to conduction is defined by:

$$\dot{Q}_{rec,cond} = \frac{\left(T_{rec,surf} - T_0\right)A_{field}}{\left(\frac{\delta_{insu}}{\lambda_{insu}} + \frac{1}{h_{air,o}}\right)(C \times F_r)} \tag{46}$$

where δ_{insu} is the insulation thickness, λ_{insu} is the thermal conductivity of the insulation, and $h_{air,o}$ is the convective heat transfer coefficient of the outside air.

The convective heat transfer coefficient of air is composed of two parts: natural and forced convective coefficients [50].

$$h_{air,o} = h_{air,nc,o} + h_{air,fc,o} \tag{47}$$

The natural convective heat transfer coefficient is calculated as:

$$h_{air,nc,o} = 1.24\left(T_{insu,w} - T_0\right)^{\frac{1}{3}} \tag{48}$$

And the forced convective heat transfer coefficient is calculated from the Nusselt number as:

$$Nu_{air,fc,o} = 0.0239 Re_{air,o}^{0.805} \left(\frac{0.785 T_{insu,w}}{T_0}\right)^{0.2} 1.167 Pr_{air,o}^{0.45} \tag{49}$$

where Re represents the Reynolds number of the air outside and Pr represents the Prandtl number. The reference temperature for the air properties calculations is $T_{air,\mathrm{o}} = \frac{T_{insu,w}+T_0}{2}$, and the characteristic length for the Reynolds number is the inside diameter of the receiver. Therefore, the forced convective heat transfer coefficient is calculated from:

$$Nu = \frac{h_{air,fc,insi} d_i}{k} \tag{50}$$

The rate of heat absorbed by the molten salt passing through the central receiver is:

$$\dot{Q}_{rec,abs} = \dot{m}_{ms} \times c_p \times (T_{ms,o} - T_{ms,in}) \tag{51}$$

where $\dot{m}_{ms}$ is the mass flow rate of the molten salt, c_p is the specific heat capacity of the molten salt, and $T_{ms,o}$ & $T_{ms,in}$ are the temperatures of the molten salt entering and leaving the receiver, respectively.

Therefore, the total heat received by the receiver is calculated as follows:

$$\dot{Q}_{rec} = \dot{Q}_{rec,em} + \dot{Q}_{rec,ref} + \dot{Q}_{rec,conv} + \dot{Q}_{rec,cond} + \dot{Q}_{rec,abs} \tag{52}$$

And the temperature of the central receiver is calculated from:

$$\frac{\dot{Q}_{rec}}{\frac{A_{field}}{F_r C}} = \frac{T_{rec,surf} - T_{ms}}{\frac{d_o}{d_o h_{ms}} + d_o \left(\frac{ln\left(\frac{d_o}{d_i}\right)}{2\lambda_{tube}}\right)} \tag{53}$$

where d_o & d_i both represent the outer and inner diameters of the absorber tube, T_{ms} represents the average temperature of the molten salt, λ_{tube} represents the conductivity of the absorber tube, and h_{ms} represent the convective heat transfer coefficient.

The convective heat transfer coefficient of the molten salt is calculated using the Dittus-Boelter equation, from the Nusselt number as [50]:

$$Nu_{ms} = 0.0239 Re_{ms}^{0.8} Pr_{ms}^{0.4} \tag{54}$$

where Re represents the Reynolds number of the molten salt inside the receiver tube and Pr represents the Prandtl number. The reference temperature for the air properties calculations is $T_{ms} = \frac{T_{ms,o}+T_{ms,i}}{2}$, and the characteristic length for the Reynolds number is the inside diameter of the receiver. Therefore, the forced convective heat transfer coefficient is calculated from:

$$Nu = \frac{h_{ms} d_i}{k} \tag{55}$$

The thermal energy efficiency of receiver is defined as:

$$\eta_{en} = \frac{\dot{Q}_{rec,abs}}{\dot{Q}_{rec}} \tag{56}$$

3.1.1.2.2 Exergy analysis.

Exergy is the measure of the departure of the system's state from the surrounding state, which is the maximum output that the system can produce when interacting with the equilibrium (surrounding) state [45]. The balance of exergy on a control volume is:

$$0 = \sum_j \left(1 - \frac{T_0}{T_j}\right) \dot{Q}_j - \dot{W}_{cv} + \sum_i \dot{m}_i ex_i - \sum_e \dot{m}_e ex_e - \dot{E}x_d \tag{57}$$

where $\dot{E}x_d$, ex, and T are the rate of exergy destructed, exergy per mass flow rate, and temperature, respectively. The subscripts i and e refer to the state at the inlet and exit, whereas the subscript 0 refers to the surrounding state.

The exergy per mass flow rate (ex) is given as [45]:

$$\mathrm{EX} = (\mathrm{H} - \mathrm{H}_0) - \mathrm{T}_0(\mathrm{S} - \mathrm{S}_0) + \left(\frac{\mathrm{V}^2 - \mathrm{V}_0^2}{2}\right) + \mathrm{G}(\mathrm{Z} - \mathrm{Z}_0) \tag{58}$$

The velocity and elevation components are neglected because their values are very small when compared to the other components.

The exergy rate carried by the solar intensity irradiation is calculated as:

$$\dot{E}x_S = \left(1 - \frac{T_0}{T_{SUN}}\right)\dot{Q}_S \tag{59}$$

where T_0,T_{sun}, and $\dot{Q}_s$ are the ambient temperature, the surface temperature of the sun, and the rate of heat received by the solar flux.

The exergy rate carried by the molten salt is calculated as:

$$\dot{E}x_{REC,ABS} = \left(1 - \frac{T_0}{T_{MS,O}}\right)\dot{Q}_{REC,ABS} \tag{60}$$

where $T_{ms,o}$ and $\dot{Q}_{rec,abs}$ are the outlet temperature of the molten salt and the rate of heat absorbed by the molten salt passing through the central receiver.

The exergy efficiency is defined as the actual theoretical efficiency divided by the maximum reversible thermal efficiency under the same conditions is defined as:

$$\eta_{ex} = \frac{\dot{E}x_{rec,abs}}{\dot{E}x_s} \tag{61}$$

3.2 Rankine Cycle

Figure 13 below shows the schematic diagram of a Rankine cycle with two stage steam turbines producing a net power output at the turbine's shaft. The operating pressures of the turbines and the condenser are shown in Table 4 together with the inlet water temperature at the heat exchanger and the mass flow rate of steam.

Table 4: Input parameters for the Rankine cycle analysis

Parameter	**Symbol**	**Values**
Pressure of the first stage turbine	P_3	12.6 [MPa]
Pressure of the second stage turbine	P_4	3.15 [MPa]
Base pressure of the system	P_1	10 [kPa]
Mass flow rate of steam	$\dot{m}_{st}$	1 [kg/s]
Temperature of the subcooled water entering the heat exchanger	T_2	320 [K]

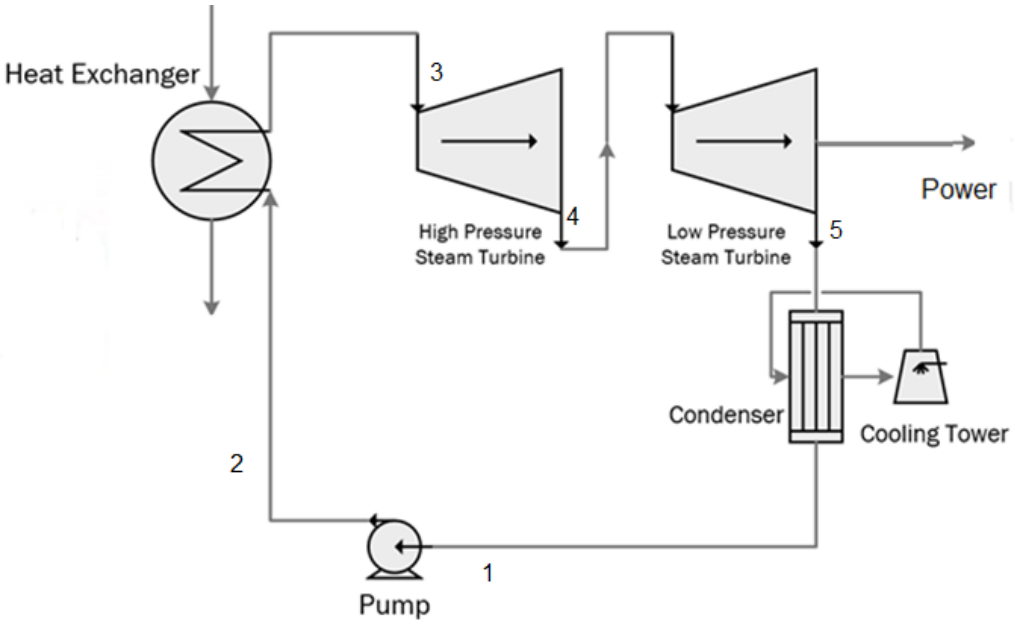

Figure 13: Rankine cycle schematic

Figure 14 shows the T-s diagram of the Rankine cycle above. The isentropic efficiencies of the turbine and pump are 85% and 80%, respectively.

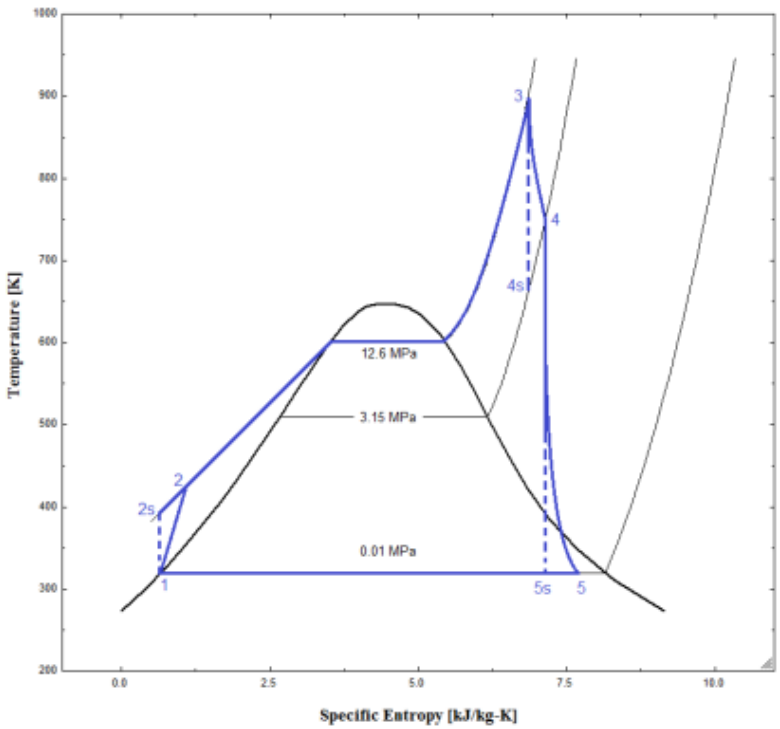

Figure 14: T-s diagram of Rankine cycle

3.2.1 Energy analysis.

This section shows the energy and exergy equations to model the Rankine cycle in the solar power conversion of steam. The equations are adopted from Xu [48].

The power generated by the turbines is calculated as:

$$\dot{W}_{turb} = \dot{m}_{st}(h_3 - h_4) + \dot{m}_{st}(h_4 - h_5) \tag{62}$$

The enthalpies of state 4 and state 5 are calculated from the turbine isentropic efficiencies as:

$$\eta_{turb} = \frac{h_3 - h_4}{h_3 - h_{4s}} \tag{63}$$

$$\eta_{turb} = \frac{h_4 - h_5}{h_4 - h_{5s}} \tag{64}$$

The power needed by the water pump is expressed as:

$$\dot{W}_p = \dot{m}_{st}(h_2 - h_1) \tag{65}$$

The actual power produced from the steam cycle is:

$$\dot{W}_{net} = \dot{W}_{turb} - \dot{W}_p - \dot{W}_{parasitic} \tag{66}$$

The parasitic losses are used for a more realistic model to account for losses occurring in the system. A 10% loss is assumed and calculated as:

$$\dot{W}_{parasitic} = 0.1(\dot{W}_{turb} - \dot{W}_p) \tag{67}$$

The rate of heat rejected by the condenser is calculated as:

$$\dot{Q}_{cond} = \dot{m}_{st}(h_5 - h_1) \tag{68}$$

The exergy carried by the condenser heat is calculated as follows:

$$\dot{E}x_{cond} = \left(1 - \frac{T_0}{T_{cond}}\right)\dot{Q}_{cond} \tag{69}$$

The energy and exergy efficiencies of the steam cycle are defined as:

$$\eta_{en} = \frac{\dot{W}_{net}}{\dot{Q}_{rec,abs}} \tag{70}$$

$$\eta_{ex} = \frac{\dot{W}_{net} + \dot{E}x_{cond}}{\dot{E}x_{rec,abs}} \tag{71}$$

3.3 Electrolyzer

The operation temperature of the SOEC is over 1023 K [13]. The modeling of the process phenomena inside the cell is done using planar rectangular SOECs in order to estimate the electric potential and the energy needs of the cell. This type of modeling is used because of its flexibility, easy-production, and compact characteristics describing the performance. The electrolyzer cell coupled with the Rankine cycle is shown in the figure below as single-celled. An active surface area of 0.04 m^2 is considered, assuming the cells are assembled in stacks making the whole electrolyzer part [14].

The net power output produced by the Rankine cycle is supplied to the electrolyzer. The electrolyzer breaks down the H_2O molecule into hydrogen and oxygen using the electricity supplied from the electrical generator at the turbine output shaft. The hydrogen produced is very pure and can be stored for later purposes. In the next section, the equations used to get the amount of hydrogen produced by the electrolyzer are given. The electrical conversion efficiency of the electrolyzer is taken to be 70% from which the rate of hydrogen produced is calculated. The lower heating value (LHV) of hydrogen is taken to be 191.2 MJ/kg [51].

3.3.1 Energy analysis.

The equations used to calculate the rate of hydrogen produced are presented below. The equations are based on the study in [29].

The rate of hydrogen produced is calculated using the electrical conversion efficiency of the electrolyzer given as:

$$\eta_{electrolyzer} = \frac{\dot{m}_{H_2} LHV}{\dot{W}_{net}} \tag{72}$$

where the efficiency of the electrolyzer is estimated as 70% and the LHV of hydrogen is given in [11] as 191.2 MJ/kg.

3.4 Overall System

The analysis of the whole system is done by combining the analysis of each subsystem shown above. Several assumptions are made while carrying out the analysis to simplify the system and make it easier to carry out the steady state analysis. The assumptions made are:

- System is running at steady state with constant solar isolation.
- Kinetic and potential energies are neglected.
- No pressure drop and heat loss in the pipelines.
- The parasitic efficiency of the whole system is 88%, which is typical for this type of cycle [48].
- The condenser, heat exchanger, and receiver all operate under constant pressure.

Chapter 4: Results and Discussion

In this chapter, the results of the analysis done on EES are represented for each subsystem, namely solar collectors, the Rankine cycle, electrolyzer, and overall system analysis. The results for the base case with the input variables shown in the previous section is shown first, then the parametric analyses showing the effects of several variables are shown.

4.1 Solar Energy Sources

The analysis is shown below for the solar collectors, parabolic trough, and heliostat field. The input variables for each collector are represented in the tables below and the results of the analysis with these variables are shown for a base case study.

4.1.1 Parabolic trough solar collector.

The equations listed above were run into EES (Engineering Equations Solver) with the following input variables shown in Table 5. These input parameters were used to calculate the amount of useful energy input to the Therminol VP-1, surface temperature of the collector, the amount of solar energy considered as heat input to the collector, and the collector's thermal efficiency. The results of the base study are listed in Table 6.

Table 5: Input parameters for analysis of parabolic trough

Parameter	**Symbol**	**Value**
Ambient Temperature	T_0	298.15 K
Solar Irradiation	G_b	$1041\ W/m^2$
Therminol (HTF) density	ρ_{HTF}	1060 kg/m^3 [40]
Stefan-Boltzmann constant	σ	$5.67 \times 10^{-8}\ W/m^2K^4$
Thermal conductivity of air	k_{air}	0.024 W/m K
Thermal conductivity of HTF	k_r	0.096 W/m K [40]
Kinematic viscosity of HTF	υ_{HTF}	$9.9 \times 10^{-7}\ m^2/s$
Receiver mass flow rate	$\dot{m}_r$	0.8 kg/s
Temperature at receiver output	T_{ro}	663 K
Temperature at receiver input	T_{ri}	334 K

The results above are verified with the results obtained in the study [52] and the values are within an acceptable margin of error. The thermal efficiency of the solar collector is acceptable, but the main interest is the overall thermal efficiency of the system when coupled with the Rankine cycle and the electrolyzer. Finally, some

parametric analysis is carried out in EES to investigate the effect of varying the solar intensity in the region, the mass flow rate of the heat transfer fluid inside the receiver, and the temperature at the outlet of the receiver.

Table 6: Results of EES analysis for parabolic trough collector

Parameter	**Symbol**	**Value**
Useful energy input	$\dot{Q}_u$	51.2 kW
Amount of solar radiation	$\dot{Q}_{solar}$	72.7 MW
Temperature of collector	T_c	827 K
Collector thermal efficiency	$\eta_{c,th}$	71.4 %

To follow up, parametric analysis was done to investigate the effect of several variables on the performance of the parabolic trough.

4.1.1.1 Effect of irradiation intensity.

The solar irradiation in Abu Dhabi varies across the day with the peak value $1041\ W/m^2$. Varying this solar intensity is important to study the effect on the useful energy input to the receiver. Figure 15 below shows the effect of the solar intensity on the useful energy input to the receiver. The energy input is linearly increasing as the solar irradiation is increasing; the increase is from 300-1100 W/m^2. The maximum energy input that can be obtained at the collector's receiver is around 55,000 kW for a maximum solar intensity of 1100 W/m^2 which is the peak sun irradiation in Abu Dhabi. At the lowest solar flux of 300 W/m^2, the useful energy rate from the collector is around 15,000 kW which simulates that increasing the solar flux results in higher temperatures of the molten salt at the outlet of the receiver. However, the increase in solar flux doesn't seem to increase the efficiency, as illustrated in the figure below. The efficiency increase is just from 73.1% to 73.7%, a total of 0.6%. This is logical since lowering the solar flux also decreases the useful energy rate from the collector and knowing that the flux is also low, the efficiency will stay the same. These results show that the parabolic trough will capture more energy in high solar intensity times, therefore raising the temperature of the heat transfer fluid, and therefore raising the temperature of the steam in the heat exchanger entering the turbine which will produce more electrical net power output at the turbine when coupled with the collector.

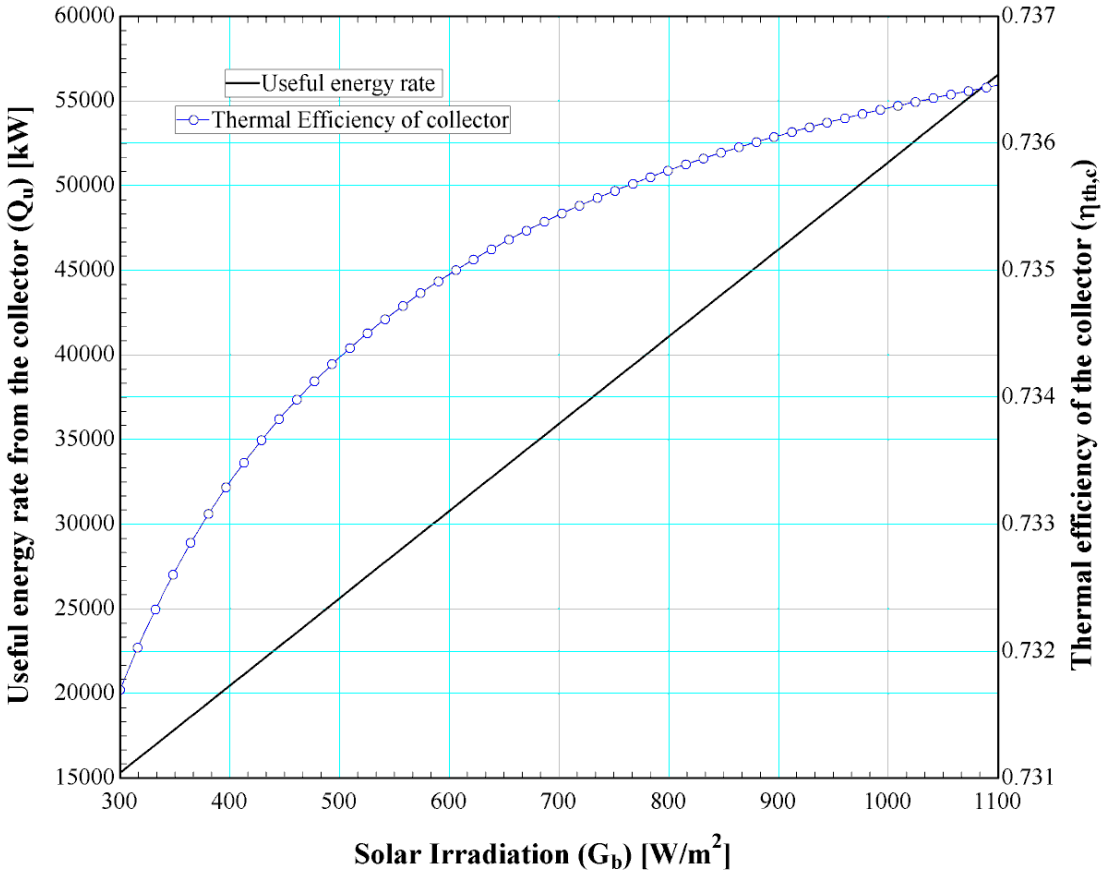

Figure 15: Effect of solar irradiation on the useful energy rate from the collector and the thermal efficiency

4.1.1.2 Effect of HTF mass flow rate.

The receiver of the parabolic trough contains Therminol VP-1, a heat transfer fluid that is used widely in parabolic trough plants because of its good thermal properties. The mass flow rate of this HTF is crucial in the performance of the parabolic solar collector. Increasing the flow rate from 2 to 20 kg/s will result in an increase in both the useful energy rate from the collector and the thermal efficiency. The increase in useful energy rate is from 36,000 to 52,000 kW. This increase will result in an increase in the outlet temperature of the HTF in the receiver since more energy is captured and delivered to the HTF. The thermal efficiency of the collector increases dramatically from 45% to 72% as the mass flow rate increases. Since the solar irradiation here is kept constant but the captured useful energy rate in the collector is increased, the efficiency therefore increases. However, increasing the mass flow rate beyond 20 kg/s will result in keeping the thermal efficiency almost constant at 72%. Also, the useful energy captured will not increase with the further

increase in mass flow rate of more than 20 kg/s, where the captured energy rate is constant at 52,000 kW. It is important to increase the mass flow rate of HTF since it increases both the efficiency of the solar collector and the captured useful energy rate, and therefore will increase the outlet temperature of the HTF and increase the overall efficiency of the system.

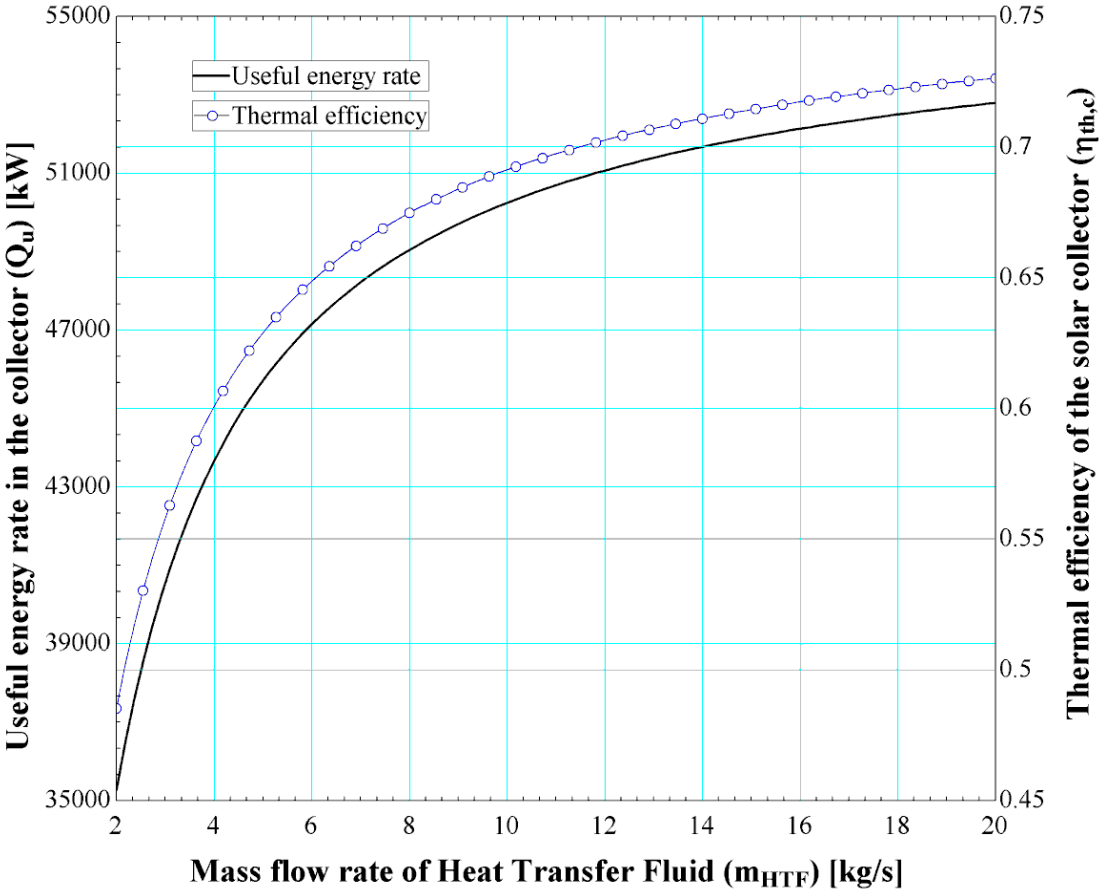

Figure 16: Effect of the mass flow rate of the HTF on the useful energy rate from the collector and the thermal efficiency

4.1.1.3 Effect of total aperture area of the parabolic trough.

The aperture area of the parabolic solar trough represents the geometric properties of the collector. It is the area which the sun's rays shines upon and are then reflected to the receiver pipe. As observed from Figure 17 below, as the aperture is increased from 10 to 100 m^2, the useful energy rate from the collector is increased from around 10,000 to 73,000 kW. This huge increase in the useful energy also increases the outlet temperature of the HTF since heat transfer takes place in the heat exchanger. This case can be observed in reality since increasing the aperture area means the solar flux from the sun is shining upon a larger surface area and hence

more rays are reflected onto the receiver tubes containing the HTF. The increase in the temperature of the HTF means the steam entering the turbine will also have higher temperatures since the HTF exchanges heat to the water, converting it to steam in the heat exchanger. However, the increase in thermal efficiency of the parabolic trough is not huge; the increase is from 70% at 10 m^2 aperture area to 71.5% at 100 m^2 aperture area. The 1.5% increase in thermal efficiency shows that the aperture area has a negligible effect on increasing the thermal efficiency of the parabolic trough, making it less appealing in optimizing the performance of the overall system.

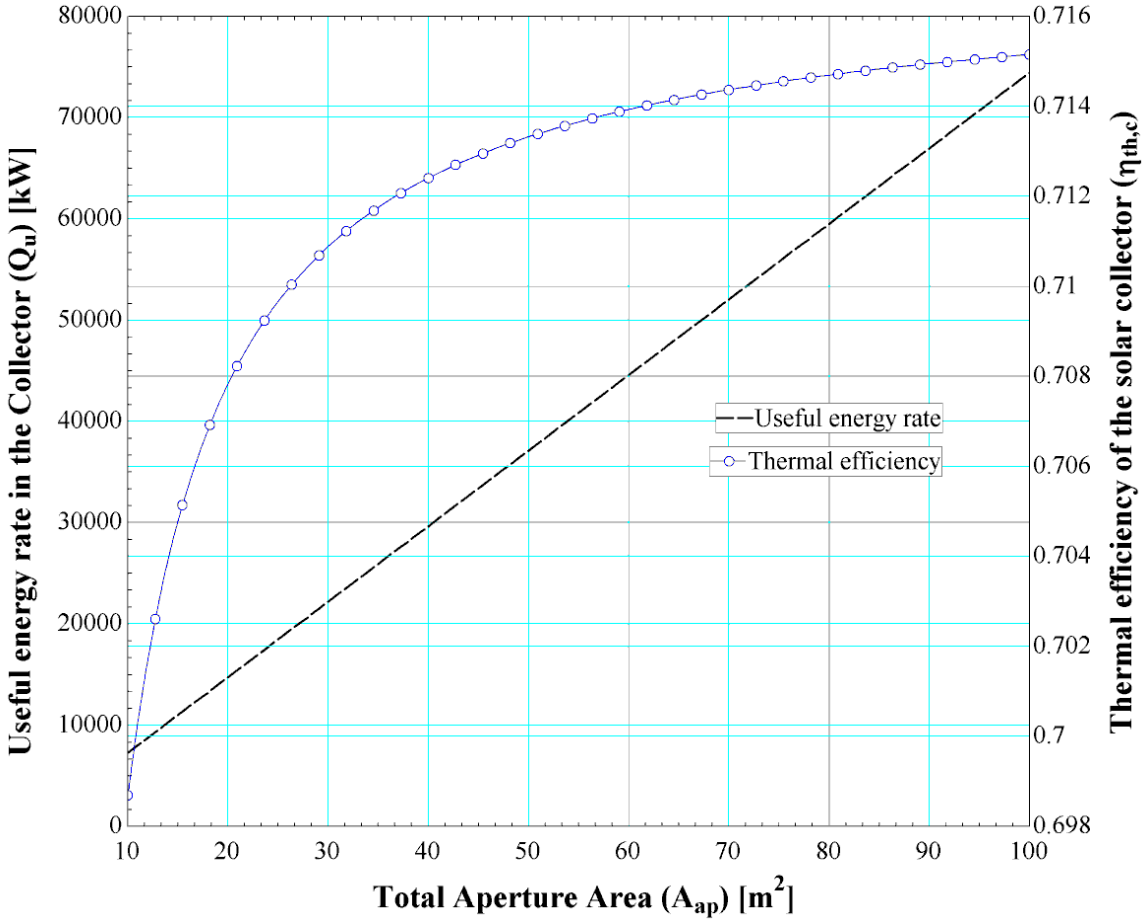

Figure 17: Effect of the total aperture area of the parabolic trough on the useful energy rate from the collector and the thermal efficiency

4.1.2 Heliostat field solar collector.

The equations governing the heliostat field performance were imported into EES for thermodynamic analysis. The input parameters for the heliostat field are shown in Table 7. The base case analysis is done with these input parameters and the results are shown in Table 8.

Table 7: Input parameters for analysis of heliostat field

Parameter	Symbol	Value
Ambient Temperature	T_0	298 K
Ambient Pressure	P_0	101325 Pa
Solar Irradiation	I	1000 W/m^2
Thermal conductivity of Insulation	k_{insu}	0.015 W/m K
Thermal conductivity of tube	k_{tube}	23.9 W/m K
Mass flow rate of molten salt	$\dot{m}_{ms}$	1.5 kg/s
Dynamic viscosity of molten salt	μ_{ms}	0.525 kg/m s
Thermal conductivity of molten salt	k_{ms}	0.5358 W/m k

Table 8: Results of EES analysis for heliostat field collector

Parameter	Symbol	Value
Receiver's Surface Temperature	$T_{rec,surf}$	550 ℃
Total heat received by the receiver	$\dot{Q}_{rec}$	1.38 MW
Energy efficiency of the receiver	$\eta_{en,rec}$	75.6 %

Furthermore, the heat losses in the receiver of the heliostat field are shown in the bar chart below. The types of heat losses were reflective, conductive, emissive, and convective. All of those losses depended on the surface temperature of the receiver which is calculated from the incident heat on the receiver. The incident heat on the receiver depends on the heliostat efficiency of directing solar flux from the sun onto the receiver carrying the molten salt.

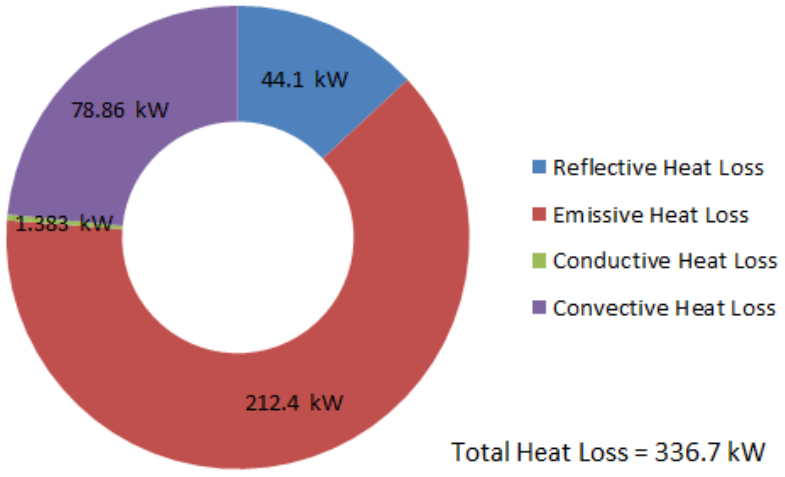

Figure 18: Breakdown of the heat loss in the receiver

Parametric analysis is carried out in EES to investigate the effect of varying the solar flux, outlet temperature of the molten salt, concentration ratio, and the view factor on the energy efficiency of the receiver, total heat loss, and the surface temperature.

4.1.2.1 Effect of incident solar flux.

The effect of varying the solar flux on the performance of the heliostat field is shown in Figure 19 below in terms of thermal efficiency and the receiver's surface temperature. As the solar irradiation is increased from 300 to 1100 W/m^2, the thermal energy efficiency of the heliostat field increases from around 74.8% to 82.6%. The increase in thermal efficiency is mainly due to the fact that more energy is captured and reflected onto the central receiver when the solar intensity is high, therefore increasing the efficiency as observed. The solar intensity in Abu Dhabi varies across the year where it is highest in June and July, assuring high operating efficiency during these two months.

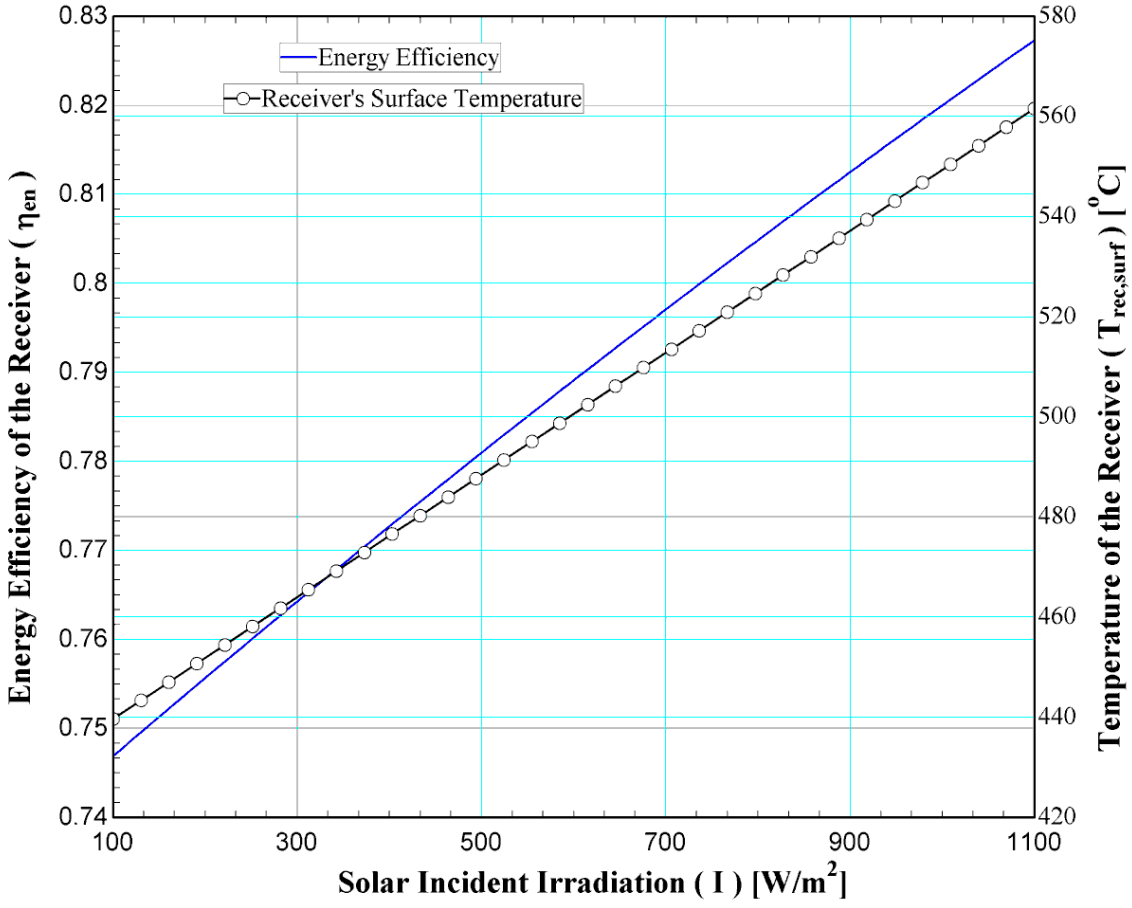

Figure 19: Effect of the solar irradiation on the energy efficiency and surface temperature of the receiver

Moreover, increasing the solar intensity also increases the surface temperature of the central receiver, which is an important factor since the outlet temperature of the molten salt is dependent on it. When the solar intensity is increased from 300 to 1100 W/m^2, the surface temperature of the receiver increases from 440°C to 560°C, a 20% increase in surface temperature. This increase in surface temperature will result in an increase in molten salt temperature. Increasing the outlet temperature of the molten salt will result in higher net electrical power at the Rankine cycle since the temperature of the steam entering the turbine will also increase in the counter flow heat exchanger.

4.1.2.2 Effect of the outlet temperature of the molten salt.

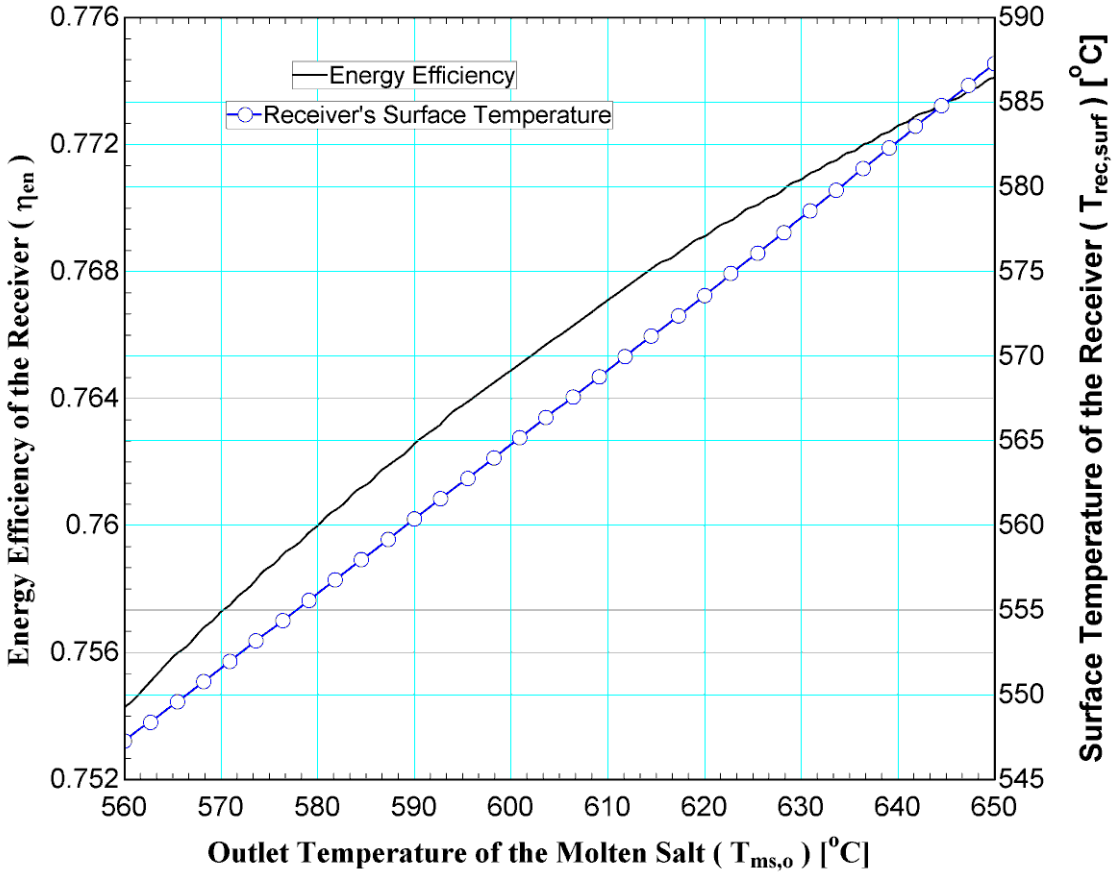

Figure 20: Effect of the outlet temperature of molten salt on the energy efficiency and surface temperature of the receiver

As discussed before, the increase in the surface temperature of the central receiver will result in an increase of the outlet temperature of the molten salt. As shown in Figure 20, the increase of outlet temperature of molten salt will clearly increase the thermal efficiency of the heliostat field. The efficiency of the field at

560°C temperature of molten salt is 75.3% which increases to 77.4% when the temperature is 650°C. The increase in thermal efficiency is very small compared to the huge increase in the salt's temperature; however, the electrical output at the steam turbine in the Rankine cycle will increase and with it the hydrogen production rate will increase. For the outlet temperature of the molten salt to increase, the heliostat field captures more energy which results in lower heat losses. The emissive and convective heat losses contribute to most of the heat losses occurring in the heliostat field, and therefore, this increase in molten salt temperature will lower these heat losses but keep the thermal efficiency nearly the same since the lower heat losses are accounted by higher absorbed heat loss in the receiver by the molten salt.

4.1.2.3 Effect of the concentration ratio.

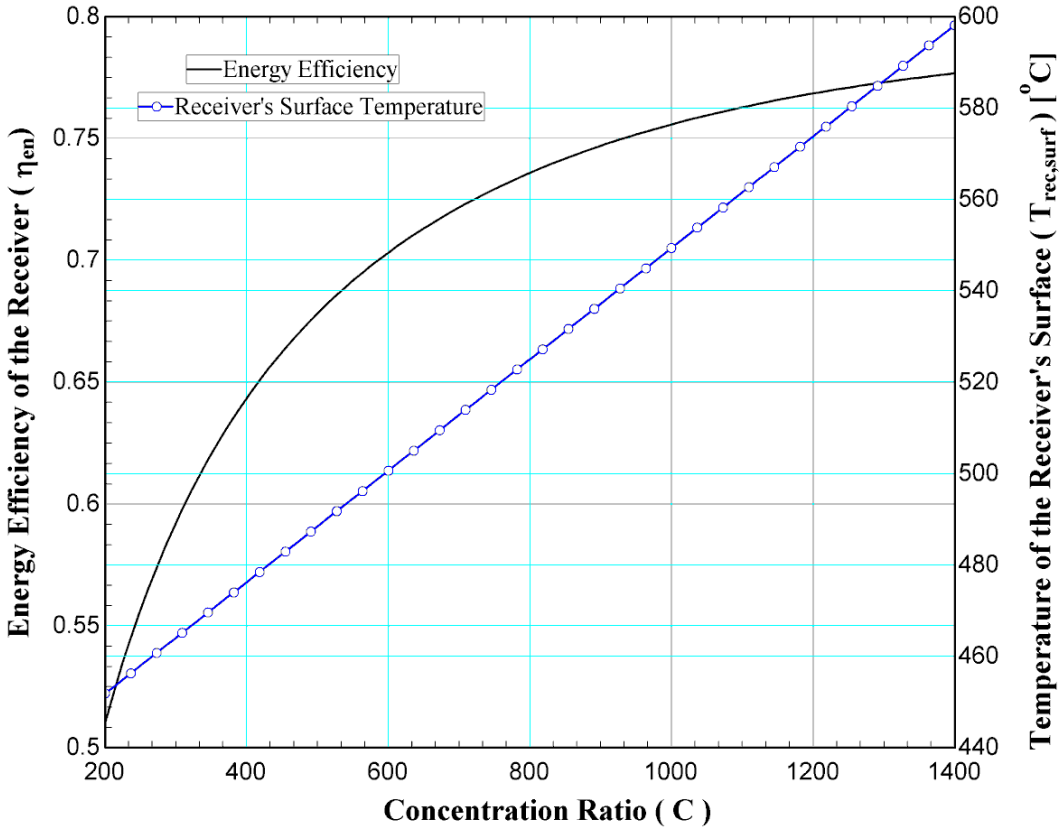

Figure 21: Effect of concentration ratio on the energy efficiency and surface temperature of the receiver

The term "concentration ratio" is used to describe the amount of light energy concentrated over the aperture area by a collector. The increase in concentration ratio will result in an increase in more sun rays concentrated at the mirrors of the heliostat field and reflected onto the central receiver. As the concentration ratio is increased

from 200 to 1400, the thermal efficiency of the heliostat field increases from 51.4% to 78%. This large increase in the thermal efficiency is due to the fact that a high concentration ratio enables the mirrors to concentrate more light energy onto the central receiver, increasing the temperature, and thus increasing the thermal efficiency. However, if the concentration ratio is further increased above 1400, the increase in efficiency will be very small as observed from Figure 21. This is mainly due to the fact that the optical mirrors can concentrate light energy but to a specific geometric limit which results in a very small efficiency increase with the increase in concentration ratio. Moreover, the increase in concentration ratio increases the surface temperature of the central receiver from 445°C to around 600°C which is a very high temperature to heat up the water in the heat exchanger and convert it to steam with very high temperatures (~1000K).

4.1.2.4 Effect of the view factor.

The view factor is a dimensionless number describing the orientation of the reflectors with respect to the central receiver. The higher the view factor, a better orientation and reflection of sun's rays is achieved. Increasing the view factor from 0.1 to 1 increases the thermal efficiency of the heliostat field. The increase in efficiency stops until the view factor is 0.7 and then the efficiency decreases dramatically till reaching a view factor of 1. The increase in efficiency is from 74% to around 77% when the view factor increases from 0.1 to 0.7; then the efficiency decreases rapidly from the maximum at 77% to 63% as the view factor increases slightly from 0.7 to 1. Additionally, the surface temperature of the central receiver increases linearly with the increase in view factor, from 440°C at a view factor of 0.1 to 580°C at a view factor of 1 as shown in Figure 22 below. The increase in surface temperature is very high, a 24% increase in surface temperature from changing the view factor alone. Later, when the overall system analysis is done, an optimization algorithm is carried out in order to maximize the overall thermal efficiency and the amount of hydrogen produced. Keeping the view factor at a value between 0.6-0.8 will result in higher thermal efficiency of the solar collector, which in return increases the efficiency of the overall system.

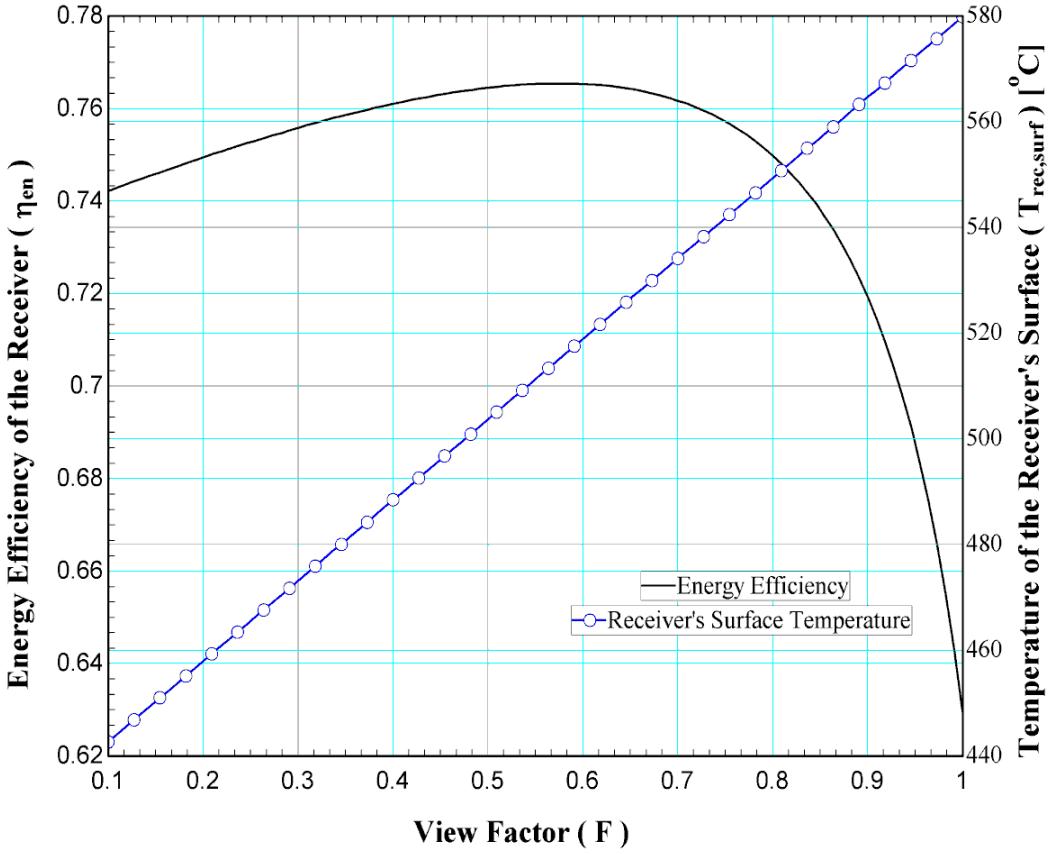

Figure 22: Effect of view factor on the energy efficiency and the surface temperature of the receiver

4.2 Rankine Cycle

The equations were analyzed in EES and the Rankine cycle efficiency and the net power output were calculated for the base case with the constants as shown in Table 9.

Table 9: Input parameters for the Rankine cycle analysis

Parameter	**Symbol**	**Values**
Pressure of the first stage turbine	P_3	12.6 [MPa]
Pressure of the second stage turbine	P_4	3.15 [MPa]
Base pressure of the system	P_1	10 [kPa]
Mass flow rate of steam	$\dot{m}_{st}$	1 [kg/s]
Temperature of the subcooled water entering the heat exchanger	T_2	320 [K]

Thermodynamic analysis was carried out on the power system with the above parameters, and the following state properties define the Rankine cycle performance for both the parabolic trough and heliostat field collectors as solar collectors.

Table 10: State properties in the power cycle with heliostat field collector

State point	Temperature [℃]	Pressure [kPa]	Enthalpy [kJ/kg]
1	45.90	10.000	191.7
2	47.00	12,600	207.0
3	911.0	12,600	4378
4s	619.7	3,150	3726
4	662.4	3,150	3823
5s	45.90	10.000	2422
5	45.90	10.000	2632

Table 11: State properties in the power cycle with parabolic trough collector

State point	Temperature [℃]	Pressure [kPa]	Enthalpy [kJ/kg]
1	45.90	10.000	191.7
2	47.00	12,600	207.1
3	704.4	12,600	3863
4s	449.9	3,150	3342
4	484.6	3,150	3420
5s	45.90	10.000	2270
5	45.90	10.000	2442

After carrying out the analysis for the base case study, the energy efficiency of the Rankine cycle was about 29.14% with a net power output of 972.2 kW including the power consumed by the pump and the parasitic losses assumed. The mass flow rate of steam inside the cycle can be varied, but the optimum value used for the highest efficiency is 1 kg/s. Moreover, the temperature of the subcooled water entering the steam generator heat exchanger can also be varied but a value of 400K was used as an ideal optimum value for the highest net power output and energy efficiency. Parametric analysis was done on the Rankine cycle to test the variation of some parameters on the performance of the cycle. The parametric analysis is shown below with the appropriate graphs.

4.2.1 Effect of molten salt outlet temperature.

The water in the Rankine cycle subsystem is heated up to superheated steam using the heat exchanger to transfer the heat from the molten salt to the water in the steam cycle. The temperature of the molten salt outlet depends on how much energy the receiver absorbed from the heat flux on the solar collectors. By varying the outlet

temperature of the molten salt as shown in Figure 23 below, increasing the temperature led to an increase in both the energy efficiency of the cycle and the net power output.

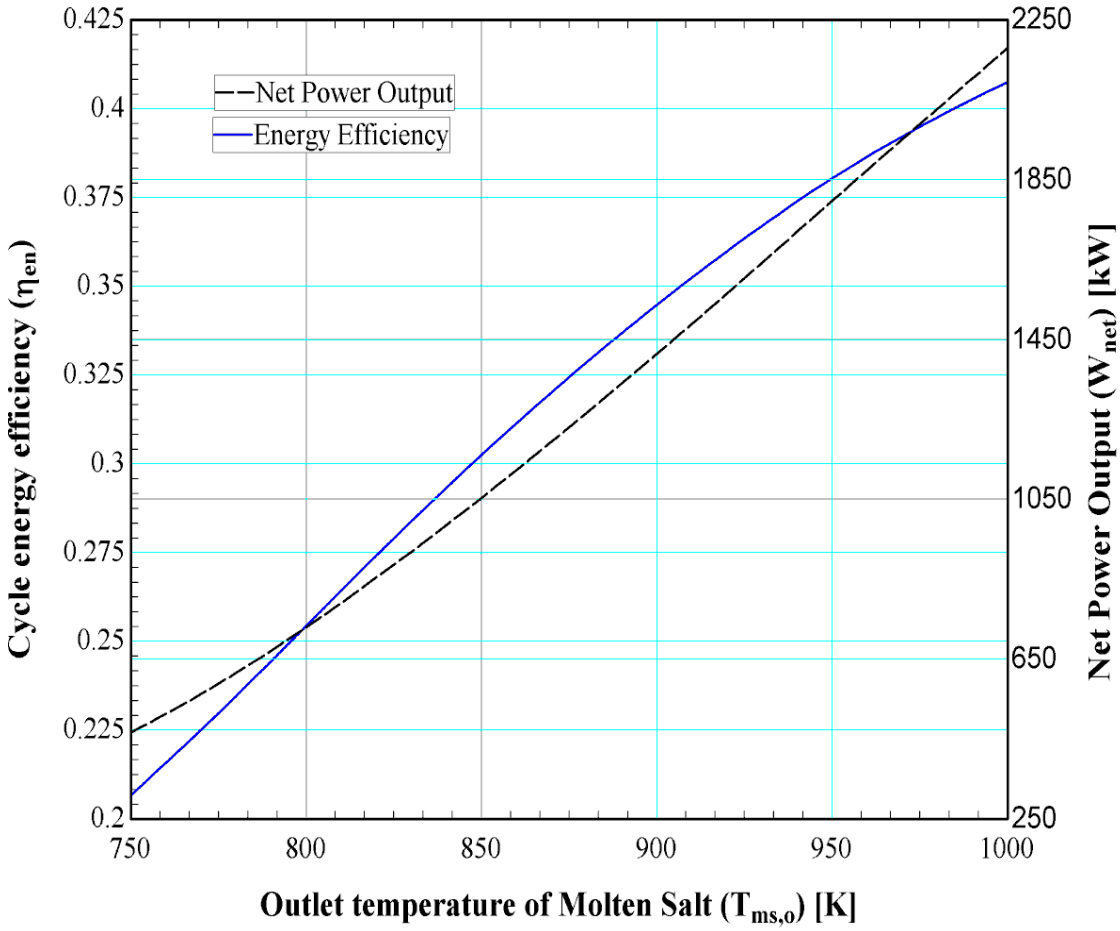

Figure 23: Effect of outlet temperature of molten salt on the energy efficiency and power output of the steam cycle

At 750K, the energy efficiency of the cycle is 21% with a power output of around 550 kW which is considered not good enough. As the temperature increased from 750 to 900K, a linear increase in efficiency to 33% and an increase in net power output to 1300 kW are observed. Knowing this, as the temperature of the molten salt increases, both the efficiency and power output increased, but there is a limit to the increase of the molten salt temperature since the amount of heat that is absorbed by the receiver is not always increasing, and also the pipes inside the heat exchanger cannot withstand high temperatures (>1200K) of fluid or else they may melt.

4.2.2 Effect of subcooled water entering heat exchanger.

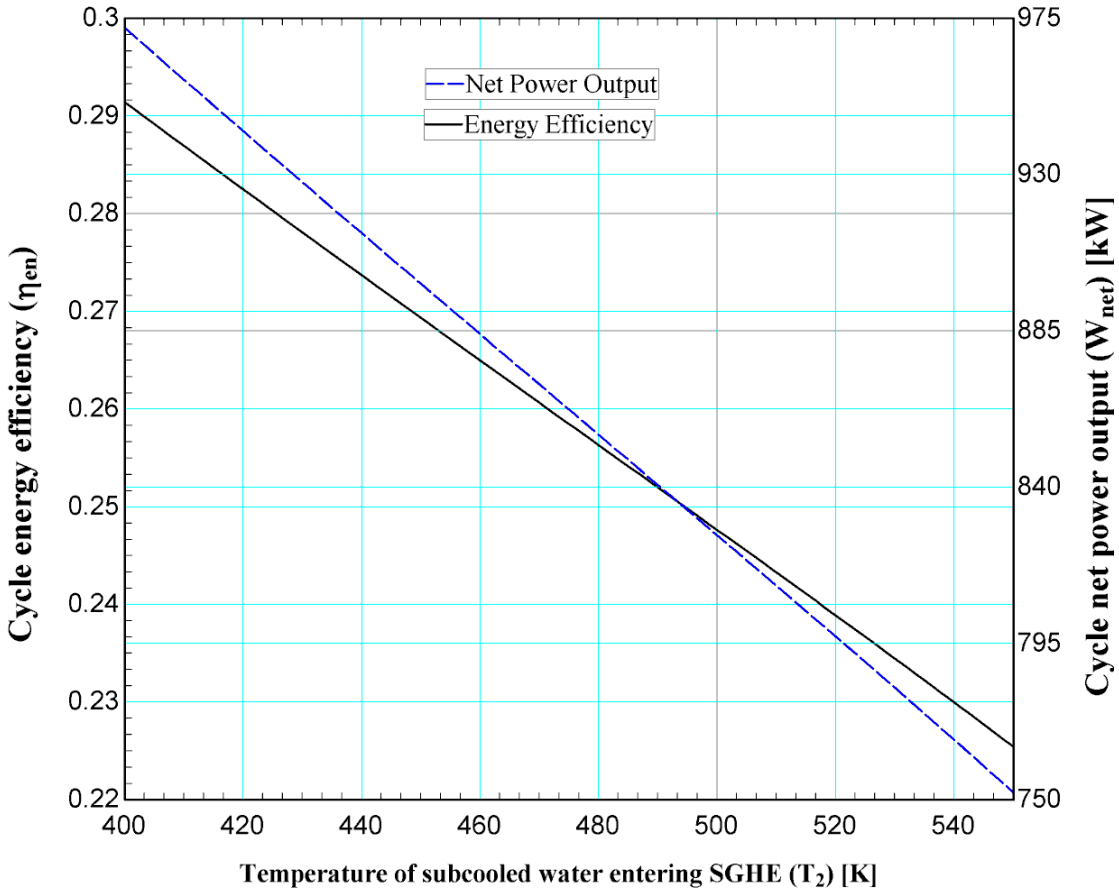

Figure 24: Effect of increasing the temperature of subcooled water on the efficiency and net power output of the cycle

In the Rankine cycle, the subcooled water pumped from the lowest pressure at state 2 is heated to superheated steam at state 3 using the heat exchanger. The temperature of water at state 2 is a design variable that can be set keeping physical limitations in mind. With the increase in temperature, the energy efficiency and net power output decreases as shown in Figure 24. As the temperature is increased from 400K to 500K, the energy efficiency decreases from 29% to 24.5%, as well as a decrease in the net power output from 975 kW to 810 kW. The percentage decrease in the efficiency and power output is not very crucial, but is still considerable. This decrease in efficiency and power output can be translated physically as the temperature at state 3 which is the inlet to the turbine will increase, increasing the turbine output. However, the enthalpy at state 2 is high compared to state 1 and therefore the pumping work is very high compared to the turbine work leading to a decrease in efficiency. As the pumping work is huge, the net power output will also

decrease respectively since the pump is consuming a lot of power from the turbine to pump the water from the pressure at state 1 to the high pressure at state 2.

4.2.3 Effect of steam mass flow rate.

The water in the Rankine cycle goes through different states, from liquid water to superheated steam to saturated liquid-vapor mixture. Figure 25 below shows the relation between the cycle energy efficiency and the mass flow rate of steam. The effect of increasing the mass flow rate of steam in the Rankine cycle is investigated on the cycle efficiency and the net power output. The mass flow rate of steam, measured in kg/s, is the dependent variable and it is changed from 0.4 to 2 kg/s. For the cycle energy efficiency, it has a negative correlation with the mass flow rate of steam. At a mass flow rate of 0.4 kg/s, the cycle efficiency starts at 45% and it decreases till it reaches a value of 15% at a mass flow rate of 2 kg/s. The efficiency shows a sharp decrease at an almost linear behavior until the efficiency reaches 30%, and then decreases in a parabolic behavior. For the net power output, measured in kW, it exhibits a negative correlation with the mass flow rate of steam. It starts at 1500 kW when the mass flow rate is 0.4 kg/s and drops till it reaches 500 kW at a mass flow rate of 2 kg/s, which is a high percentage decrease in net power output (~50% decrease). The net power output decreases rapidly at first with a linear relation until it reaches 900 kW; then the rate of decrease keeps decreasing till it reaches 500 kW. The increase of steam mass flow rate has an effect on both the pumping work and the work output and both turbines. For this reason, increasing the mass flow rate increases the pumping work more than it increases the turbine work output, and therefore, the net power output of the system decreases which leads to the decrease in thermal efficiency of the Rankine cycle as illustrated in the figure below.

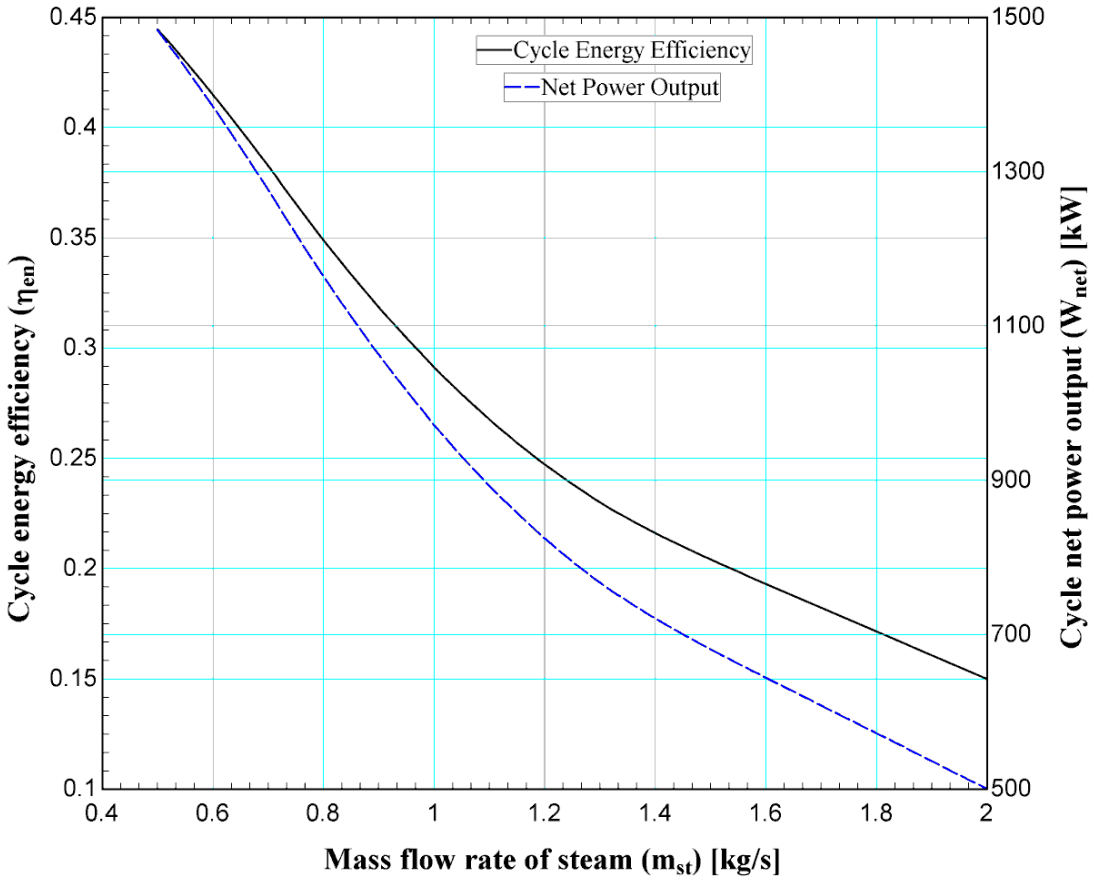

Figure 25: Effect of steam mass flow rate on the cycle efficiency and the net power output

4.3 Electrolyzer

The equation of the electrolyzer is imported into EES together with the other sub-system equations and a value for the rate of hydrogen produced is calculated. Parametric analyses were done to investigate the effects of varying solar flux, heliostat field area and parabolic trough area, mass flow rates of steam and heat transfer fluid (HTF), and temperatures of molten salt and subcooled water inlet on the amount of hydrogen produced.

4.3.1 Effect of solar flux.

The effect of increasing the solar irradiation on the net power output and hydrogen production rate is shown in Figure 26 below. It is clear that a heliostat field will produce a higher hydrogen mass flow rate and more net power output at the steam cycle when compared to the parabolic trough. In the graph, the independent variable is the solar irradiation which is increased from 300 and 1100 W/m^2, leading to an increase in both hydrogen production rate and net power output. The net power

output using the parabolic trough solar collector is almost 900 kW at a solar irradiation value of 300 W/m^2 and it increases linearly to a value of around 1500 kW at a solar irradiation of 1100 W/m^2. The increase in power output is almost 75kW per 100 W/m^2 in solar flux. Moreover, the increase in solar irradiation also increased the hydrogen production rate. At a solar irradiation of 300 W/m^2, the hydrogen mass flow rate is around 0.0533 kg/s, which keeps increasing linearly till it reaches around 0.0883 kg/s at a solar irradiation value of 1100 kW/m^2 using the parabolic trough solar collector.

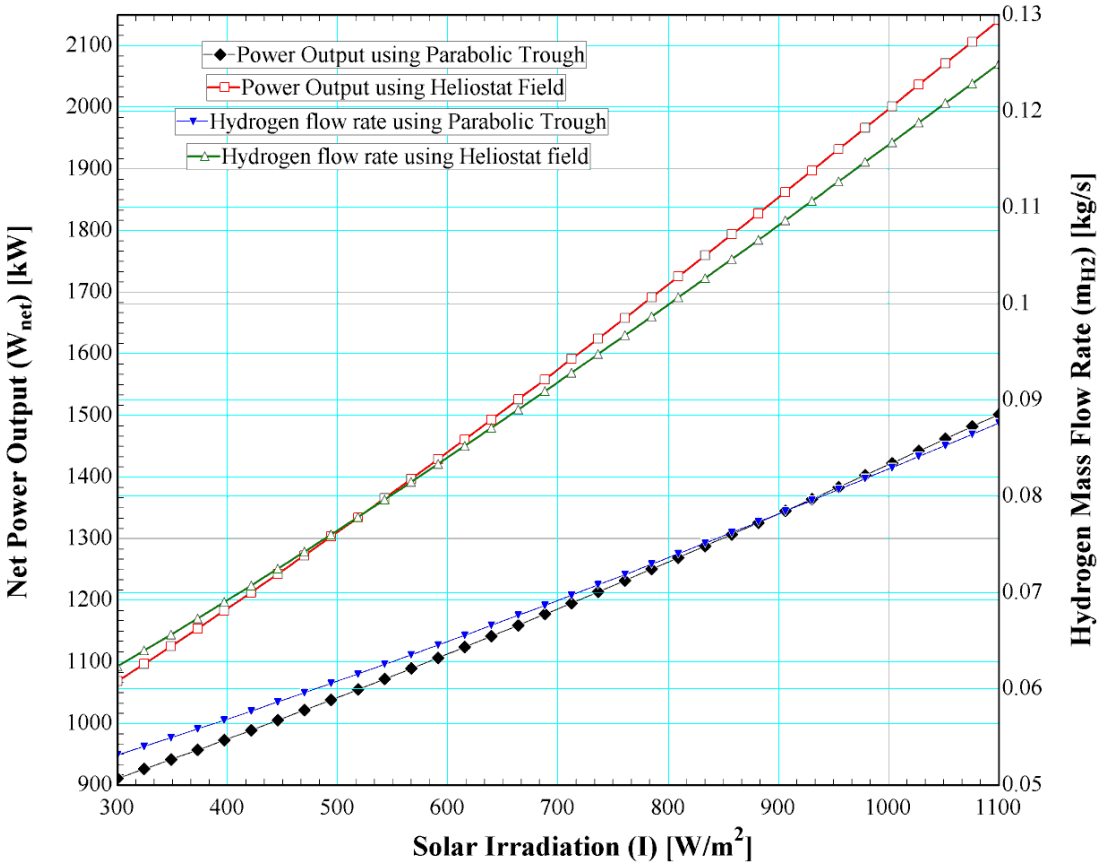

Figure 26: Effect of the solar irradiation on the net power output and the mass flow rate of hydrogen produced

Similarly, using the heliostat field collector also increased both the net power output and the hydrogen production rate when the solar flux increased from 300 to 1100 W/m^2. The net power output is almost 1066 kW when the solar irradiation is equal to 300 W/m^2 and keeps linearly increasing until it reaches 2150 kW at a solar irradiation value of 1100 W/m^2. This means that for every 100 W/m^2 increase in solar irradiation, the net power output increases by 135 kW. As for the hydrogen mass flow

rate, the production rate is around 0.0633 kg/s at solar irradiation of 300 W/m^2, and follows the linear relation till it reaches around 0.125 kg/s at solar irradiation of 1100 W/m^2. The increase in solar irradiation means more energy is captured by both solar collectors and will lead to a greater net power output and hydrogen production. The heliostat field had the higher net power output and hydrogen production since it has higher thermal efficiency and operating temperature when compared to the parabolic trough solar collector.

4.3.2 Effect of subcooled water temperature.

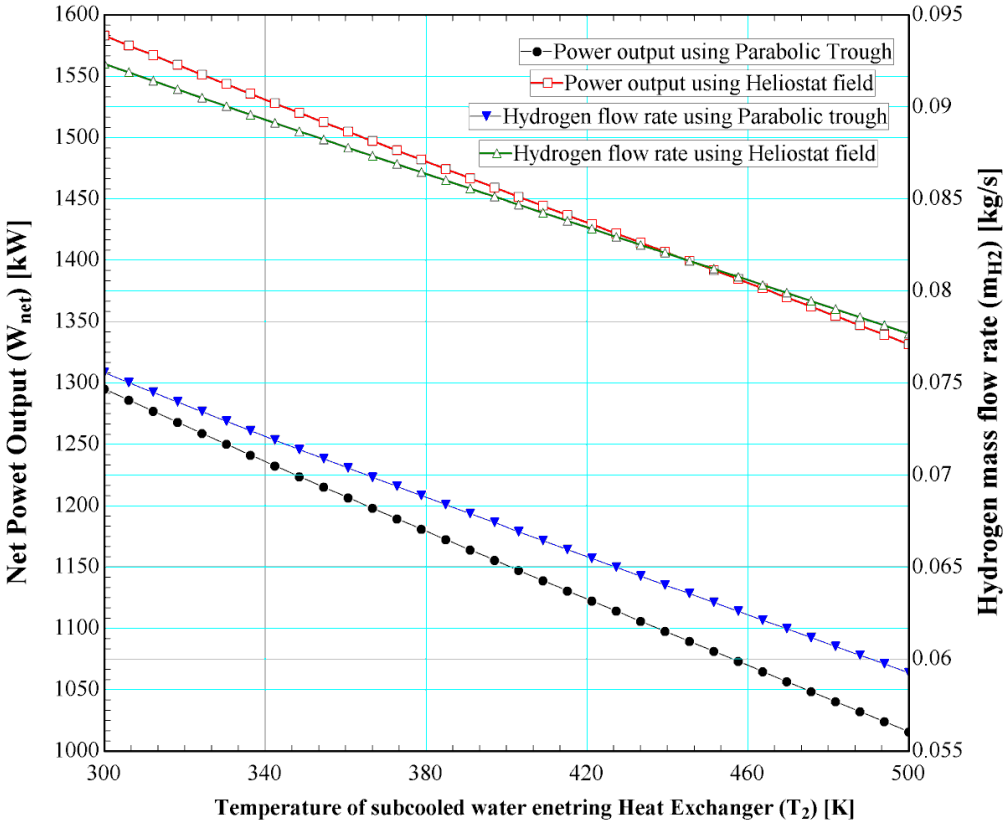

Figure 27: Effect of the temperature of subcooled water in Rankine cycle on the net power output and the mass flow rate of hydrogen produced

The effect of increasing the temperature of the subcooled water in the Rankine cycle is shown in Figure 27 below on the net power output and the rate of hydrogen produced by the electrolyzer. The temperature of the subcooled water is increased from 300 to 500 K, resulting in a decrease in net power output linearly from 1300 kW to 1020 kW using the parabolic trough as the solar collector, and decreasing the net power output from 1570 kW to 1330 kW when using the heliostat field as the solar collector unit. Increasing the temperature of the subcooled water will definitely

increase the pumping work required to raise the pressure from state 1 to state 2, and therefore will decrease the net power output accordingly. As a result, the hydrogen production rate will also decrease when the power output is low as illustrated in the figure below. Moreover, the hydrogen production rate also decreases with the increase in the temperature of the subcooled water as shown in Figure 27. The hydrogen production rate at a temperature of 300 K of subcooled water is around 0.076 kg/s when using the parabolic trough solar collector which decreases as the temperature of the subcooled water is 500 K to 0.058 kg/s. Using the heliostat field collector will yield a hydrogen mass flow rate of 0.093 kg/s at 300 K of subcooled water which decreases to 0.077 kg/s at 500K. The decrease in hydrogen production rate is mainly due to the fact that the net power output decreases with the increase in subcooled water temperature, which in return decreases the hydrogen production rate.

4.3.3 Effect of steam mass flow rate.

In the Rankine cycle, the mass flow rate of steam is very crucial to the performance of the cycle under constant operating temperature. Figure 28 below shows the effect of increasing the mass flow rate of steam on the net power output of the cycle and the hydrogen production rate in the electrolyzer. The mass flow rate increases from 0.4 to 2 kg/s in the Rankine cycle; as a result, the net power output of the cycle decreases from 1800 kW at 0.4 kg/s to 980 kW at 2 kg/s when using the parabolic trough as the solar collector. Also, the net power output decreases when using the heliostat field as the solar collector from 2080 kW at 0.4 kg/s to 1150 kW at 2 kg/s. The decrease in net power output is very rapid for both parabolic and heliostat solar collectors when increasing the mass flow rate from 0.4 to around 1.2 kg/s, since the power output decreases in this region at 400 kW per 0.4 kg/s increase in mass flow rate. After that, as the mass flow rate increases from 1.2 to 2 kg/s, and the decrease in net power output is not significant for both parabolic and heliostat solar collectors. Moreover, the hydrogen production rate also decreases with the increase in steam mass flow rate from 0.4 to 2 kg/s. The hydrogen production rate when using the parabolic solar collector is 0.105 kg/s when the mass flow rate is 0.4 kg/s and then decreases to 0.055 kg/s at a mass flow rate of 2 kg/s. When using the heliostat as the solar collector, the hydrogen production rate is 0.120 kg/s at steam flow rate of 0.4 kg/s and decreases to 0.067 kg/s at a steam flow rate of 2 kg/s. The decrease in

hydrogen production rate is logical since the net power output decreases with the increase in steam flow rate; therefore, the hydrogen production will also decrease as a result.

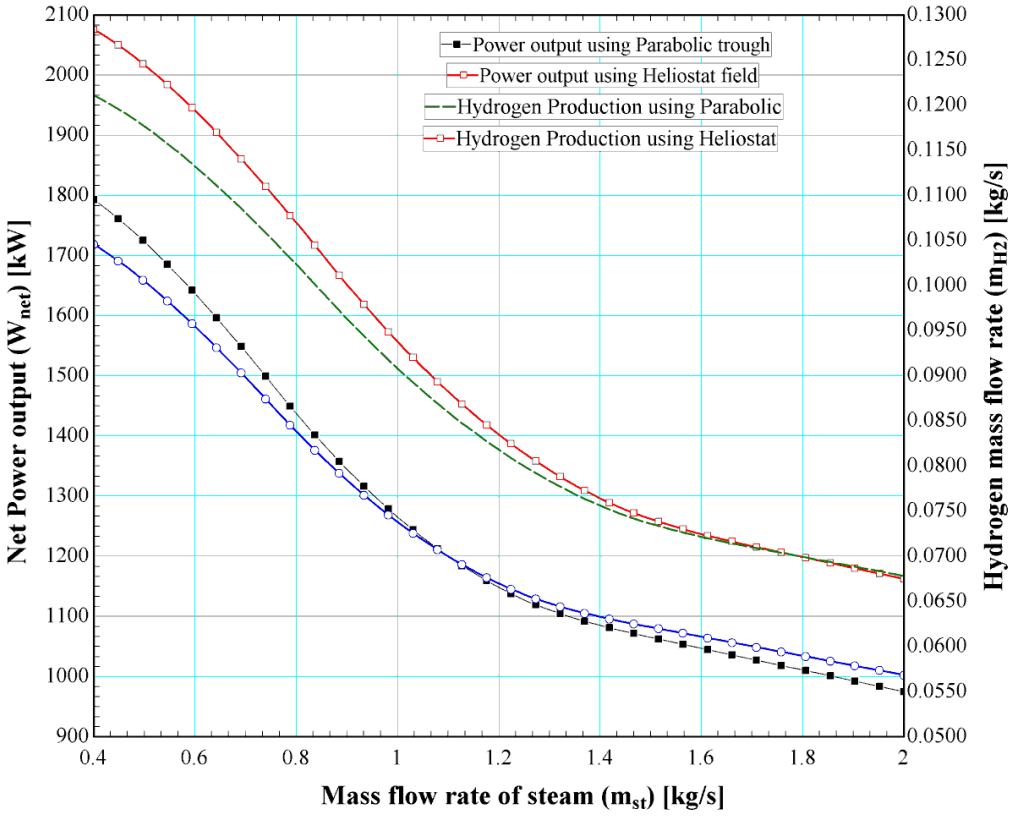

Figure 28: Effect of the steam mass flow rate on the net power output and the mass flow rate of hydrogen produced

4.4 Overall System

The analysis of the overall system is shown below for the two solar collectors: the parabolic trough and the heliostat field. The analysis of the whole system is done by combining the analysis of each subsystem shown above. Several assumptions are made while carrying out the analysis to simplify the system and make it easier to carry out the steady state analysis. The assumptions made are:

- System is running at steady state with constant solar isolation.
- Kinetic and potential energies are neglected.
- No pressure drop and heat loss in the pipelines.
- The parasitic efficiency of the whole system is 88%, which is typical for this type of cycle [48].
- The condenser, heat exchanger, and receiver all operate under constant pressure.

4.4.1 Effect of solar flux.

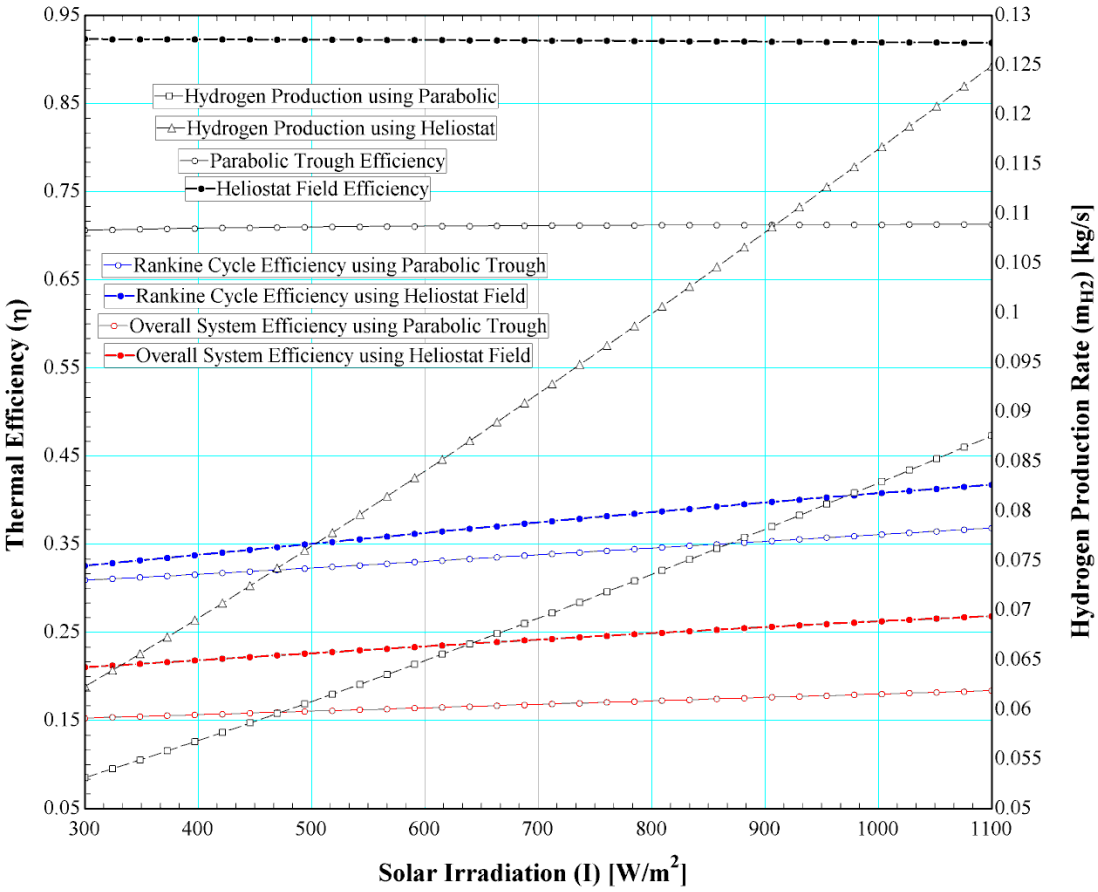

Figure 29: Effect of the solar flux on the thermal efficiency of each subsystem and the overall system and on the rate of hydrogen produced with both parabolic trough and heliostat field collectors

The performance of the overall system when using both parabolic trough and heliostat field solar collectors is studied with the variation of different independent parameters. The variation of solar irradiation on the thermal efficiency of each subsystem and the overall system is shown in Figure 29 above together with the effect on the mass flow rate of hydrogen produced at the electrolyzer. The solar flux is increased from 300 to 1100 W/m^2 at which the thermal efficiency of the parabolic trough very slightly increases from 71% and the heliostat field efficiency also increases marginally from 92%. The thermal efficiency of the Rankine cycle increases from 31 to 37% when using the parabolic trough whereas it increases from 33 to 43% when using the heliostat field solar collector. Additionally, the overall thermal efficiency of the whole system increases from 15% at 300 W/m^2 to 17% at 1100 W/m^2 when using parabolic troughs whereas the overall efficiency increases from

21% to 27% when using the heliostat field solar collector. The increase in overall thermal efficiency is very small due to the fact that increasing the solar irradiation has no effect on the efficiency of the collectors but slightly increases the efficiency of the Rankine cycle because of the increased temperature of the molten salt in the receiver due to high solar incident. On the other hand, since the efficiency of the Rankine cycle increases with the increase in solar flux, the amount of hydrogen produced also increases due to the fact that net power output increases. The increase in hydrogen production rate is from 0.053 kg/s at 300 W/m^2 to 0.087 kg/s at 1100 W/m^2 when using the parabolic trough collector. Using the heliostat field solar collector increases the hydrogen production rate from 0.063 kg/s at 300 W/m^2 to around 0.125 kg/s at 1100 W/m^2. As a result, higher hydrogen production is achieved using the heliostat field, but at the price of higher running and initial costs, since heliostat fields are very sensitive to changes in operation variables and the direction of the sun, unlike parabolic troughs where sun tracking technologies are present and working effectively.

4.4.2 Effect of parabolic trough aperture area.

The effect of the aperture area on the thermal efficiency of the overall efficiency considering each subsystem and the effect on hydrogen production rate when using the parabolic trough is shown in Figure 30 below. Upon increasing the aperture area of the parabolic trough from 10 to 80 m^2, the efficiency of each subsystem increases which leads to an increase in the efficiency of the overall system. The efficiency of the parabolic trough is almost constant with the increase in aperture area as discussed in the analysis of the parabolic trough. However, the efficiency of the Rankine cycle increases slightly from 35% at 10 m^2 aperture area to 40% at 80 m^2 area. This increase in the thermal efficiency of the Rankine cycle leads to an increase in the overall efficiency of the whole system from 16% to 20% with the increase in aperture area. Moreover, the increase of the aperture area from 10 to 80 m^2 leads to an increase in the hydrogen production rate from 0.0775 kg/s at 10 m^2 to 0.086 kg/s at 80 m^2 aperture areas, which is considered a slight but acceptable increase in mass flow rate.

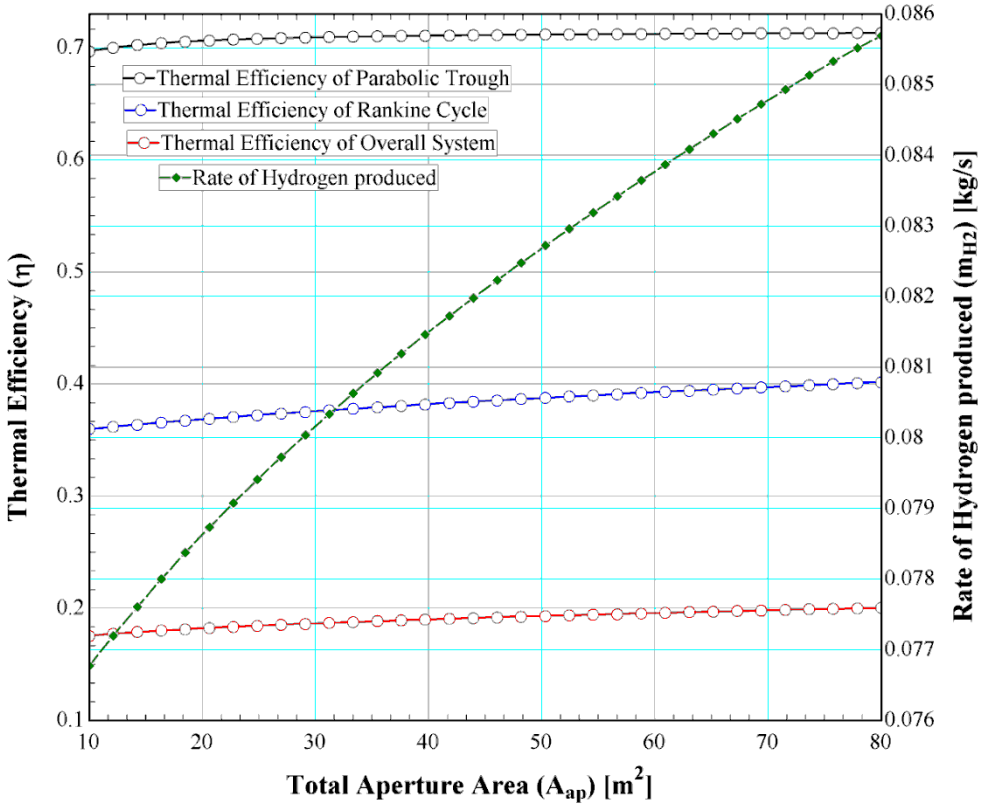

Figure 30: Effect of the parabolic trough aperture area on the thermal efficiency of each subsystem and the overall system and on the rate of hydrogen produced

4.4.3 Effect of molten salt mass flow rate in parabolic trough receiver.

The figure below shows the effect of increasing the mass flow rate of the molten salt in the parabolic trough receiver (HTF) on the thermal efficiency of the whole system considering the overall system and the effect on the hydrogen production rate. As the mass flow rate is increased from 5 kg/s to 15 kg/s, the thermal efficiency of the parabolic trough increases slightly from 68% to 73% which shows the little effect of the mass flow rate on the performance of the parabolic trough. As for the Rankine cycle, the thermal efficiency increases from 29% to 47% at a mass flow rate of 15 kg/s. This is due to the fact that increasing the mass flow rate of the HTF will result in increased inlet temperature at the turbine, since the counter flow heat exchanger enables the heat transfer from the HTF to the water, and increasing either mass flow rates will increase the inlet temperature to the two-stage turbine. The overall system efficiency will therefore increase from 14% at 5 kg/s to 25% at 5 kg/s since more net power output is produced at the turbine in the Rankine cycle, increasing the overall thermal efficiency. The effect on the hydrogen production rate

is illustrated above showing a significant increase from 0.04 kg/s at a 5 kg/s flow rate of HTF to 0.21 kg/s of hydrogen flow rate at 15 kg/s of HTF mass flow rate. The increase in hydrogen production is due to the fact that more net power output is produced by the Rankine cycle; therefore the electrolyzer output will yield higher hydrogen production as a result. Of course, there is a limit to increasing the mass flow rate of the HTF inside the receiver's tube due to material design and heat transfer effectiveness.

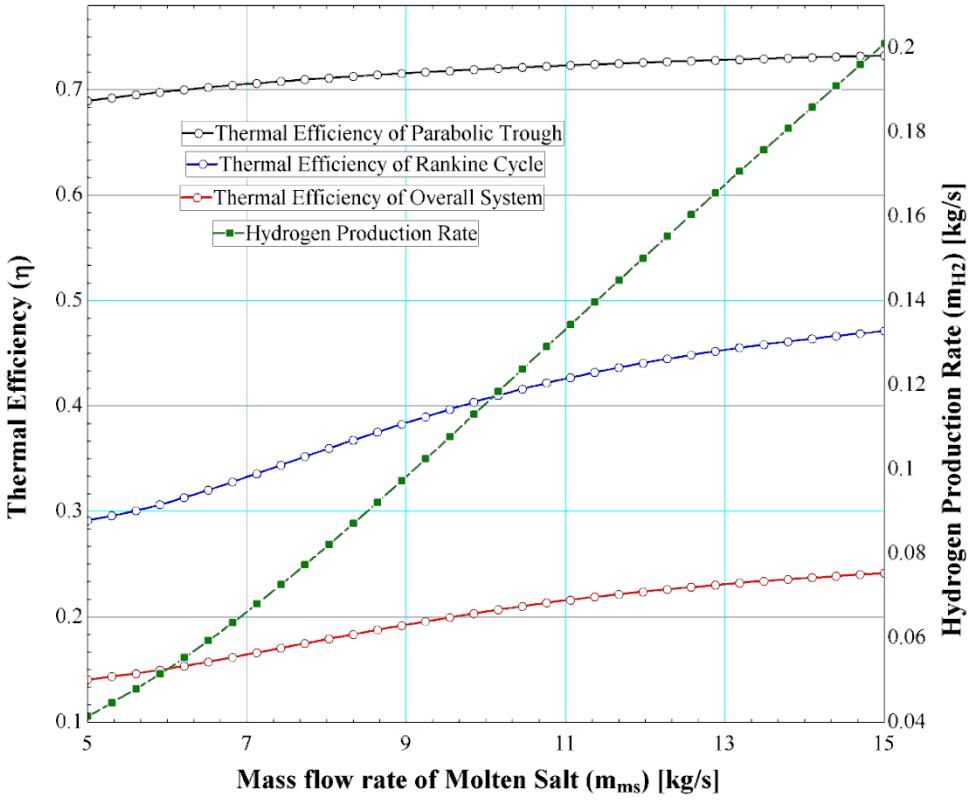

Figure 31: Effect of molten salt mass flow rate in the parabolic trough receiver on the thermal efficiency of each subsystem and the rate of hydrogen produced

4.4.4 Effect of heliostat field area.

The heliostat field area is an independent variable that can be increased or decreased to increase the performance of the overall system. Upon increasing the heliostat field area from 10,000 m^2 to 50,000 m^2, the thermal efficiency of the heliostat field increases from 76% to 92%, which is a significant increase considering the increase in area of the field means more sun rays are reflected onto the central receiver as a percentage of the incoming solar incident, and in return the efficiency is much improved. Increasing the total field area also increases the thermal efficiency of the Rankine cycle but to a negligible amount; the increase is from 35% to 38%. With

that, the overall thermal efficiency of the whole system increases accordingly from 20% at 10,000 m^2 of field area to 23% at 50,000 m^2 of heliostat field area. The increase in hydrogen production is not that significant either as the hydrogen mass flow rate is 0.085 kg/s at 10,000 m^2 and increases to 0.0924 kg/s at 50,000 m^2. The reason is that the heliostat field uses several reflector mirrors to concentrate the solar incident onto one point (central receiver), and increasing the field area, which is increasing the number of reflective mirrors, doesn't increase the temperature of molten salt inside the receiver by a huge amount. This is because a small heliostat field area (10,000 m^2) can reach the operating temperatures of the heliostat collector (1000°C) at the central receiver since it is optimized to reach those temperatures.

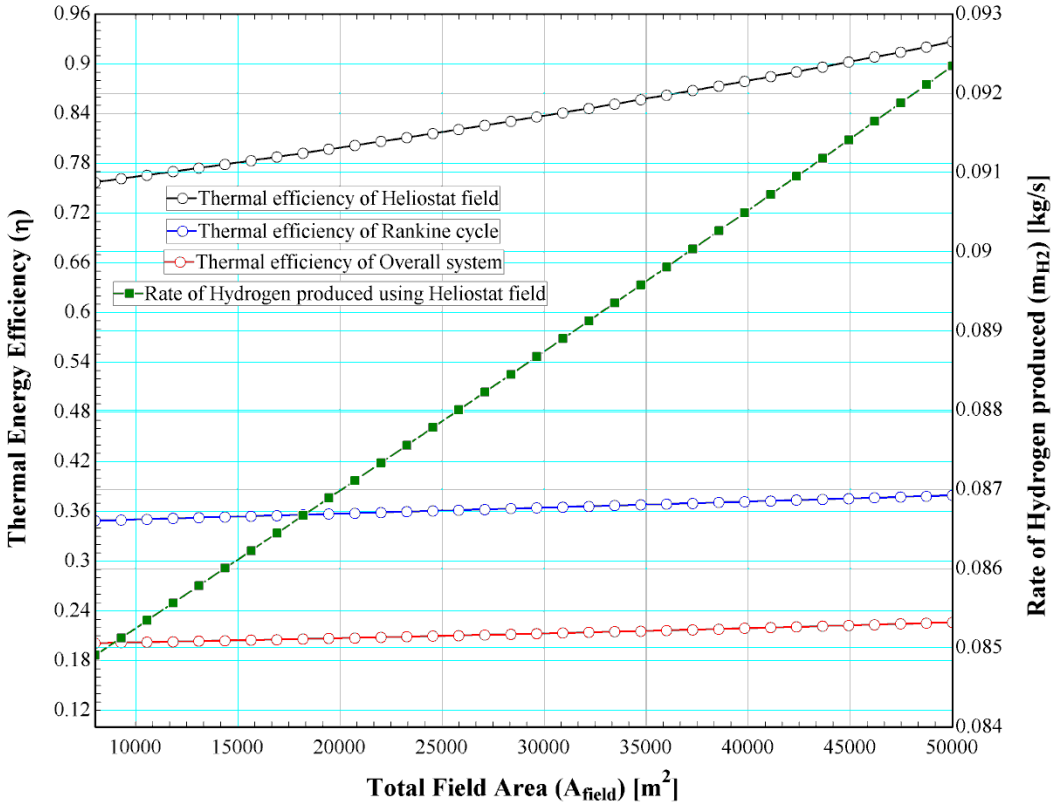

Figure 32: Effect of heliostat field area on the thermal efficiency of each subsystem and the rate of hydrogen produced

4.4.5 Effect of heliostat field concentration ratio.

As discussed before, the concentration ratio describes the concentration of light rays onto the central receiver, if the concentration number is high, then the heliostat field is effective. Increasing the concentration ratio from 300 to 1400 increases the thermal efficiency of the heliostat field from 76% to 92% expectedly

since the mirrors are more effective optically to concentrate the solar incident onto the central receiver of the heliostat field, increasing the heat absorbed by the molten salt, and hence increasing the thermal efficiency. The increase in thermal efficiency of the heliostat field is very rapid when the concentration ratio is increased from 300 to 900 since the efficiency change is 15% as compared to when increasing the concentration ratio from 900 to 1400 where the increase in efficiency is only 2%. The Rankine cycle thermal efficiency also increases from 23% to 41% since the temperature of the molten salt increases with the increase in heat absorption by the receiver which in turn increases the temperature at the turbine inlet when the counter flow heat exchanger dissipates the heat to the water converting it to superheated steam at the turbine inlet. With the increase in temperature at the turbine inlet, the net power output also increases which results in an increase of thermal efficiency of the steam cycle. Additionally, the overall system's thermal efficiency also increases from 12% to 27% when the concentration ratio is increased from 300 to 1400.

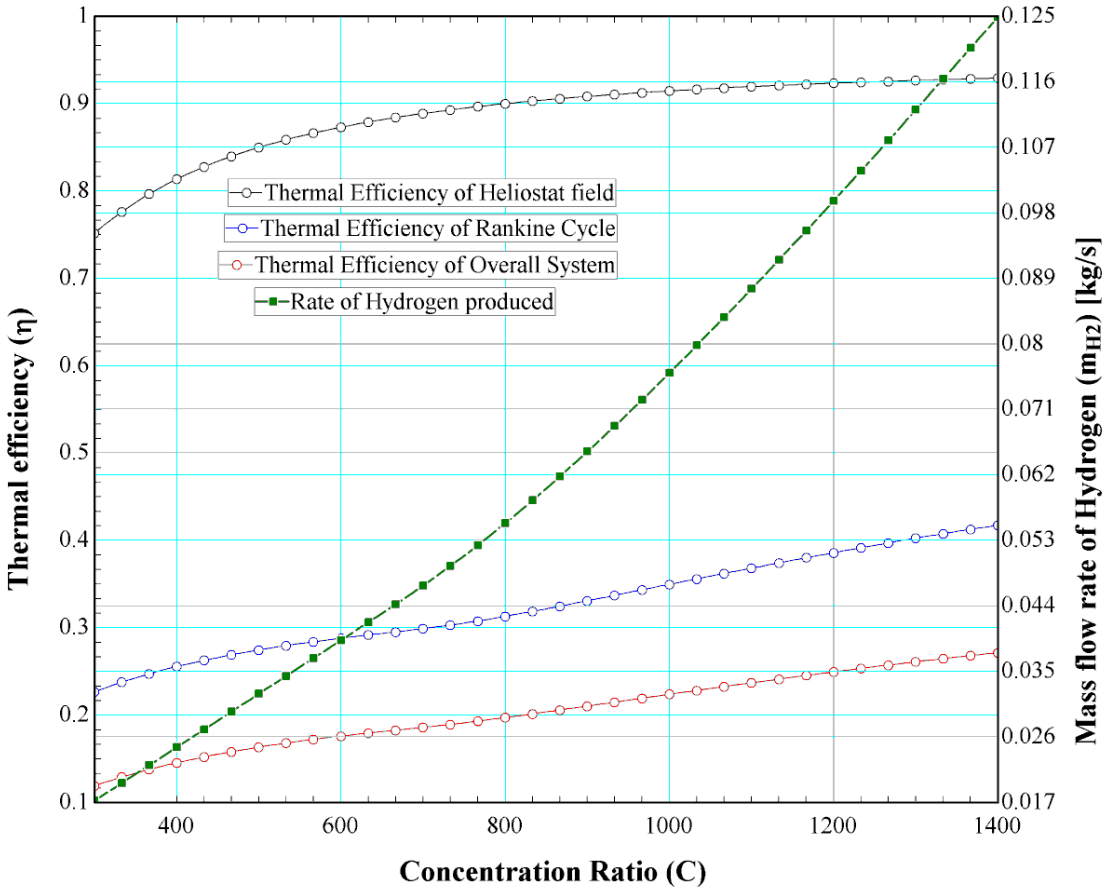

Figure 33: Effect of heliostat field concentration ration on the thermal efficiency of each subsystem and the rate of hydrogen produced

4.4.6 Effect of molten salt outlet temperature in heliostat field.

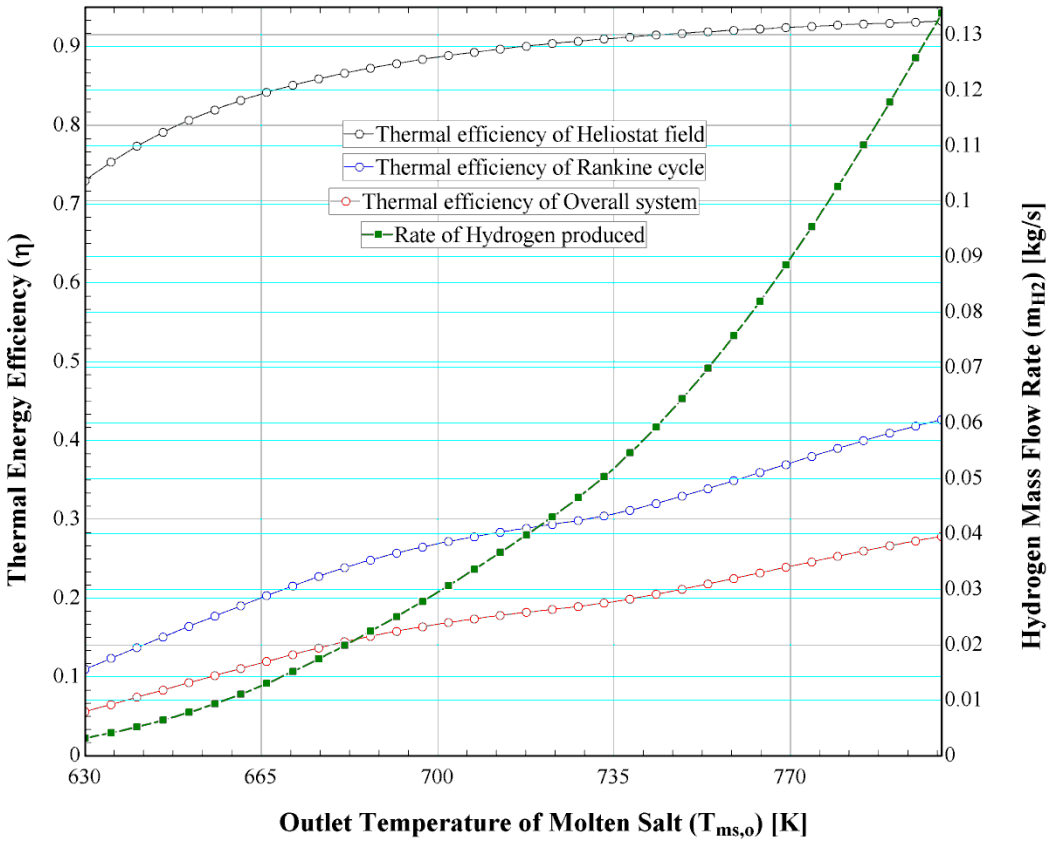

Figure 34: Effect of molten salt outlet temperature in the heliostat field receiver on the thermal efficiency of each subsystem and the rate of hydrogen produced

As seen from Figure 34, the increase in the outlet temperature of the molten salt in the heliostat receiver increases the thermal efficiency of the collector field from 72% at 630 K temperature of molten salt to 92% at 790K molten salt temperature. The increase in thermal efficiency is very rapid when the temperature is increased from 630 to around 710 K, since the increase in efficiency is 18% for an 80 K increase in molten salt temperature. The thermal efficiency of the Rankine cycle also increases from a very low 12% at a temperature of 630K to 40% when a high temperature of around 790 K is achieved. The increase in thermal efficiency of the Rankine cycle is not limited to 790 K since increasing the molten salt temperature further yields a greater increase in efficiency of the Rankine cycle. The maximum temperature of molten salt that can be achieved depends on the other heliostat geometric variables, mass flow rate of molten salt, and the solar flux acting on the field. Later in the optimization section, the best high temperature of molten salt will yield a higher thermal efficiency of the Rankine cycle of more than 40%. With the increase in both

the heliostat field and Rankine cycle efficiencies, the overall system thermal's efficiency also increases from a very low 8% due to the low molten temperature, to 27% at a temperature of 790 K. Higher molten temperatures will result in even higher thermal efficiency for the overall system and hence more hydrogen production at the electrolyzer. The hydrogen production rate also increases accordingly with the increase in molten salt temperature from 0.003 kg/s to 0.135 kg/s. The mass flow rate of hydrogen produced at the higher temperatures can also increase due to the fact that the inlet temperature at the turbine will be high, resulting in more net power output, producing more hydrogen mass flow rate.

4.5 Optimized Results

Tables 12 and 13 show the optimized results for energy efficiency and hydrogen production rate at the electrolyzer. The Direct Search method inside EES is used for the optimization by varying the incident solar flux, turbine pressures, heliostat field area, ambient conditions, mass flow rate of steam, mass flow rate of heat transfer fluid, and molten salt outlet temperature.

The maximum rate of hydrogen produced is 0.3322 kg/s optimized in EES and the highest overall thermal efficiency is 25.35% for the parabolic trough solar collector. On the other hand, the maximum overall thermal efficiency when using the heliostat field is 27% and the maximum hydrogen production rate is 0.411 kg/s.

Table 12: Optimized results for overall thermal efficiency

Parameter	Parabolic Trough Collector	Heliostat Field Collector
I	1100 [W/m^2]	1100 [W/m^2]
A_{ap}	80 [m^2]	A_{field} =50,000 [m^2]
P_2	12 [MPa]	5 [MPa]
P_4	1 [MPa]	4.5 [MPa]
$\dot{m}_s$	0.4 [kg/s]	0.4 [kg/s]
$\dot{m}_{ms}$	7.4 [kg/s]	7.4 [kg/s]
$T_{ms,i}$	300 [K]	400 [K]
$T_{ms,o}$	800 [K]	980 [K]
$\boldsymbol{\eta_{overall}}$	25.35 %	27 %

Table 13: Optimized results for the amount of hydrogen produced

Parameter	Parabolic Trough Collector	Heliostat Field Collector
I	804 [W/m^2]	1000 [W/m^2]
A_{ap}	53 [m^2]	A_{field} =50,000 [m^2]
P_2	12 [MPa]	12 [MPa]
P_4	1 [MPa]	1 [MPa]
$\dot{m}_s$	0.756 [kg/s]	0.8 [kg/s]
$\dot{m}_{ms}$	15 [kg/s]	10 [kg/s]
$T_{ms,i}$	300 [K]	300 [K]
$T_{ms,o}$	800 [K]	1000 [K]
$\mathbf{m_{H2}}$	0.3322 [kg/s]	0.411 [kg/s]

4.6 Economic Analysis

Preliminarily cost analysis is done on both thermal power plants to estimate the cost of electricity based on the solar advisor model (SAM). SAM is a full-year cost analysis developed by the National Renewable Energy Laboratory (NREL) to help solar stakeholders in assessing the cost of concentrating solar power electricity generation systems [53]. The cost analysis is carried out for parabolic troughs and heliostat fields for total installed cost and cost of electricity. Several financial assumptions are maintained for the analysis. These assumptions include a 30-year analysis period, an inflation rate of 2.5%, and a composite income tax rate of 40% [53].

Table 14: Cost analysis of parabolic and heliostat power plants

	Parabolic Trough Plant	**Heliostat Field Plant**
Design Inputs		
Turbine kWe (gross/net)	1265	2000
Heat Transfer Fluid	Therminol-VP1	Molten Salt
Solar Field Temperature (K)	663	838
Solar Multiple	1.3	1.8
Thermal Storage Hours	-	-
Cost & Performance Inputs		
System Availability	94%	91%
Turbine Efficiency	33%	40%
Collector Reflectance	0.94	0.95
Solar Field ($/m^2)	295	200
Power Block ($/kWe-gross)	940	1140
Operation and Maintenance (O&M) ($/kW-yr)	70	65
Cost & Performance outputs		
Total Installed Costs ($/kW)	4,982	8,879
Installed Cost ($/W)	4.6	6.3
Cost of Electricity ($/kWh)	3.76	5.12
Cost of Hydrogen ($/kg$H_2$-day)	238.63	415.25

Firstly, SAM was used to estimate the cost of the parabolic trough technology. As mentioned before, the solar power plant is the LS-3 plant with Therminol VP-1 as the heat transfer fluid. The solar field outlet temperature is 663K. The design parameters of the collector are shown in Table 2. The design inputs together with cost and performance inputs and outputs are shown in Table 14. An estimate for the cost of

electricity is then generated, and the cost of hydrogen production per kilogram is estimated [54]. Secondly, a similar analysis is done on the heliostat field plant to estimate the cost of hydrogen produced using SAM. Inside the SAM software, the location, plant characteristics, and power cycle are chosen from a variety listed in the program. All the geometric and technical data for the proposed systems are used as inputs and the localized cost of electricity values are generated. This LCOE is then used to estimate a value for the cost of hydrogen production per kilogram a day. The economic analysis shows a higher cost of hydrogen production per day when using the heliostat field power plant coupled with the electrolyzer. 1 kg of hydrogen produced comes at a cost of USD 415.25 per day whilst costing USD 238.63 when utilizing the parabolic trough plant.

4.7 Performance Comparison

Table 15 shows a comparison between the Rankine cycle used in this research with the Brayton cycle and the reheat-regenerative Rankine cycle. The comparison is shown in terms of the cycle net power output using a concentrating parabolic trough collector as the input to the system. The first system is a simple Brayton cycle using air as the working fluid. The air is compressed in an air compressor to high temperatures and then sent to the receiver of the collector. Inside the receiver's tubes, air is further heated up before entering the gas turbine where power output is produced. Part of this power output is used to drive the air compressor, completing the cycle. The second cycle is a simple Rankine cycle with a reheater between the two-stage steam turbines. The reheater further increases the temperature of the steam using heat from the molten salt inside the heat exchanger. Regenerative feed water heaters are also utilized inside the system for increasing the thermal efficiency of the cycle. Steam at intermediate pressures is withdrawn and mixed directly with feed water in a contact heater and the resultant mixture is fed to the second feed water pump. The schematics of both cycles are shown in Figures 35 and 36.

Table 15: Performance comparison of different cycles

Cycle	Net power output
CSP plant with Rankine Cycle	1.26 MW
CSP plant with Brayton Cycle	3.5 MW [55]
CSP plant with reheat-regenerative Rankine Cycle	5 MW [56]

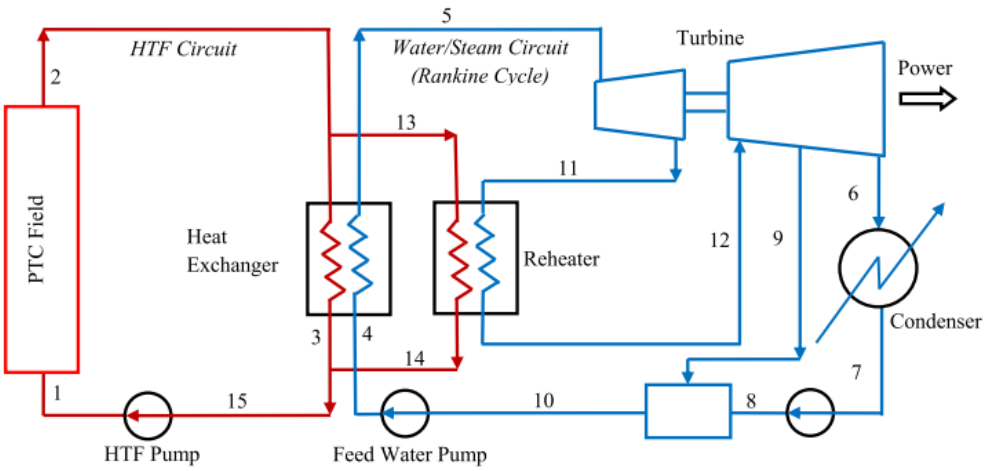

Figure 35: Reheat-regenerative Rankine cycle with parabolic trough collector [56]

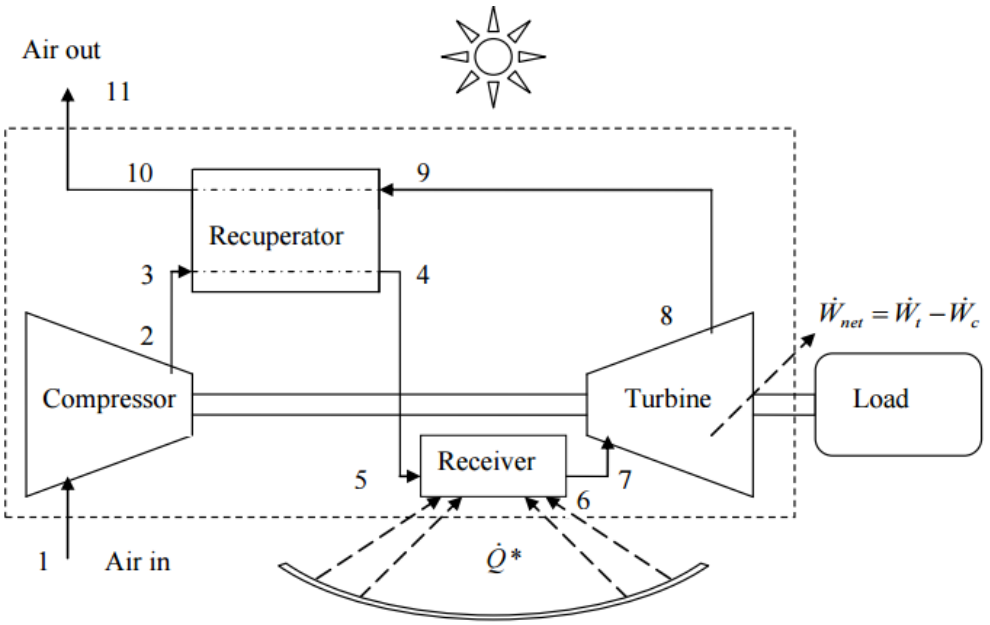

Figure 36: Brayton cycle with parabolic trough collector [55]

Chapter 5: Model Validation

In the earlier section, the present analysis is based on the energy balance of each subsystem. The thermodynamic analysis of the heat exchanger and the Rankine cycle depends only on the thermal properties of molten salt and water at each state in the cycles. These thermodynamic properties are well developed and presented from the literature. The analysis for the central receiver is based on the thermal model obtained from Li et al. [50] for the heliostat field. The analysis for the parabolic trough receiver is based on the model provided in Duffie et al. [43]. Firstly, the parabolic solar collector model is validated by the experimental study in [57] as shown in Figure 37. The graph shows the heat loss calculations for both the experimental model and the proposed model in this thesis. As observed, the proposed model shows good correlation with the experimental work. The small error difference is due to the assumptions made in the calculation of the heat loss coefficients. Also, the thermal efficiency of the collector when the ambient temperature is 298K is presented by Dudley as 73% which agrees with the results obtained for the proposed model with 72.3% thermal efficiency.

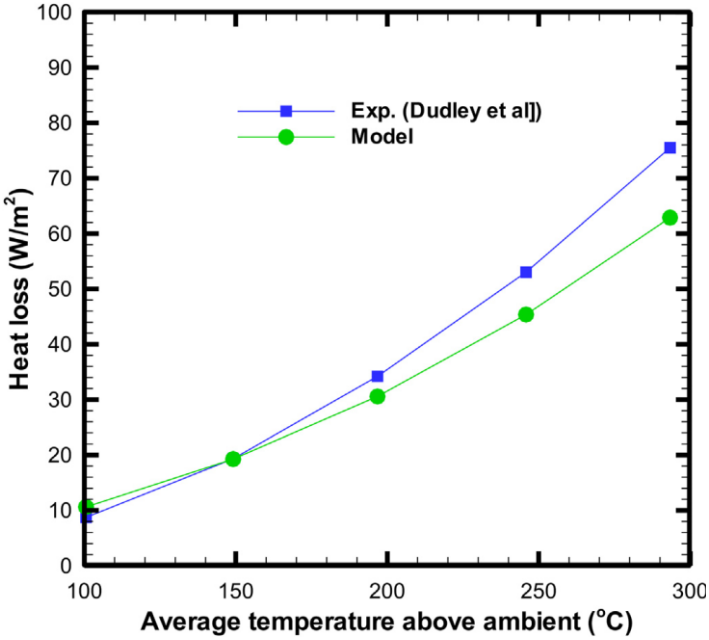

Figure 37: Validation of the parabolic solar collector model [52]

Moreover, the analysis for the central receiver of the heliostat field is modified and used to calculate the thermal performance based on the input parameters given in the thermodynamic analysis section. The thermal efficiency of the central receiver was

calculated as 75.6% which agrees with the results obtained by Xu et al. [48]. Therefore, the results obtained in this thesis are reasonable and valid, and are useful for guiding the design and operation of hydrogen production solar plants.

Chapter 6: Conclusions and Future Work

6.1 Conclusions

The demand for energy is increasing in the UAE, and this thesis provides good alternatives in sustainability to produce power and hydrogen from sources other than fossil fuels. The proposed system was studied and analysis was carried out on each subsystem and the overall system. The functionality of the system was provided in terms of coupling concentrated solar collectors to the conventional Rankine cycle and then to an electrolyzer. The thermodynamic analysis was based on energy and exergy analysis from equations obtained from the literature as shown in this thesis. Parametric analysis was also carried out on each subsystem and the overall system to investigate the effects of controlled variables on the performance of each component.

The analysis carried out in this thesis required data and numbers obtained from research papers and specification sheets of the components in question. The energy and exergy equations were taken from well-known books and journal articles. From the analysis shown in the section above, it is concluded that the coupling of an electrolyzer to a Rankine cycle powered by a concentrated solar collector could indeed solve future power generation problems and provide a different energy carrier in the UAE.

The energy and exergy analysis carried out in the section above draws many conclusions:

a. Thermal efficiencies for the parabolic trough ranged from 50-73% with the later achieved at a high mass flow rate of molten salt of 20 kg/s and the highest solar incident of 1100 W/m^2 which is possible in the UAE during the months of May-July.
b. Thermal efficiency of the heliostat field ranges from 74% to 92%. Higher solar incident and high concentration ratio achieve a maximum efficiency of 90%. Using a total field area of 50,000 m^2, the energy efficiency of the heliostat collector reaches 92% which is the best efficiency given the conditions of the system.
c. The maximum efficiency obtained from the Rankine cycle is around 45% using a steam mass flow rate of 15 kg/s. Of course, the piping sizes and

materials will limit the mass flow rate as will the fact that the optimized value at which it absorbs all the heat from the molten salt in the heat exchanger.

d. The overall system efficiency is highest at 27% when using the heliostat field which is considered low. However, thermal power plants using solar energy tend to have lower efficiencies but at the cost of zero greenhouse gas emissions and a cleaner environment.
e. Hydrogen production rate is a maximum of 0.411 kg/s or 24.56 kg/h when using heliostat field, when the incident irradiation is at its maximum and the highest mass flow rate of molten salt that can be achieved without cavitation or eroding the pipe material.
f. Increasing the aperture area of the parabolic trough had negligible effects on the energy efficiency at 70%, overall system thermal efficiency of 18%, and therefore on the hydrogen production rate which turned out to be 0.0855 kg/s at the highest aperture area.
g. The mass flow rate of Therminol inside the parabolic trough receiver increases the efficiency from 50 to 73% as well as the useful energy rate.
h. The increase in view factor increases the efficiency of the heliostat field up to 77% at 0.7 view factor, and then decreases the efficiency to 61% when the view factor is increased from 0.7 to 1.
i. The outlet temperature of molten salt increases as long as the receiver absorbed more heat energy. The increase in temperature meant a higher inlet turbine temperature which increased power output, and therefore higher mass flow rate of hydrogen produced.
j. Hydrogen that is not used right away can be stored for later usage using thermal storage technologies.
k. Underground storage for hydrogen in salt caverns or in depleted oil and gas reservoirs is a good idea for large-scale storage.
l. The use of a reheat system between the two stage turbines will increase the net power output and therefore the hydrogen production.
m. Open feed water heaters could lead to increased thermal efficiency, producing more net electricity, and therefore more mass flow rate of hydrogen.
n. Heliostat field collectors are proven for higher overall efficiency and have the highest hydrogen production flow rate at 0.2 kg/s.

o. The efficiency of the electrolyzer used was 70%. The option to choose another highly efficient electrolyzer will result in the production of more hydrogen.
p. The mass flow rate of water to the electrolyzer for molecule-level breakdown is kept constant and was not included in the analysis.

6.2 Recommendations and Future Work

Many adjustments can be made to increase the thermal efficiency, net power output, and hydrogen production rate of the overall system for future research. These recommendations could also provide better performance for a realistic plant in the industry. The recommendations that will lead to improved performance and results are listed below.

i. Experimental setup was needed to test the claims shown above using equations from the literature. The thesis was conducted using a theoretical approach and the results shown may vary experimentally.
ii. The materials used and equipment was not discussed in this thesis and it would be very useful to conduct research on those materials and equipment to take cost and affordability into account when carrying out the analysis.
iii. The integration of solar collectors and the hydrogen production unit can be done commercially but keeping in mind that it has to be a remote area where the solar incident is highest. Also, remote areas can be good for thermal storage of hydrogen underground that can be used as automobile fuel.
iv. At night, thermal storage options can be used to store energy during day light where the solar flux is available. By this, a 24/7 operation of the thermal power plant can be possible.
v. New research claims some gas turbines to be running on hydrogen as the fuel. They have lower efficiencies, but could serve as replacements for fossil fuels.
vi. A secondary organic Rankine cycle (ORC) or another smaller Rankine cycle can be used with the normal one to make use of the heat dumped at the condenser to further power production.
vii. Different solar collectors can be used achieving higher temperatures. Parabolic dish collectors achieve very high temperatures that will increase power output and hydrogen production but will cost more.

viii. Several ways can be used to improve the efficiency of the Rankine cycle such as regeneration, open and closed feed-water heaters, and a reheat option at the two-stage turbine.

ix. There is a heat loss at the operation of the electrolyzer that can be utilized in a micro heat cycle or coupled with a steam turbine to increase the efficiency.

References

[1] U. S. D. o. State, "Fourth Climate Action Report to the UN Framework Convention on Climate Change: Projected Greenhouse Gas Emissions," ed. Washington D, USA: U.S Department of State, 2007.

[2] R. Rapier, "Global Carbon Dioxide Emissions — Facts and Figures." [Online]. Available: http://www.energytrendsinsider.com/2012/07/02/global-carbon-dioxide-emissions-facts-and-figures/. [Accessed: 14-Apr-2015].

[3] J. Hallett, "Climate change 2001: The scientific basis. Edited by J. T. Houghton, Y. Ding, D. J. Griggs, N. Noguer, P. J. van der Linden, D. Xiaosu, K. Maskell and C. A. Johnson. Contribution of Working Group I to the Third Assessment Report of the Intergovernmental Panel on Climate Change, Cambridge University Press, Cambridge. 2001. 881 pp. ISBN 0521 01495 6," *Quarterly Journal of the Royal Meteorological Society*, vol. 128, pp. 1038-1039, 2002.

[4] V. Smil, *Energy : a beginner's guide*. Oxford: Oneworld, 2009.

[5] S. A. Kalogirou, "Solar thermal collectors and applications," *Progress in Energy and Combustion Science*, vol. 30, pp. 231-295, 2004.

[6] R. W. Mar and J. C. Swearengen, "Materials issues in solar thermal energy systems," *Solar Energy Materials*, vol. 5, pp. 37-53, 1981/7// 1981.

[7] B. Stine, W and W. Harrigan, R, "Power Cycles for Electricity Generation," in *Power From the Sun*, M. Geyer, Ed., ed: John Wiley and Sons, Inc., 1986.

[8] Wikipedia contributors, "Hydrogen Economy." [Online]. Available: http://en.wikipedia.org/wiki/Hydrogen_economy. [Accessed: 29-Apr-2015].

[9] Wikipedia contributors, "Thermochemical Cycle." [Online]. Available: http://en.wikipedia.org/wiki/Thermochemical_cycle#Cycles_based_on_the_sulfur_chemistry. [Accessed: 29-Apr-2015].

[10] Wikipedia contributors.. "Steam Reforming." [Online]. Available: http://en.wikipedia.org/wiki/Steam_reforming. [Accessed: 29-Apr-2015].

[11] A. A. AlZaharani, I. Dincer, and G. F. Naterer, "Performance evaluation of a geothermal based integrated system for power, hydrogen and heat generation," *International Journal of Hydrogen Energy*, vol. 38, pp. 14505-14511, 2013.

[12] Y. Bo, Z. Wenqiang, X. Jingming, and C. Jing, "Status and research of highly efficient hydrogen production through high temperature steam electrolysis at

INET," *International Journal of Hydrogen Energy*, vol. 35, pp. 2829-2835, 2010.

[13] C. M. Stoots, J. E. O'Brien, M. G. McKellar, G. L. Hawkes, and S. Herring, "Engineering process model for high-temperature electrolysis system performance evaluation," 2005.

[14] R. Rivera-Tinoco, C. Mansilla, and C. Bouallou, "Competitiveness of hydrogen production by High Temperature Electrolysis: Impact of the heat source and identification of key parameters to achieve low production costs," *Energy Conversion and Management,* vol. 51, pp. 2623-2634, 2010.

[15] W. Dönitz and E. Erdle, "High-temperature electrolysis of water vapor—status of development and perspectives for application," *International Journal of Hydrogen Energy,* vol. 10, pp. 291-295, 1985.

[16] M. A. Laguna-Bercero, "Recent advances in high temperature electrolysis using solid oxide fuel cells: A review," *Journal of Power Sources,* vol. 203, pp. 4-16, 2012.

[17] D. Palmer, (1997). "Hydrogen in the Universe."[Online]. Available: http://imagine.gsfc.nasa.gov/ask_astro/index.html. [Accessed: 5-May-2014].

[18] A. Midilli and I. Dincer, "Key strategies of hydrogen energy systems for sustainability," *International Journal of Hydrogen Energy,* vol. 32, pp. 511-524, 2007.

[19] M. Momirlan and T. N. Veziroglu, "The properties of hydrogen as fuel tomorrow in sustainable energy system for a cleaner planet," *International Journal of Hydrogen Energy,* vol. 30, pp. 795-802, 2005.

[20] I. Dincer and T. A. H. Ratlamwala, "Development of novel renewable energy based hydrogen production systems: A comparative study," *Energy Conversion and Management,* vol. 72, pp. 77-87, 2013.

[21] Y. Chen, P. Lundqvist, A. Johansson, and P. Platell, "A comparative study of the carbon dioxide transcritical power cycle compared with an organic rankine cycle with R123 as working fluid in waste heat recovery," *Applied Thermal Engineering,* vol. 26, pp. 2142-2147, 2006.

[22] X. R. Zhang and H. Yamaguchi, "An experimental study on evacuated tube solar collector using supercritical CO2," *Applied Thermal Engineering,* vol. 28, pp. 1225-1233, 2008.

[23] W. J. Yang, C. H. Kuo, and O. Aydin, "A hybrid power generation system: solar-driven Rankine engine-hydrogen storage," *International Journal of Energy Research,* vol. 25, pp. 1107-1125, 2001.

[24] D. Shapiro, J. Duffy, M. Kimble, and M. Pien, "Solar-powered regenerative PEM electrolyzer/fuel cell system," *Solar Energy,* vol. 79, pp. 544-550, 2005.

[25] Ö. F. Selamet, F. Becerikli, M. D. Mat, and Y. Kaplan, "Development and testing of a highly efficient proton exchange membrane (PEM) electrolyzer stack," *International Journal of Hydrogen Energy,* vol. 36, pp. 11480-11487, 2011.

[26] Y. Shin, W. Park, J. Chang, and J. Park, "Evaluation of the high temperature electrolysis of steam to produce hydrogen," *International Journal of Hydrogen Energy,* vol. 32, pp. 1486-1491, 2007/8// 2007.

[27] L. Mingyi, Y. Bo, X. Jingming, and C. Jing, "Thermodynamic analysis of the efficiency of high-temperature steam electrolysis system for hydrogen production," *Journal of Power Sources,* vol. 177, pp. 493-499, 2008.

[28] H. Zhang, S. Su, X. Chen, G. Lin, and J. Chen, "Configuration design and performance optimum analysis of a solar-driven high temperature steam electrolysis system for hydrogen production," *International Journal of Hydrogen Energy,* vol. 38, pp. 4298-4307, 2013.

[29] T. A. H. Ratlamwala, I. Dincer, and M. Aydin, "Energy and exergy analyses and optimization study of an integrated solar heliostat field system for hydrogen production," *International Journal of Hydrogen Energy,* vol. 37, pp. 18704-18712, 2012.

[30] P. Ahmadi, I. Dincer, and M. A. Rosen, "Energy and exergy analyses of hydrogen production via solar-boosted ocean thermal energy conversion and PEM electrolysis," *International Journal of Hydrogen Energy,* vol. 38, pp. 1795-1805, 2013.

[31] C. Yilmaz and M. Kanoglu, "Thermodynamic evaluation of geothermal energy powered hydrogen production by PEM water electrolysis," *Energy,* vol. 69, pp. 592-602, 2014.

[32] P. Ahmadi and I. Dincer, "Exergoenvironmental analysis and optimization of a cogeneration plant system using Multimodal Genetic Algorithm (MGA)," *Energy,* vol. 35, pp. 5161-5172, 2010.

[33] P. Ahmadi, I. Dincer, and M. A. Rosen, "Performance assessment and optimization of a novel integrated multigeneration system for residential buildings," *Energy and Buildings,* vol. 67, pp. 568-578, 2013.

[34] M. Ozturk and I. Dincer, "Thermodynamic analysis of a solar-based multi-generation system with hydrogen production," *Applied Thermal Engineering,* vol. 51, pp. 1235-1244, 2013.

[35] M. D. Islam, I. Kubo, M. Ohadi, and A. A. Alili, "Measurement of solar energy radiation in Abu Dhabi, UAE," *Applied Energy,* vol. 86, pp. 511-515, 2009.

[36] A. B. Zavoico, "Solar Power Tower Design Basis Document" Sandia National Laboratories, Report no. SAND2001-2100, Rev.0., San Francisco (CA): Nexant; 2001. p. 21-4.

[37] M. J. Montes, A. Abánades, and J. M. Martínez-Val, "Performance of a direct steam generation solar thermal power plant for electricity production as a function of the solar multiple," *Solar Energy,* vol. 83, pp. 679-689, 2009.

[38] E. Zarza, M. E. Rojas, L. González, J. M. Caballero, and F. Rueda, "INDITEP: The first pre-commercial DSG solar power plant," *Solar Energy,* vol. 80, pp. 1270-1276, 2006.

[39] LUZ International Limited, "Solar electric generating system IX technical description," LUZ, International Limited; 1990.

[40] (2012) "Therminol." [Online]. *Heat transfer fluids by Solutia Inc*. Available: www.therminol.com/pages/products/vp-1.asp. [Accessed: 25-Apr-2015].

[41] L. Valenzuela, E. Zarza, M. Berenguel, and E. F. Camacho, "Control concepts for direct steam generation in parabolic troughs," *Solar Energy,* vol. 78, pp. 301-311, 2005.

[42] R. E. Forristall, *Heat transfer analysis and modeling of a parabolic trough solar receiver implemented in engineering equation solver*: National Renewable Energy Laboratory, 2003.

[43] J. A. Duffie and W. Beckman, "Solar Engineering of Thermal Processes," 2nd ed. New York: John Wiley & Sons; 2006.

[44] J. C. Gomez, SolarPaces, and L. National Renewable Energy, *Heat capacity uncertainty calculation for the eutectic mixture of biphenyl/diphenyl ether used as heat transfer fluid preprint*. Golden, Colo.: National Renewable Energy Laboratory.

[45] F. A. Al-Sulaiman, "Exergy analysis of parabolic trough solar collectors integrated with combined steam and organic Rankine cycles," *Energy Conversion and Management,* vol. 77, pp. 441-449, 2014.

[46] R. Petela, "Exergy analysis of the solar cylindrical-parabolic cooker," *Solar Energy,* vol. 79, pp. 221-233, 2005.

[47] A. Bejan, G. Tsatsaronis, and M. J. Moran, *Thermal Design and Optimization*: Wiley, 1996.

[48] C. Xu, Z. Wang, X. Li, and F. Sun, "Energy and exergy analysis of solar power tower plants," *Applied Thermal Engineering,* vol. 31, pp. 3904-3913, 2011.

[49] D. L. Siebers and J. S. Kraabel, "Estimating convective energy losses from solar central receivers," 1984.

[50] X. Li, W. Kong, Z. Wang, C. Chang, and F. Bai, "Thermal model and thermodynamic performance of molten salt cavity receiver," *Renewable Energy,* vol. 35, pp. 981-988, 2010.

[51] I. Staffell, "The energy and fuel data sheet," in *W1P1 - Revision 1*, U. o. Birmingham, Ed., ed, 2011.

[52] F. A. Al-Sulaiman, "Energy and sizing analyses of parabolic trough solar collector integrated with steam and binary vapor cycles," *Energy,* vol. 58, pp. 561-570, 2013.

[53] C. Turchi, M. Mehos, C. K. Ho, and G. J. Kolb, "Current and future costs for parabolic trough and power tower systems in the US market," *SolarPACES 2010,* 2010.

[54] C. Turchi, "Parabolic trough reference plant for cost modeling with the solar advisor model (SAM)," National Renewable Energy Laboratory (NREL), Golden, CO.2010.

[55] W. le Roux, G, J. Meyer, B, and T. Bello-Ochende, "Solar thermal power generation using the Brayton cycle," University of Pretoria, Department of Mechanical and Aeronautical Engineering 2013.

[56] N. B. Desai and S. Bandyopadhyay, "Optimization of concentrating solar thermal power plant based on parabolic trough collector," *Journal of Cleaner Production,* vol. 89, pp. 262-271, 2015.

[57] V. E. Dudley, G. J. Kolb, A. R. Mahoney, T. R. Mancini, C. W. Matthews, M. Sloan, *et al.*, "Test results: SEGS LS-2 solar collector," Sandia National Labs., Albuquerque, NM (United States)1994.

Vita

Mohamed Shahin Shahin was born on the 6th of May 1991 in Cairo, Egypt. He started school in Sharjah at Hetteen School up to 3rd grade. He then joined Al Kindy School in Abu Dhabi and didn't stay there long before moving to Emirates Private School where he finished his secondary schooling in 2008. He then joined the American University of Sharjah for his Computer Science major before changing to Mechanical Engineering and obtaining his Bachelor's degree and graduated in 2013. He published his first journal paper with his senior design members under the supervision of Dr. Essam Wahba on aerodynamic drag reductions.

Mr. Shahin then joined the American University of Sharjah to pursue his Master's degree in Mechanical Engineering. He was awarded a graduate teaching assistant scholarship from 2013-2015 and worked as a teaching assistant. During his time as a GTA, he was assigned the job of teaching recitations and assisting professors in the Mechanical Engineering labs. During his Master's time, he submitted 2 papers that will be published in reputed journals.